eXPRESS Polymer Letters Vol.4, No.7 (2010) 396
Available online at www.expresspolymlett.com
DOI: 10.3144/expresspolymlett.2010.49

Editorial corner

The first impact factor has been given to Express Polymer Letters

*T. Czigány**

Department of Polymer Engineering, Budapest University of Technology and Economics, Műegyetem rkp. 3., H-1111, Budapest, Hungary

Express Polymer Letters, a journal launched in January 2007, achieved a great success by the fact that the Journal Citation Reports® of 2009, issued by Thomson Reuters, published the first calculated impact factor of the journal, which is 1.452 (The impact factor of a journal is the average number of citations in a given year to those papers that were published during the two preceding years).

By this impressive initial impact factor the high level of eXPRESS Polymer Letters has been acknowledged, which means that we are already within the first half of all journals with impact factor all over the world. Taking into account these journals dealing with polymers or polymer related materials science and technology topics, eXPRESS Polymer Letters is already within the first third of them. This rapid and remarkable result was generated by the consequent, rigorous peer reviewing process and by the good quality, predictable and reliable publication. In the past 3 years researchers of almost 60 countries submitted articles to eXPRESS Polymer Letters, but only about 30% of it was finally accepted. The continuously improving quality of the papers and the growing recognition of eXPRESS Polymer Letters is proven by the fact that the number of downloads doubles every year. From the articles published in the journal most cited and downloaded are those related to preparation and properties of nano-, bio- and self-reinforced composites and to self-healing properties of special materials, to certain technologies (such as e.g. polymer welding) and to natural polymers and their composites.

Although it is quite hard to become a member of the journal family having impact factor, it is much easier to lose this position. Therefore eXPRESS Polymer Letters makes the acceptance and approval process of the submitted papers even stricter. We do not strive for quantity, rather for quality, therefore we do not plan to increase the number of articles published in a month (presently 8–10). We wish to publish only original articles and we do our best to maintain the fast reviewing and publishing process (presently on an average 3–4 months).

Of course, this success could not have been achieved without the continuous cooperation and help of our authors, reviewers and readers, which is very much acknowledged and counted on in the future as well. This is the right occasion to thank all my colleagues of the Editorial for their hard work!

Prof. Dr. Tibor Czigány
Editor of Express Polymer Letters

*Corresponding author, e-mail: czigany@eik.bme.hu

eXPRESS Polymer Letters Vol.4, No.7 (2010) 397–403
Available online at www.expresspolymlett.com
DOI: 10.3144/expresspolymlett.2010.50

Dispersion of nano-silica in monomer casting nylon6 and its effect on the structure and properties of composites

L. F. Cai[1*], *Z. Y. Lin*[2], *H. Qian*[2]

[1]Department of Environment and Life science, Putian University, No. 1133, Mid-Xueyuan St., Putian, Fujian Province 351100, P. R. China
[2]College of Materials Science and Engineering, Huaqiao University, No. 269, Chenghuabei Rd., Quanzhou, Fujian Province 362021, P. R. China

Received 26 February 2010; accepted in revised form 24 April 2010

Abstract. To promote dispersion of nano-silica in monomer casting nylon6 (MC nylon6), nano-silica was dispersed in melted caprolactam with the assistance of ultrasound, anionic polymerization was then initiated to form silica/MC nylon6 *in-situ* nanocomposites. It was found that hydrogen bonds were formed between nano-silica and caprolactam, in the meantime, ultrasound helped to break the nanoparticles aggregations into smaller ones or even mono-dispersing particles. Therefore, the agglomerated nanoparticles were pulled apart and stabilized by caprolactam. Additionally, the rapid anionic polymerization of caprolactam also contributed to the avoidance of re-agglomeration and deposition of nanoparticles during the polymerization process, leading to the uniform distribution of nanoparticles in the polymer matrix. Mechanical tests indicated that the silica/MC nylon6 *in-situ* nanocomposites prepared according to the above strategy were simultaneously toughened, strengthened and stiffened. Thermogravimetric analysis (TGA) results showed that thermal stability of nanocomposites was notably improved compared to neat MC nylon6.

Keywords: *nanocomposites, silica, MC nylon6, in-situ anionic polymerization*

1. Introduction

Polymer-based nanocomposites have been reported as an exciting new class of materials for their markedly improved properties over neat polymers and micron-sized particle filled polymer composites [1, 2]. However, the specific characteristics of the nanocomposites can only be effective provided that the nanoparticles are well dispersed in the matrix. Due to the strong tendency of nanoparticles to agglomerate, manufacturing composites with uniformly distributed nanoparticles becomes a challenging task [3].

To break down these nanoparticles aggregations and manufacture nano-structural composites, researchers mainly focus on the following three approaches: 1) sol-gel processing [4], 2) melt compounding [5–7], and 3) *in-situ* polymerization with the presence of nanoparticles [8, 9]. During sol-gel process, the formation of a crosslinking network of organic metal oxides makes it difficult to process, and it is a disadvantage that limits the application of this method. Melt compounding is one of the most conventional processing methods. However, the previously synthesized polymers would inevitably undergo some degradation during processing. Comparatively, *in-situ* polymerization with the presence of nanoparticles seems to be rather facile. In this method, nanoparticles are dispersed in monomer first, and then the mixture is polymerized using a technology similar to bulk polymerization. It is

*Corresponding author, e-mail: cailf2002@yahoo.com.cn

obvious that the most important factor that affects the properties of composites is the dispersion of nanoparticles.

According to Tadros [10], the dispersion of ultrafine particles in medium can be divided into three procedures:

1. Wetting of particles into dispersion medium;
2. Breaking of aggregations into mono-dispersing particles or smaller aggregations;
3. Stabilization of mono-dispersing particles and smaller aggregations against re-agglomeration.

With the enlightenment of Tadros's work, the authors of the present paper plan to prepare silica/monomer casting nylon6 (MC nylon6) *in-situ* nanocomposites via anionic polymerization according to the following procedure: nano-silica was directly dispersed into melted caprolactam with the assistance of ultrasound, and then anionic polymerization was initiated to form the resulting nanocomposites. Such strategy was designed according to the following: (i) it was reported that particles with polar surface can be easily wetted by polar liquid [11]. Accordingly, nano-silica with polar silanol groups on the surface can be easily wetted by polar melted caprolactam containing amide group, (ii) the preparation of the nylon6/silica nanocomposites using *in-situ* anionic polymerization was also recently reported by Rusu and Rusu [12]. It is found that nano-silica was simply dispersed in the melted caprolactam by ordinary stirrer. Accordingly, although some of the nano-silica was homogeneously dispersed, there were still some bigger aggregations (ca. 200 nm in diameter) within the nylon6 matrix. Considering that the tremendous energy offered by ultrasonic is likely to break the nanoparticles aggregations into smaller ones or even mono-dispersing particles [13], in the present work, ultrasound was employed to disperse nano-silica in melted caprolactam. Therefore, the agglomerated nanoparticles would be pulled apart and coated with caprolactam, leading to the improved stability of smaller aggregations and mono-dispersing nanoparticles against re-agglomeration, and (iii) in comparison with classical hydrolytic polymerization of caprolactam which takes about 12–24 hrs [14, 15], the rapid anionic polymerization of caprolactam (usually within 1 hr [12, 16]) also contributed to the avoidance of re-agglomeration and deposition of nanoparticles during the polymerization process, leading to the uniform distribution of nanoparticles in polymer matrix (Figure 1). Besides, it is well known that the anionic polymerization of caprolactam proceeds well below the melting temperature of the nylon6, which could avoid the degradation in comparison with conventional melt compounding. The present paper characterized the dispersion of nano-silica in the composite and preliminarily evaluated effect of nano-silica on the structure and properties of the MC nylon6 based nanocomposites.

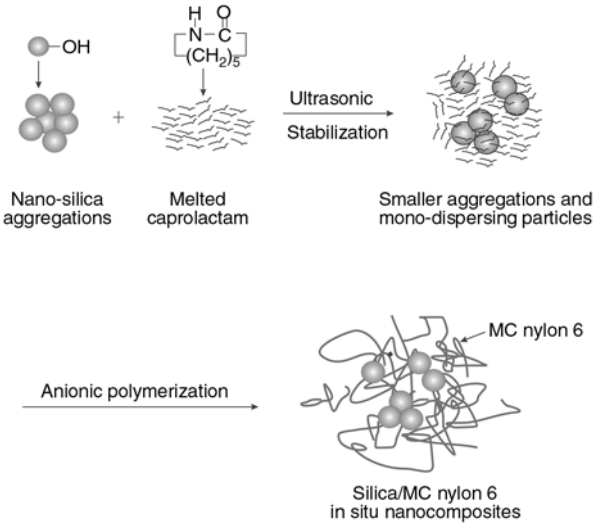

Figure 1. Schematic drawing of the proposed technology to prepare silica/MC nylon6 *in-situ* nanocomposites with uniformly distributed nanoparticles

2. Experimental

2.1. Materials

Nano-silica was supplied by Zhoushan Mingri Nanometer Material Corporation (Zhejiang, China) with an average diameter of 30±5 nm. The particles were dried at 120°C under vacuum for 24 h to eliminate the physically absorbed and weakly chemically absorbed species.

ε-caprolactam (AR grade) was obtained from Baling Company, China Petroleum and Chemical Corporation (Hunan, China). Sodium hydroxide (AR grade) and 2,4-tolylene diisocyanate (2,4-TDI, CP grade, vacuum distillated before use) were obtained from Shanghai Chemical Reagents Corporation (Shanghai, China).

2.2. Composites preparation

Silica/MC nylon6 *in-situ* nanocomposites were obtained according to the following procedure:

100 g caprolactam was melted at 120°C, then 0.40 g sodium hydroxide was added followed by vacuum treatment to eliminate the produced water, vacuum treatment was maintained about 30 min to confirm the thorough elimination of water. Then various contents of dried nano-silica (including 1.0, 2.0, 3.0 and 5.0 wt%) was dispersed in this melt by the assistance of ultrasound (ultrasonic mixer with a power of 300 W and a frequency of 40 kHz) to obtain homogeneous mixture. Finally the mixture was heated to 150°C, 0.364 g 2,4-TDI was introduced as cocatalyst, and the anionic polymerization time was 60 min.

2.3. Characterization

Fourier-transform infrared (FTIR) spectroscopy was employed to investigate the interaction between nano-silica and caprolactam. The FTIR spectra of original nano-silica and silica/caprolactam compound were recorded in KBr pellets on a Nexus-470 Fourier-transform IR spectrometer (Nicolet, United States of America). Blank scanning was performed before measurements to eliminate the influence of water vapor and CO_2 in the air.

To assess nanoparticles dispersion in the composites matrix, ultrathin film was randomly cut from the inner part of composites and observed through a JEM-100CXII transmission electron microscope (TEM, Japan).

The wide angle X-ray diffraction (WAXD) analysis was conducted using a Bruker D8 Diffractometer (Germany). The X-ray beam was nickel-filtered CuK_α radiation ($\lambda = 0.15$ nm), and data were collected from 5 to 35° (2θ) at a rate of 2°/min.

Thermogravimetric analysis (TGA) measurements were performed using a TA-5200 thermogravimetric analyzer (United States of America) from 25 to 700°C with a heating rate of 20°C/min under flowing of nitrogen.

The mechanical properties reported hereinafter are the average of five successful tests. All specimens were mechanically cut using a ZHY-W universal sample maker (CHENGDE Dahua Tester Co. Ltd., Hebei, China). Dumbbell specimens with waist dimensions of 25.0×5.0×2.0 mm were used for tensile tests in a SANS CMT-6104 (MTS, United States of America) universal tester. Notched impact strength were tested in XCJ-40 Charpy Tester (CHENGDE Materials Tester Co. Ltd., Hebei, China), the dimensions of these samples were 40.0×3.0×2.0 mm (length×width×thickness). All the specimens were conditioned at 30°C and a relative humidity of 50% for 48 h prior to the measurements, which were then tested under the same conditions.

3. Results and discussion

3.1. Interaction between nano-silica and caprolactam

According to the structure (Figure 2), nano-silica has silanol groups on the surface, while caprolactam contains amide group. At the beginning of discussion, therefore, it should be studied whether there is interaction between nano-silica and caprolactam, since it is planned to use caprolactam as dispersion medium and stabilizer for separated nanoparticles against re-agglomeration.

Figure 3 gives the FTIR spectra of caprolactam and nano-silica/caprolactam. In the spectrum of neat caprolactam, the observed N–H stretching band and the amide I mode known to be dominated by the C=O stretching band are 3218 and 1660 cm^{-1} respectively. These two bands are very broad and strong due to the fact that caprolactam possesses typical self-associated hydrogen bonds formed

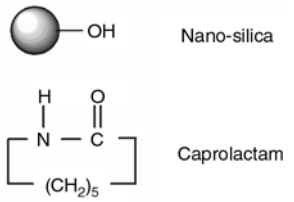

Figure 2. Schematic structure of nano-silica and caprolactam

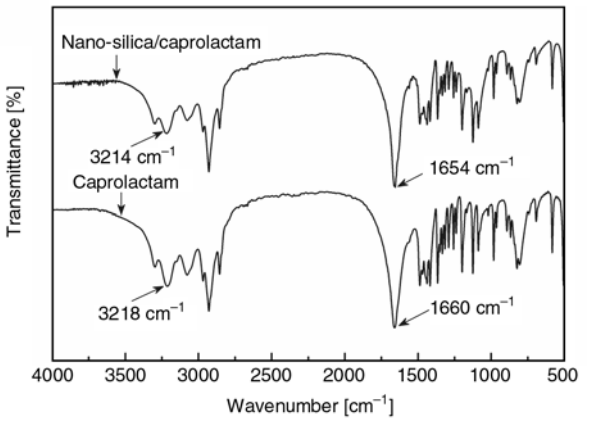

Figure 3. FTIR spectra of caprolactam and nano-silica/caprolactam compound (nano-silica content = 2.0 wt%)

between C=O and N–H. For the spectrum of nano-silica/caprolactam, the absorption of N–H (appears at 3214 cm^{-1}) and C=O(appears at 1654 cm^{-1}) show obvious displacement to lower frequency compared to neat caprolactam. In consideration of the fact that there are plentiful silanol groups on the surface of nano-silica, the above results should indicate the existence of hydrogen bonds between caprolactam and nano-silica [17].

3.2. Microstructural characterization

Filler dispersion is of great importance in the physical behaviors of polymer composites. As shown by the TEM photos in Figure 4, the nanoparticles have homogeneous dispersion in matrix. The dispersion scale of the nano-silica in matrix ranges from 25 to 70 nm, i.e. nanoparticles agglomerations were broken into smaller ones or even mono-dispersing particles since the original size of nano-silica is about 30±5 nm (see Experimental part). Clearly, this also manifests the feasibility of the strategy we proposed in the Introduction part to prepare silica/MC nylon6 *in-situ* nanocomposites with uniformly distributed nanoparticles.

Nylon6 is well known to crystallize into variously phase: the α stable crystal and among others the γ one [18]. WAXD was used to gain insight into the influence of nano-silica on the crystal form of MC nylon6. As is shown in Figure 5, the peak at 2θ = 20.3° belongs to the (200) face of the α1 form, the peak at 2θ = 21.6° belongs to the (001), (200), and (201) faces of the γ form, and the peak at 2θ = 23.9° belongs to the (002) and (202) faces of the α2 form. Therefore, it is evident that the α form is the dominant crystalline phase for both neat MC nylon6 and

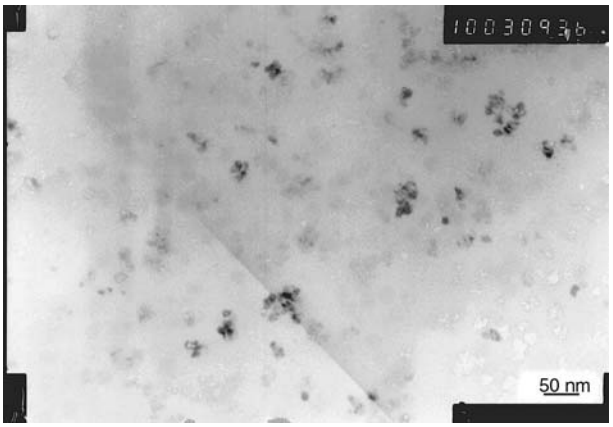

Figure 4. TEM image of a silica/MC nylon6 *in-situ* nanocomposites (nano-silica content = 2.0 wt%)

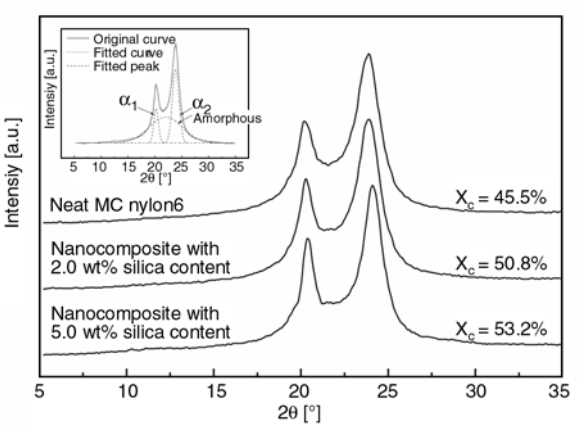

Figure 5. WAXD spectra of MC nylon6 and nanocomposites. The inset illustrates the WAXD curve treated by fitting and peak separation. X_c denotes crystalliniy.

nanocomposites (Figure 5), which is consistent with the results reported by Reynaud *et al*. [8]. In order to further studied the crystallinity of neat MC nylon6 and nanocomposites, the WAXD curves were treated with fitting and peak separation as shown in the inset of Figure 5 to get α1 form, α2 form and amorphous. The crystalliniy (X_c) was calculated according to Equation (1):

$$X_c\,[\%] = \frac{\Sigma(A_{\alpha 1-form} + A_{\alpha 2-form})}{\Sigma(A_{\alpha 1-form} + A_{\alpha 2-form} + A_{amorphous})} \cdot 100 \quad (1)$$

where $A_{\alpha 1\text{-}form}$, $A_{\alpha 2\text{-}form}$ and $A_{amorphous}$ denote the area of various fitted peaks (α1 form, α2 form and amorphous, respectively). As shown in Figure 5, the crystalliniy (X_c) of nanocomposites is higher than that of neat MC nylon6, indicating the promotion of nano-silica on the crystallization of nylon6 matrix. Similar results were also reported in nylon6/clay nanocomposites, and such promotion behaviors were generally attributed to the nucleation effect of nano-fillers [19, 20].

3.3. Thermal behavior of nanocomposties

TGA weight loss obtained in a nitrogen atmosphere for the neat MC nylon6 and nanocomposites is shown in Figure 6. It can be seen that the neat MC nylon6 exhibits two-step weight loss mechanism, while the nanocomposites show delayed decomposition in first step compared to neat MC nylon6. The temperatures at which 10, 50, and 90% weight loss occur as representative of thermal stability are

Table 1. TGA results of MC nylon6 and nanocomposites

	MC nylon6	Nanocomposites with various silica content [wt%]			
		1.0%	2.0%	3.0%	5.0%
$T_{10\%}$* [°C]	321.58	336.21	360.19	400.97	396.58
$T_{50\%}$* [°C]	440.89	437.76	435.36	444.16	444.16
$T_{90\%}$* [°C]	472.03	465.75	461.35	467.75	467.75
Residue [wt%]	0.02	1.12	2.03	2.92	5.10

*$T_{10\%}$, $T_{50\%}$ and $T_{90\%}$ denote to the temperature at various weight loss of 10%, 50% and 90%, which is calculated from the TGA thermograms

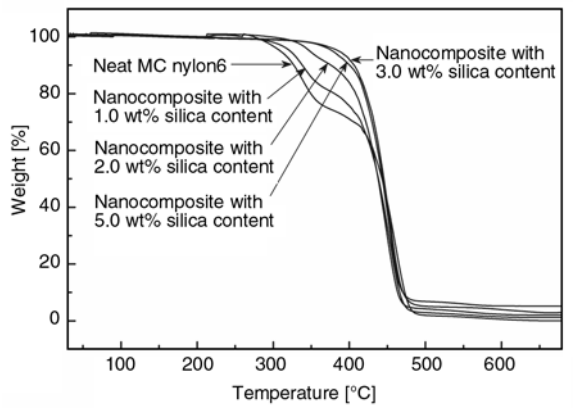

Figure 6. TGA thermograms of MC nylon6 and nanocomposites as a function of silica content

listed in Table 1. It is evident that the influence of nano-silica on thermal stability of MC nylon6 differs at different ranges of weight loss. At lower weight loss (10 and 50%), the notable tendency of improved thermal stability of the nanocomposites with increasing nano-silica content can be seen from Table 1. At present, the detailed mechanism of thermal stabilization of the filled nylon6 systems is not clearly understood. According to Theng [21] and Velde [22], the interaction between the amide groups of nylon6 molecules and the ionic groups at the clay surfaces probably suppresses thermal degradation of the composite matrix. Such explanation may also be valid for the improved thermal stability of nanocomposites as mentioned above. However, it is interesting to find that thermal stability of nanocomposites is slightly inferior to neat MC nylon6 when higher weight loss (90%) is considered. Such results indicate that the introduction of silica might change the decomposition mechanism of MC nylon6 under high temperature. Further work will be carried out on such high temperature decomposition mechanism of silica/MC nylon6 *in-situ* nanocomposites.

3.4. Mechanical properties

Figure 7 shows notched Charpy impact strength of nanocomposites as a function of nano-silica content. It is seen that the contribution of the uniformly distributed nanopartilces to the improvement of toughness under high speed deformation and to the reduction of notch sensitivity is notable, and the highest impact strength of composites (appears at 3.0 wt% of silica content) is about 1.17 times higher than that of neat MC nylon6. So far, the crack front bowing mechanism has been widely used for explaining the toughening effect in micro-sized particulate filled polymers [23]. Nevertheless, Chan *et al*. [24] inferred that in the case where the size of rigid particles is of the order of 50 nm or less, the applicability of the bowing mechanism is questionable, because such small size rigid particles may not be able to resist the propagation of the crack. From J-integral tests, they suggested that nanoparticles would trigger large-scale plastic deformation of the matrix, which consumes tremendous fracture energy. Since the above morphological investigation reveals that most of the dispersion scale of the

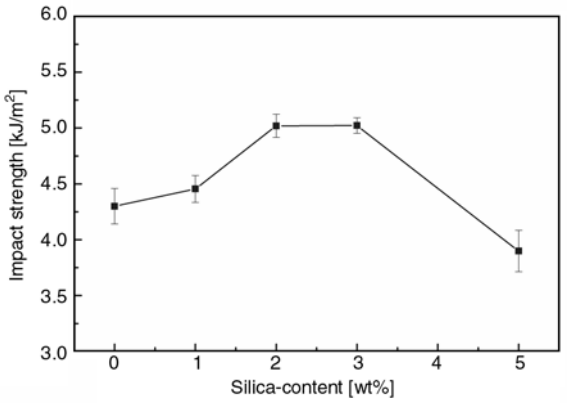

Figure 7. Notched Charpy impact strength of MC nylon6 and nanocomposites as a function of silica content

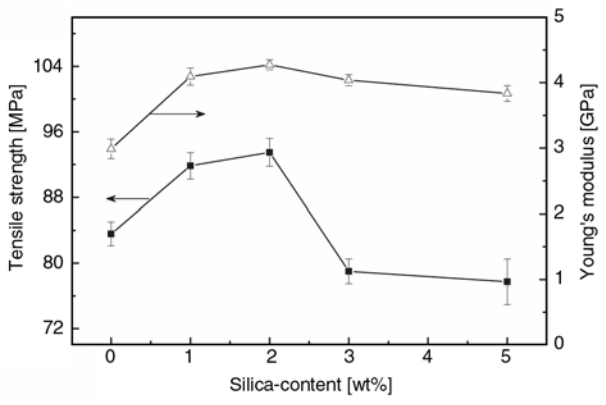

Figure 8. Tensile strength and Young's modulus of MC nylon6 and nanocomposites as a function of silica content

nanoparticles is less than 50 nm in the composites, it is believed that the mechanism proposed by Chan and co-workers should also be valid in the current study.

Tensile strength of nanocomposites as a function of nano-silica content is shown in Figure 8. In comparison with neat MC nylon6, the composites show prominent improvement of tensile strength under lower nano-silica content (2 wt%), and the highest tensile strength of composites (appears at 2.0 wt% of silica content) is about 1.12 times higher than that of neat MC nylon6. According to the above FTIR results, there are hydrogen bonds between nano-silica and amide group. Such interaction should also account for the strengthening effect, as the stress was effectively transferred [25, 26]. The filler content dependences of Young's modulus of the composites are also exhibited in Figure 8. In comparison with neat MC nylon6, all of the composites show higher Young's modulus. At a silica content of 2.0 wt%, for example, the Young's modulus shows maximum value and is about 1.43 times higher than that of neat MC nylon6. Similarly, the interaction between nano-silica and caprolactam can effectively impart the rigidity of nanoparticles to MC nylon6.

4. Conclusions

On the basis of the above discussion, the following conclusions can be drawn.

1. Caprolactam can be used as dispersion medium and stabilizer for the separated nanoparticles against re-agglomeration owing to the existence of hydrogen bond between nano-silica and caprolactam.
2. TEM photos reveal a uniform distribution of nano-silica in matrix. This manifests that the nanoparticles aggregations were broken into smaller ones or even mono-dispersing particles according to the technology we proposed in this paper.
3. Within the sensitivity of our experimental instrument, no influence of nano-silica can be noticed on the crystal form in these MC nylon6 based nanocomposites. However, nano-silica shows obvious promotion effect on the crystallization of nylon6 matrix.
4. Thermal stability of nanocomposites prepared according to the technology we proposed in this paper is notably improved compared to neat MC nylon6. And nanocomposites also receive simultaneous improvement of toughness, strength and stiffness.

Acknowledgements

The authors are grateful to the support of National Natural Science Foundation of China (Grant: 59602007).

References

[1] Zhang M. Q., Rong M. Z., Friedrich K.: Processing and properties of nonlayered nanoparticle reinforced thermoplastic composites. in 'Handbook of organic-inorganic hybrid materials and nanocomposites. Vol 2: Nanocomposites' (ed.: Nalwa H. S.) American Science Publishers, Boston, 113–150 (2003).

[2] Leuteritz A., Pospiech D., Kretzschmar B., Willeke M., Jehnichen D., Jentzsch U., Grundke K., Janke A.: Progress in polypropylene nanocomposite development. Advanced Engineering Materials, **5**, 678–681 (2003).
DOI: 10.1002/adem.200320139

[3] Rong M. Z., Zhang M. Q., Ruan W. H.: Surface modification of nanoscale fillers for improving properties of polymer nanocomposites: A review. Materials Science and Technology, **22**, 787–796 (2006).
DOI: 10.1179/174328406X101247

[4] Novak B. M.: Hybrid nanocomposite materials-between inorganic glasses and organic polymers. Advanced Materials, **5**, 422–433 (1993).
DOI: 10.1002/adma.19930050603

[5] Cho J. W., Paul D. R.: Nylon 6 nanocomposites by melt compounding. Polymer, **42**, 1083–1094 (2001).
DOI: 10.1016/S0032-3861(00)00380-3

[6] Dennis H. R., Hunter D. L., Chang D., Kim S., White J. L., Cho J. W., Paul D. R.: Effect of melt processing conditions on the extent of exfoliation in organoclay-based nanocomposites. Polymer, **42**, 9513–9522 (2001).
DOI: 10.1016/S0032-3861(01)00473-6

[7] García M., van Vliet G., ten Cate M. G. J., Chavez F., Norder B., Kooi B., van Zyl W. E., Verweij H., Blank D. H. A.: Large-scale extrusion processing and characterization of hybrid nylon-6/SiO_2 nanocomposites. Polymers for Advanced Technologies, **15**, 164–172 (2004).
DOI: 10.1002/pat.458

[8] Reynaud E., Jouen T., Gauthier C., Vigier G., Varlet J.: Nanofillers in polymeric matrix: A study on silica reinforced PA6. Polymer, **42**, 8759–8768 (2001).
DOI: 10.1016/S0032-3861(01)00446-3

[9] Paul D. R., Robeson L. M.: Polymer nanotechnology: Nanocomposites. Polymer, **49**, 3187–3204 (2008).
DOI: 10.1016/j.polymer.2008.04.017

[10] Tadros T. F.: Industrial applications of dispersions. Advances in Colloid and Interface Science, **46**, 1–47 (1993).
DOI: 10.1016/0001-8686(93)80032-7

[11] James R. O.: Characterization of colloids in aqueous systems. in 'Ceramic powder science' (eds.: Messing G. L., Mazdiyansi K., Haber R. A.) American Ceramic Society, Westerville, 349–410 (1987).

[12] Rusu G., Rusu E.: Nylon 6/SiO_2 nanocomposites synthesized by in situ anionic polymerization. High Performance Polymers, **18**, 355–375 (2006).
DOI: 10.1177/0954008306063392

[13] Joung G. R., Sang W. P., Kim H. S., Lee J. W.: Power ultrasound effects for in situ compatibilization of polymer-clay nanocomposites. Materials Science Engineering: C, **24**, 285–288 (2003).
DOI: 10.1016/j.msec.2003.09.057

[14] Mougin N., Veith C. A., Cohen R. E., Gnanou Y.: Anionic polymerization of lactams in the presence of metal dialkoxyaluminum hydrides: Presentation of a new mechanism. Macromolecules, **25**, 2004–2016 (1992).
DOI: 10.1021/ma00033a026

[15] Rusu G., Ueda K., Rusu E., Rusu M.: Polyamides from lactams by centrifugal molding via anionic ring-opening polymerization. Polymer, **42**, 5669–5678 (2001)
DOI: 10.1016/S0032-3861(01)00059-3

[16] Kircher K.: Chemical reaction in plastics processing. Hanser, Munich (1987).

[17] Xue Q.: Spectroscopy in the study of macromolecular structure (in Chinese). High Education Publishers, Beijing (1995).

[18] Lin L., Argon A. S.: Deformation resistance in oriented nylon 6. Macromolecules, **25**, 4011–4024 (1992).
DOI: 10.1021/ma00041a025

[19] Jiang T., Wang Y-H., Yeh J-T., Fan Z-Q.: Study on solvent permeation resistance properties of nylon6/clay nanocomposite. European Polymer Journal, **41**, 459–466 (2005).
DOI: 10.1016/j.eurpolymj.2004.10.024

[20] Katoha Y., Okamoto M.: Crystallization controlled by layered silicates in nylon 6-clay nano-composite. Polymer, **50**, 4718–4726 (2009).
DOI: 10.1016/j.polymer.2009.07.019

[21] Theng B. K. G..: The chemistry of clay-organic reactions. Halsted Press, New York (1974).

[22] Velde B.: Introduction to clay minerals: Chemistry, origins, uses, and environmental significance. Chapman and Hall, London (1992).

[23] Lange F. F.: The interaction of a crack front with a second-phase dispersion. Philosophical Magazine, **22**, 983–992 (1970).
DOI: 10.1080/14786437008221068

[24] Chan C-M., Wu J-S., Li J-X., Cheung Y-K.: Polypropylene/calcium carbonate nanocomposites. Polymer, **43**, 2981–2992 (2002).
DOI: 10.1016/S0032-3861(02)00120-9

[25] Cai L. F., Huang X. B., Rong M. Z., Ruan W. H., Zhang M. Q.: Effect of grafted polymeric foaming agent on the structure and properties of nano-silica/polypropylene composites. Polymer, **47**, 7043–7050 (2006).
DOI: 10.1016/j.polymer.2006.08.016

[26] Cai L. F., Mai Y. L., Rong M. Z., Ruan W. H., Zhang M. Q.: Interfacial effects in nano-silica/polypropylene composites fabricated by in-situ chemical blowing. Express Polymer Letters, **1**, 2–7 (2007).
DOI: 10.3144/expresspolymlett.2007.2

eXPRESS Polymer Letters Vol.4, No.7 (2010) 404–414
Available online at www.expresspolymlett.com
DOI: 10.3144/expresspolymlett.2010.51

Effect of organo-modified montmorillonite on poly(butylene succinate)/poly(butylene adipate-co-terephthalate) nanocomposites

B. W. Chieng, N. A. Ibrahim, W. M. Z. Wan Yunus*

Chemistry Department, Faculty of Science, Universiti Putra Malaysia, 43400 UPM Serdang, Selangor, Malaysia

Received 6 March 2010; accepted in revised form 24 April 2010

Abstract. The composite material based on poly(butylene succinate) (PBS), poly(butylene adipate-co-terephthalate) (PBAT) and organo-modified montmorillonite (OMMT) were prepared by melt blending technique and characterized. Sodium montmorillonite (Na-MMT) was successfully modified by octadecylammonium (ODA) and dimethyldioctadecylammonium (DDOA) salts to become OMMT through cation exchange technique which is shown by the increase of basal spacing of clay by XRD. The addition of the OMMT to the PBS/PBAT blends produced nanocomposites which is proved by XRD and TEM. Tensile tests showed increase in tensile strength and modulus which is attributed to the existence of strong interactions between PBS/PBAT and clay, particularly with OMMT. Highest tensile strength of nanocomposite was observed at 1 wt% of OMMT incorporated. TGA study showed that the thermal stability of the blend increased after the addition of clays. SEM micrographs of the fracture surfaces show that the morphology of the blend becomes homogeneous and smoother with presence of OMMT.

Keywords: *nanocomposites, biodegradable, OMMT*

1. Introduction

Nanocomposites based on biodegradable polyester and layered silicate have been extensively investigated because of their potential applications in the fields related to environmental protection. Biodegradable polymers are degradable polymers in which the degradation results from the action of naturally occurring microorganism such as bacteria, fungi and algae. Although biodegradable polymers have started making inroads into commercial applications, there is still lot of potential in the improvement of their properties for commercial large scale application.

Montmorillonite is one of the commercial layered silicates and has been widely used as reinforcing filler in the preparation of nanocomposites. However, the hydrophilic nature of montmorillonite limits its compatibility with organophilic polymers. Thus, chemical modification has been developed to make montmorillonite compatible with organophilic polymer. This can be readily achieved by modifying the montmorillonite with alkylammonium salts to form organo-montmorillonite (OMMT).

Poly(butylene succinate) (PBS) is a biodegradable aliphatic thermoplastic which synthesized by polycondensation of 1,4-butanediol with succinic acid. PBS possesses many desirable properties including biodegradability, melt processability, and thermal and chemical resistance. It can be processed in the field of textiles into melt-blown, multifilament, monofilament, flat and split yarn [1]. However, other properties such as gas barrier properties, melt viscosity for further processing and so on, are frequently insufficient for various end-use applica-

*Corresponding author, e-mail: norazowa@science.upm.edu.my

tions [2]. Poly(butylene adipate-co-terephthalate) PBAT, trade name ECOFLEX® is an aliphatic/aromatic copolyester based on the monomers 1,4-butanediol, adipic acid and terephthalic acid. It is fully biodegradable polymer and is resistant to water. Typical applications are packaging films, agricultural films and compose bags.

Blending two or more polymers is an economic technique for producing new polymer materials at low cost and desirable properties combination for specific end use. They can be developed much more quickly than new polymers and require much less capital investment. However, thermodynamic immiscibility of polymers had limited the use of polymer blends in industry. These immiscible blends are characterized by a two phase morphology, narrow interphase, poor physical and chemical interactions across the phase boundaries, and poor mechanical properties. Many studies have focused on improving the compatibility between polymer components, either by adding third component, or by inducing a chemical reaction which leads to the modification of polymer interface [3]. To improve the properties of PBS, many researchers introduce clays to the PBS system [4–6]. Researchers also tried to improve the properties of PBS by blending with other polymers [7]. Jacob *et al.* [8] have studied the compatibility between PBS and PBAT. They revealed that this blend is immiscible but only one T_g was observed due to the close proximity of individual T_g's of both PBS and PBAT. Other reports have shown that OMMT can act as compatibilizer for immiscible polymer blends [9–15] which exhibit remarkable improvement in their properties compared to the pristine polymer or the conventional composite [16, 17]. The interlayer cations between the silicate layers such as Na^+ are exchanged with organic cations to increase the organonophilicity of the clay layers. This lowers the interfacial energy and improves wetting by the polymer matrix [16].

In this study, the OMMT was used as compatibilizer to improve the miscibility of the PBS/PBAT blends. The PBS/PBAT composites were prepared by the melt blending technique and the effect of OMMT on physical, mechanical and thermal properties was investigated. The compatibility between the PBS and PBAT was studied by examining the fracture surface of the tensile test specimens under SEM.

2. Experimental

2.1. Materials

Poly(butylene succinate) PBS, was supplied by Showa Highpolymer Co. Ltd. (Japan) under tradename 'BIONOLLE', grade #1020. The PBS pellets were dried in an oven at 60°C for 24 hours before processing. The poly(butylene adipate-co-terephthalate) PBAT, trade name ECOFLEX® F BX 7011 was supplied by BASF. PBAT was supplied in pellet form and used as received. Properties of BIONOLLE and ECOFLEX are summarized in Table 1. Na-MMT (Kunipia F) with cation exchange capacity of 119 meq/100 g was obtained from Kunimine Ind. Co. Japan and used as received. Octadecylamine and dimethyldioctadecylammonium bromide was purchased from Acros Organics and used as an organic modifier of montmorillonite.

Table 1. Properties of BIONOLLE and ECOFLEX

Properties	BIONOLLE	ECOFLEX
Melting point	116°C	110°C
Glass transition	–31°C	–29°C
Melt mass-flow rate (190°C/2.16 kg)	20–29 g/10 min	2.7–4.9 g/10 min
Molecular weight (M_w)	~40 000	40 000
Crystallinity	30–50%	~20%

2.2. Preparation of OMMT

The organo-modified montmorillonite (OMMT) was prepared according to the published method with slight modification [18]. The octadecylammonium-montmorillonite (ODA-MMT) was prepared by adding a dispersed 20.00 g of sodium montmorillonite in 800 ml of distilled water at 80°C into a solution of 13.476 g octadecylamine and 4.81 ml concentrated hydrochloric acid in 200 ml hot distilled water. The resultant suspension was vigorously stirred for 1 hour. The precipitate was repeatedly filtered and washed with hot distilled water until no chloride ion was detected with 0.1 N $AgNO_3$ solution. It was then dried at 60°C for 24 hours. The OMMT was ground with a mortar and sieved into particles of size less than 100 μm which will then used for the preparation of nanocomposites. Similar procedure was adopted to prepare dimethyldioctadecylammonium-montmorillonite (DDOA-MMT) with DDOA as intercalation agent.

2.3. Preparation of poly(butylene succinate) (PBS)/poly(butylene adipate-co-terephthalate) (PBAT)/clay nanocomposites

Nanocomposites containing a thermoplastic blend and clay were produced by melt compounding. The blend composition was kept constant (PBS 70 wt% + PBAT 30 wt%), whereas the clay content was varied between 0 and 7 wt%. PBS, PBAT and clay were manually premixed in a container and fed into Brabender at 130°C and rotor speed of 50 rpm. The residence time was maintained at 10 minutes for all the preparation. The products were then compression molded into sheets of 1 mm thickness by an electrically heated hydraulic press with a force of 1500 kN at 125°C for 10 minutes. The sample sheets were then use for further characterization.

2.4. X-ray diffraction (XRD)

X-ray diffraction measurement was carried out by using a Shimadzu XRD 600 X-ray diffractometer with CuK_α radiation ($\lambda = 1.542$ Å) operated at 30 kV and 30 mA. Data were collected within the range of scattering angles (2θ) of 2 to 10° at the rate of 2°/min. The basal spacing of the clay was derived from the peak position (d_{001} reflection) in the XRD diffractogram according to the Bragg equation ($\lambda = 2d\sin\theta$).

2.5. Fourier Transform Infrared (FTIR)

Fourier transform infrared spectra were recorded using a Spectrum BX Perkin Elmer using KBR disk method in the range of frequency 280 to 4000 cm^{-1} at 25°C. FTIR spectrum was recorded using transmission method. For each spectrum, 128 consecutive scans with 4 cm^{-1} resolution were averaged.

2.6. Tensile properties

Tensile properties test were carried out by using Instron 4302 series IX. The samples were cut into the dumbbell shape follow the ASTM D638 (type V) standard. Average thickness and average width of the gauge section of each specimen were calculated using three measurements of the thickness and width respectively. A digital micrometer, Mitutoyo (Japan) with an accuracy of 0.001 mm was used in the measurements. Load of 1.0 kN was applied at constant crosshead speed of 10 mm/min at room temperature. Tensile strength and tensile moduli were evaluated from the stress-strain data. Seven specimens were tested and the average of the values was taken.

2.7. Thermogravimetric Analysis (TGA)

Thermogravimetric analysis was performed using a Perkin Elmer TGA7. The weight of the samples used was about 10.0 mg and were heated from 35 to 600°C at the heating rate of 10°C/min. The analysis was carried out in nitrogen atmosphere with nitrogen flow rate of 20 ml/min. The weight loss of samples were recorded and plotted as the function of temperature.

2.8. Scanning Electron Microscopy (SEM)

Scanning Electron Microscopy was done using JEOL scanning microscope JSM-6400, Japan operated at 20 kV. Fracture surfaces were obtained from plain strain fracture tensile tested specimens. The fracture surfaces were sputter coated with gold. A selective dissolution of polyester in dimethylformamide (DMF) was used to distinguish phases. The sample was held in DMF for 10 minutes, removed and dried. The surface of the blend was examined for changes in its phase morphology.

2.9. Transmission Electron Microscopy (TEM)

Transmission Electron Microscopy image were obtained using a Hitachi H-700 TEM operated at an accelerating voltage of 100 kV to observe the nanoscale structures of the composites. All samples were ultrathin-sectioned using a microtome equipped with a diamond knife. The samples were collected in a trough filled with water and placed on a 200 mesh copper grid.

3. Results and discussion

3.1. Characterization of OMMT

3.1.1. Fourier Transform Infrared (FTIR)

FTIR spectra of Na-MMT and OMMT (ODA-MMT and DDOA-MMT) are illustrated in Figure 1. For the unmodified montmorillonite, Na-MMT, the presence of broad band at 3400 cm^{-1} indicates the

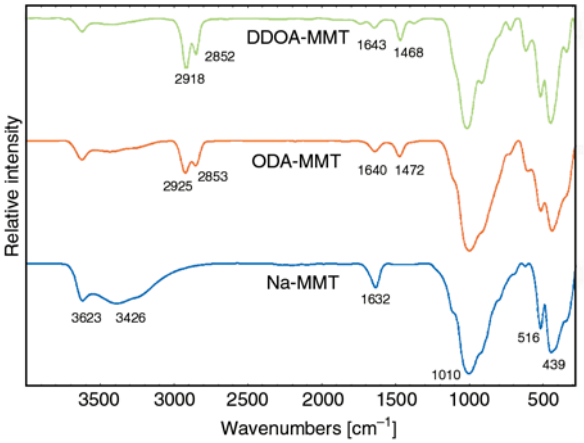

Figure 1. FTIR spectra of Na-MMT, ODA-MMT and DDOA-MMT

presence of the free water molecules vibration. This less intense band is ascribed to water hydrogen bonded to other water molecules within the interlayer of the montmorillonite. These molecules are involved with the structure of the hydration sphere of the Na^+ cation within the montmorillonite interlayer. It also shows that the hydrophilic nature of Na-MMT and water present in the Na-MMT. The infrared spectrum of Na-MMT exhibited four unique characteristic peaks which correspond to the O–H stretching (3623 cm^{-1}), Si–O stretching (1010 cm^{-1}), Al–O stretching (516 cm^{-1}) and Si–O bending (439 cm^{-1}). The OMMT presents three new peaks in the FTIR spectrum compared to Na-MMT. The Bands around 2918 and 2852 cm^{-1} are attributed to the C–H asymmetric and symmetric stretching vibrations of surfactant, respectively. The band around 1468 cm^{-1} is assigned to the CH_2 methylene (scissoring) vibration. The existence of these three new peaks in OMMT confirm the intercalation of alkylammonium ion in the interlayer spaces of montmorillonite [19]. This can further be confirmed with XRD observation.

On the other hand, the OMMT also become more organophilic as shown by the reduction in intensity of free O–H stretching peak. Furthermore, the H–O–H bending vibration of the water molecules is sensitive to the clay surface property transformation from hydrophilic to organophilic. The shifting of the H–O–H bending (1632 cm^{-1}) to a higher frequency (~1640 cm^{-1}), indicationg that H_2O is less hydrogen bonded and total sorbed water content decreases. Hydrophobic cations in organoclay will weaken the hydrogen bonding of the water. For the weaker hydrogen bond, lower energy is required for H–O–H bending vibration and thus a higher frequency of the H–O–H can be observed [20]. IR spectrum of OMMT keeps all the characteristic absorption bands of the host structure Na-MMT, it indicates that surfactants are intercalated into the silicate layer of Na-MMT. Therefore the clay was successfully modified to become OMMT.

3.1.2. X-ray diffraction analysis (XRD)

The changes of basal spacing of the resulted materials can reflect the intercalation of surfactant cation into montmorillonite interlayer spaces [21]. The natural montmorillonite, Na-MMT has 1.24 nm of basal spacing at $2\theta = 7.12°$ before it was modified with different surfactants. This basal spacing value is similar to the value obtained from the XRD measurement of previous work [22]. The values of 2θ and basal spacing of clays are summarized in Table 2. The XRD patterns for the clays are illustrated in Figure 2. After being modified by the surfactant ODA and DDOA, the basal spacing of the clay increase from 1.24 to 2.83 and 3.20 nm respectively. These indicated that the exchange cation is intercalated into the galleries of silicate layers after it is exchanged with the sodium ion. Thus montmorillonite is successfully modified by the surfactant and OMMT is formed.

Table 2. Basal spacing of Na-MMT, ODA-MMT and DDOA-MMT

Clay	Exchange cations	2θ [°]	Basal spacing [nm]
Na-MMT	Na^+	7.12	1.24
ODA-MMT	$CH_3(CH_2)_{17}NH_3^+$	3.12	2.83
DDOA-MMT	$[CH_3(CH_2)_{17}]_2N(CH_3)_2^+$	2.76	3.20

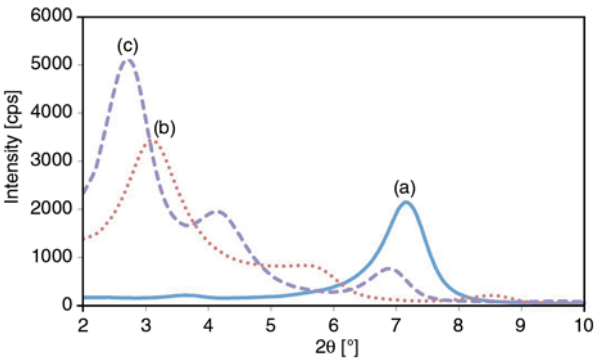

Figure 2. XRD patterns of (a) Na-MMT, (b) ODA-MMT and (c) DDOA-MMT

There are three peaks observed for DDOA-MMT. The three spacings are attributed to the arrangement of the DDOA surfactant molecule in the clay layers and the presence of unmodified clay. The peak at 2θ = 6.88° (1.28 nm) is a similar space to the Na-MMT, so this spacing is attributed to unmodified Na-MMT. The peak at 2θ = 4.14° (2.13 nm) may be due to the molecular arrangement with the surfactant molecules laying flat to the surface, and peak at2θ = 2.76° (3.20 nm) is attributed to the surfactant molecules at 90° to the surface [23].

On the other hand, ODA-MMT shows only two peaks in the XRD pattern [24]. The peak at 2θ = 3.12° (2.83 nm) corresponds to the basal spacing of ODA-MMT. Another peak at 2θ = 5.75° (1.54 nm) attributed to the arrangement of surfactant molecules parallel to the surface of clay [23].

3.2. Characterization of nanocomposites

3.2.1. X-ray diffraction analysis

The nanostructure of layered silicate nanocomposites is established using XRD analysis at low angles (2θ < 10°). Figure 3 shows the XRD pattern of Na-MMT and PBS/PBAT/Na-MMT composites at different clay loadings. Due to the hydrophilic nature of Na-MMT, it is hardly intercalated into the polymer blend. The basal spacing of composites with the clay loading of 1 and 3 wt% could not be detected, which may be due to low clay content or absence of any ordered layer structure. This lack of intergallery clay diffraction is due to the exfoliation and random distribution of the clay platelets within the polymer blend [25]. When 5 and 7 wt% of Na-MMT is added to the polymer blend, the diffraction angle of Na-MMT is shifted from 7.12° (1.24 nm) to lower angle 6.48° (1.36 nm) and 6.58° (1.34 nm) respectively. The intensity of the characteristic peak of Na-MMT was reduced significantly, but almost retains its position, indicating the formation of a conventional or phase separated composites [26]. Such structure was expected since polymer matrices have no interaction with the highly hydrophilic Na-MMT surface.

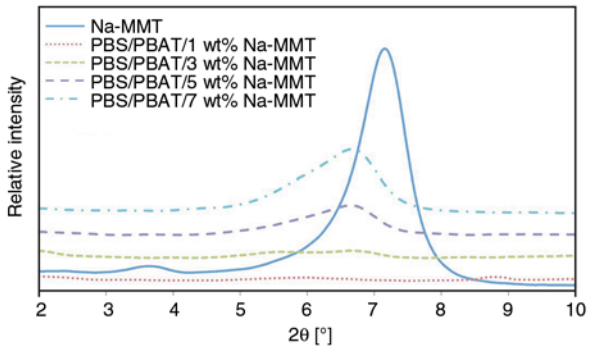

Figure 3. XRD patterns of Na-MMT and PBS/PBAT composites at different Na-MMT clay loadings

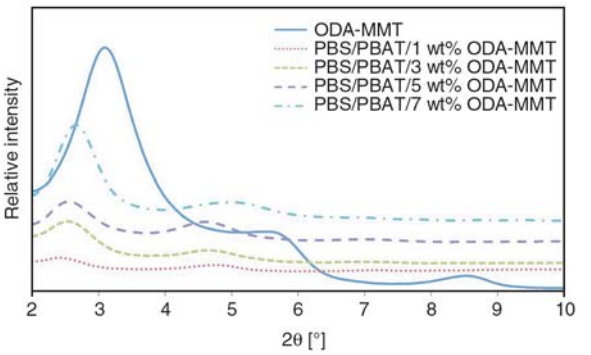

Figure 4. XRD patterns of ODA-MMT and PBS/PBAT composites at different ODA-MMT clay loadings

The intercalation of the polymer chains would increase the interlayer spacing compared with that of clay, which would shift the peak towards a lower angle. Figure 4 shows the XRD pattern of ODA-MMT and PBS/PBAT/ODA-MMT nanocomposites. ODA-MMT shows a characteristic peak at diffraction angle of 3.12° corresponding to basal spacing 2.83 nm. The increases in the basal spacing of ODA-MMT from 2.83 to 3.59, 3.45, 3.44 and 3.31 nm when 1, 3, 5 and 7 wt% of ODA-MMT respectively incorporated into PBS/PBAT, indicated that the polymer chain is successfully intercalated into the clay layers forming intercalated type nanocomposites.

Figure 5 shows the XRD pattern of DDOA-MMT and PBS/PBAT/DDOA-MMT composites. DDOA-MMT shows a sharp peak at diffraction angle of 2.76° corresponding to 3.20 nm of basal spacing.

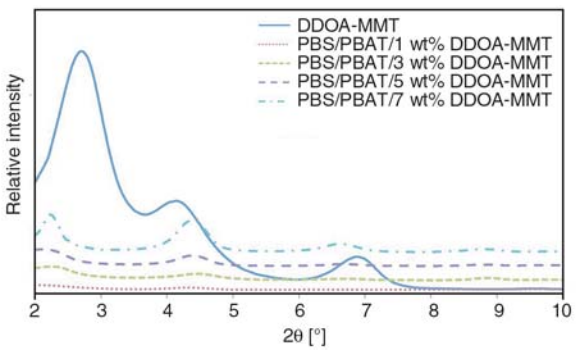

Figure 5. XRD patterns DDOA-MMT and PBS/PBAT composites at different DDOA-MMT clay loadings

Table 3. Basal spacing of PBS/PBAT composites at various clay loadings

Sample	2θ [°]	Basal spacing [nm]
Na-MMT	7.12	1.24
PBS/PBAT/1 wt% Na-MMT	–	–
PBS/PBAT/3 wt% Na-MMT	–	–
PBS/PBAT/5 wt% Na-MMT	6.48	1.36
PBS/PBAT/7 wt% Na-MMT	6.58	1.34
ODA-MMT	3.12	2.83
PBS/PBAT/1 wt% ODA-MMT	2.46	3.59
PBS/PBAT/3 wt% ODA-MMT	2.56	3.45
PBS/PBAT/5 wt% ODA-MMT	2.57	3.44
PBS/PBAT/7 wt% ODA-MMT	2.67	3.31
DDOA-MMT	2.76	3.20
PBS/PBAT/1 wt% DDOA-MMT	–	–
PBS/PBAT/3 wt% DDOA-MMT	2.31	3.81
PBS/PBAT/5 wt% DDOA-MMT	2.28	3.88
PBS/PBAT/7 wt% DDOA-MMT	2.24	3.93

The increases in the basal spacing of DDOA-MMT from 3.20 to 3.81, 3.88, and 3.93 nm when 3, 5 and 7 wt% of DDOA-MMT respectively incorporated into PBS/PBAT, indicated that the polymer chain is successfully intercalated into the clay layers. The existence of sharp peaks shows that all the composites still retain an ordered structure. For the case of PBS/PBAT/1 wt%, the characteristic peak of the original clay disappeared, indicating that the clay was fully exfoliated in the blend matrix. Thus, it could be said that it forming the exfoliated type of nanocomposite and will be confirmed by TEM. Basal spacing of all nanocomposites was summarized in Table 3.

3.2.2. Transmission Electron Microscopy (TEM)

The dispersion of layered silicates in the composites were observed by TEM as shown in the Figure 6, which presents PBS/PBAT composites with 1 wt% of (a) Na-MMT and (b) DDOA-MMT. The dark lines are the cross section of intercalated silicate layers and the bright areas are the matrix.

In PBS/PBAT/Na-MMT, the clay persists as tactoids of agglomerates throughout the polymer matrix as shown in Figure 6a. This incomplete dispersal of the reinforcing phase inhibits ideal surface contact between the polymer and clay, creating large regions of clay tactoids in the composite. This observation is in agreement with the XRD result which shows little shifting in the diffraction peak of

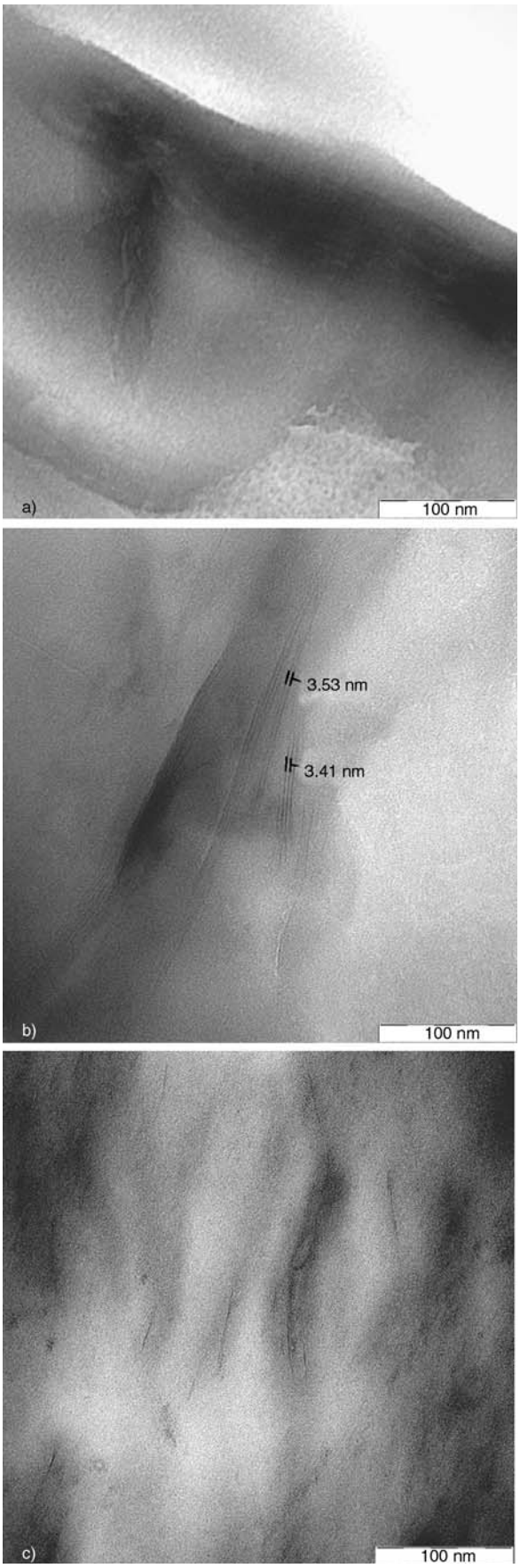

Figure 6. TEM images of PBS/PBAT composite with 1 wt% of (a) Na-MMT (b) ODA-MMT and (c) DDOA-MMT

Na-MMT for PBS/PBAT/Na-MMT composites and formed as immiscible or phase separated micro-composites. PBS/PBAT/ODA-MMT (Figure 6b) shows that the layers of clay were disordered and the PBS/PBAT matrix was intercalated into the gallery of the clay. It is consistent with the XRD result shows that a large increase in basal spacing of the clay and formed intercalated type of nano-composites.

On the other hand, TEM image of PBS/PBAT/DDOA-MMT shown in Figure 6c demonstrate single silicate layers homogenously dispersed in the polymer matrix, indicates the formation of a fully exfoliated nanocomposite. This finding shows that DDOA-MMT exhibits better dispersion of clay layers in the PBS/PBAT matrix, and is in accordance with the XRD observation shown in Figure 5, supports the formation of an exfoliated type nanocomposite. Because of that, better homogeneity and tensile properties were achieved for the PBS/PBAT/DDOA-MMT which will be proved by SEM and tensile tests.

3.2.3. Tensile roperties

The tensile properties of PBS/PBAT/Na-MMT and PBS/PBAT/OMMT composites at various contents of clays are shown in Figure 7 and Figure 8, respectively. The tensile strength of pristine PBS/PBAT blend is 21.20 MPa. Tensile strength of PBS/PBAT/Na-MMT decreased as the clay content increases. This is due to the hydrophilic nature of Na-MMT which is incompatible with the hydrophobic polymer matrix. However, the reduction could also be attributed to poor dispersion and agglomeration of Na-MMT in the blends as shown in Figure 6a.

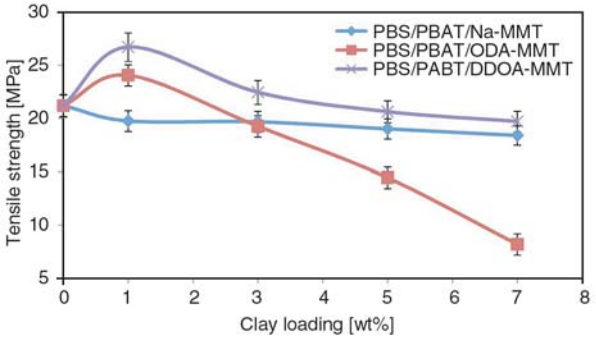

Figure 7. Tensile strength of PBS/PBAT composites

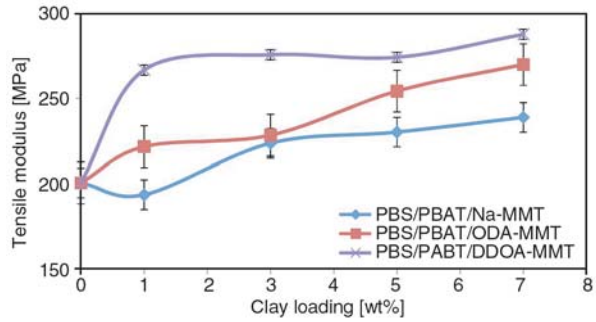

Figure 8. Tensile modulus of PBS/PBAT composites

It is clearly seen that the highest tensile strength was achieved at 1 wt% of OMMT clay loading. This suggests that OMMT acts as reinforcing filler, which increases interaction at the phase boundaries upon the addition of OMMT. Strong interphase interaction between the matrix and the dispersed phase is believed reduce the stress concentration point when tensile load is applied. The OMMT is able to act as reinforcing filler due to its high aspect ratio and platelet structure. However, when the amount of clay is above 1 wt%, only a part of the clay locates in the interfacial area, and the excess is dispersed in the matrix affecting its homogeneity and consequently the tensile strength of the blends [27, 28]. Some of the clay is present in the form tactoids, remained partially intercalated and stacked, which weakened the reinforcing effect [29]. Thus, the reinforcing effect is reduced for nanocomposites with higher clay loading owing to poor dispersion of clay and hence unable to transfer stress efficiently. When comparing the OMMT as filler for PBS/PBAT blend, it is observed that at 1 wt% clay loading the reinforcing effect of DDOA-MMT is more noticeable.

Incorporation of clay into PBS/PBAT blend also increases the tensile modulus [30]. Clay has been found to be efficient in stiffening polymers [31]. The tensile modulus of PBS/PBAT/ODA-MMT increased up to 269.9 MPa, whereas the tensile modulus of PBS/PBAT/DDOA-MMT increased up to 287.7 MPa. The increase in tensile modulus is mainly due to the high aspect ratio and rigidity of clay layers. However, the tensile modulus increase in PBS/PBAT/OMMT is higher than PBS/PBAT/Na-MMT at all clay loadings. This indicates that OMMT is more compatible with polymer blend compared to Na-MMT, and hence increase the stiffness of the nanocomposites. Once again the OMMT act as reinforcing filler better than the unmodified clay, Na-MMT. The enhancement of tensile modulus was reasonably ascribed to the

constraint of the polymer chains by their interaction with the clay surfaces [32].

3.2.4. Thermogravimetric Analysis (TGA)

Generally, introduction of clay into polymeric matrices can improve their thermal stabilities since the clay can hinder the permeability of volatile degradation products out of the materials. The dispersed clay generates a barrier which delays the release of thermal degradation products in comparison the pristine polymer [22]. Figures 9 and 10 show the TG and DTG thermograms respectively of PBS/PBAT blend and PBS/PBAT composites. The weight loss of the blend and nanocomposites due to degradation is monitored as a function of temperature. The characteristic thermal parameters selected were onset temperature, which is the initial weight loss temperature, and maximum degradation temperature, which is the highest thermal degradation rate temperature. The results are summarized in the Table 4.

The PBS/PBAT blend shows the onset temperature of 215.3°C, which increased to 223.6, 237.5 and 234.0°C when Na-MMT, ODA-MMT and DDOA-MMT clays respectively incorporated into the blend. The incorporation of clay into polymer matrix was found to enhance the thermal stability. The improved thermal stability attributed to an ablative reassembling of the silicate layers which may occur on the surface of the nanocomposites creating a physical protective barrier on the surface of the material which hinder the diffusion of volatiles and assist the formation of char after decomposition [33]. However, the OMMT gave higher thermal stability compared to the hydrophilic Na-MMT indicating better interaction between PBS/PBAT matrix and OMMT. The maximum degradation temperature (T_{max}) also increased by compounding the PBS/PBAT with OMMT.

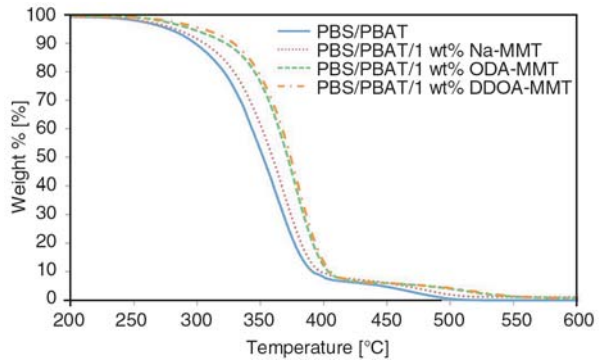

Figure 9. TG thermograms of PBS/PBAT and PBS/PBAT composites

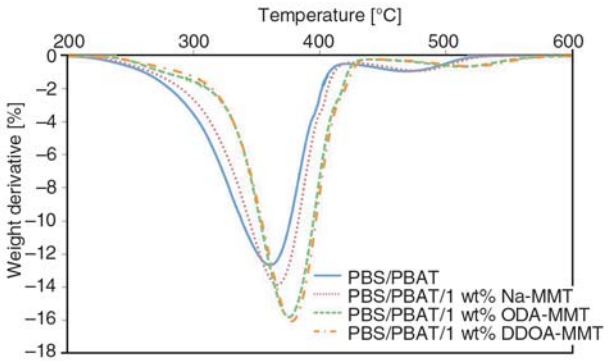

Figure 10. DTG thermograms of PBS/PBAT and PBS/PBAT composites

Table 4. TG results of PBS/PBAT and PBS/PBAT composites

Sample	Onset temperature [°C]	Maximum degradation temperature T_{max} [°C]
PBS/PBAT	215.3	360.4
PBS/PBAT/Na-MMT	223.6	366.6
PBS/PBAT/ODA-MMT	237.5	375.4
PBS/PBAT/DDOA-MMT	234.0	377.0

3.2.5. Scanning Electron Microscopy (SEM)

The fracture surface of the nanocomposites was examined by scanning electron microscope to study the morphology of the surface. Figure 11 shows SEM micrographs of fractured surface of PBS/PBAT blend and its nanocomposites at magnification of 1000×.

According to Jacob *et al.* [8], if the blend components have different melt viscosities, the morphology of the resulting blend will show the finely dispersed phase of the component with lower viscosity. Higher viscosity will lead to coarse dispersion of phases in a spherical domain. However in the case of blends containing higher concentrations of PBS, a reversal of the continuous phase was visible. Thus for PBS/PBAT blend, the PBAT with higher viscosity formed the continuous phase as shown by red arrows in the Figure 11a. This can further confirmed by etching the PBS/PBAT blend with dimethylformamide (DMF). PBS is soluble in DMF, while PBAT is insoluble. The DMF was used to dissolve the soluble phase. Figure 12 represents the micrograph of the PBS/PBAT blend after

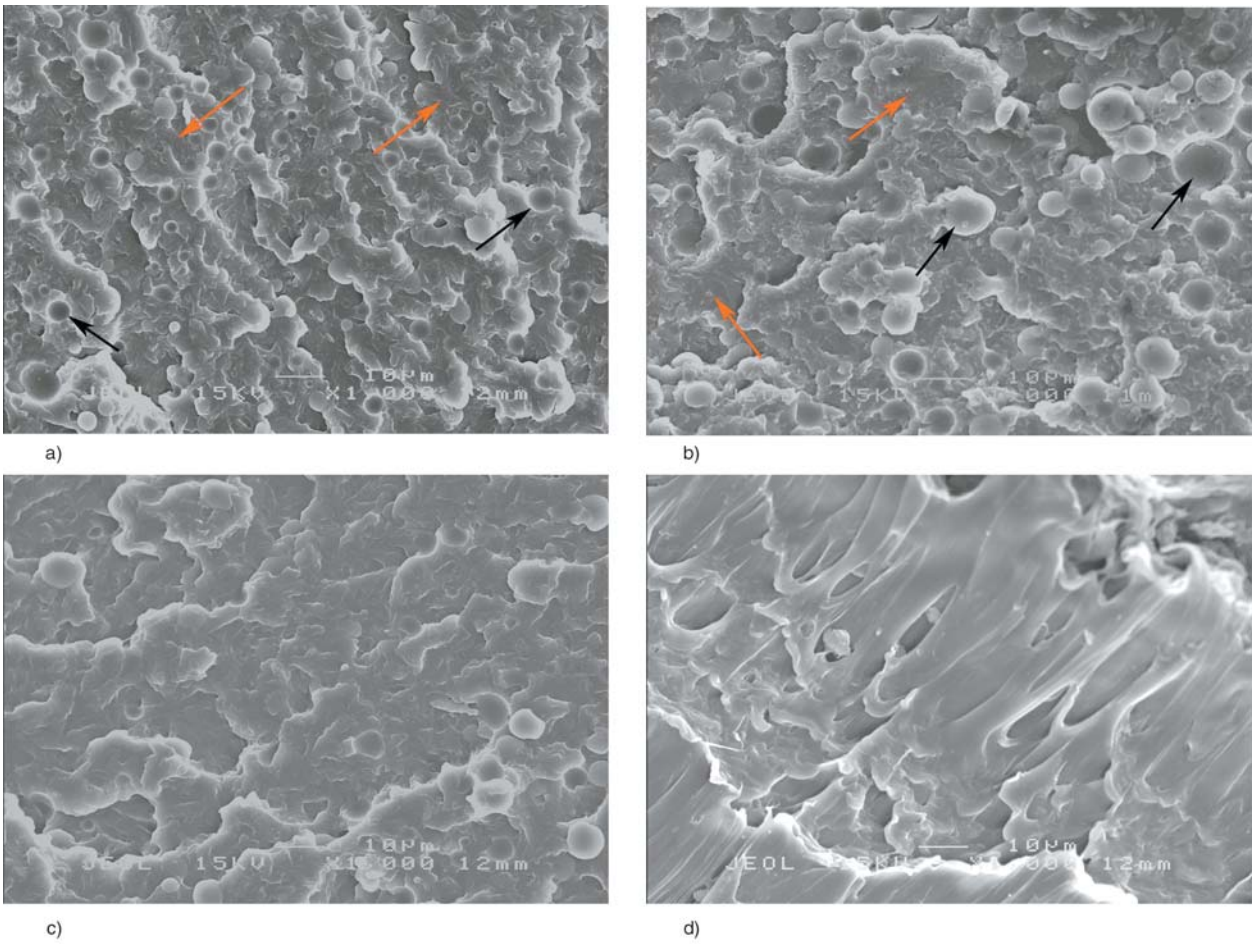

Figure 11. SEM images of (a) PBS/PBAT, and PBS/PBAT composite with 1 wt% of (b) Na-MMT, (c) ODA-MMT and (d) DDOA-MMT

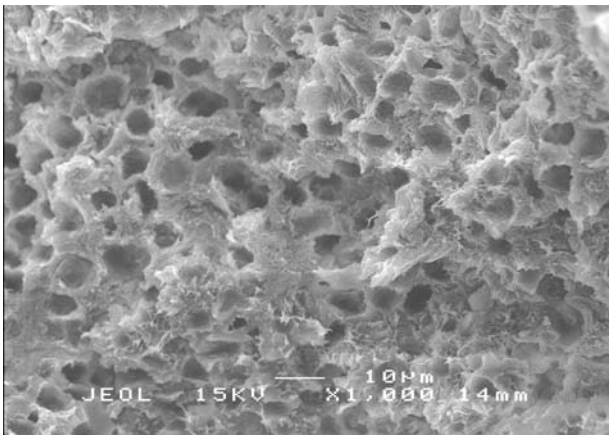

Figure 12. SEM micrograph of PBS/PBAT blend after etching with DMF

etching with DMF. The micrograph clearly showed that the PBS phase dissolved in the DMF and PBAT phase stayed intact during the etching process. However, PBS/PBAT nanocomposites dissolved in DMF solvent during the same etching process. This means that the PBS/PBAT blend was a miscible blend after incorporation of OMMT. This finding reveals that OMMT can improve the miscibility of the blend.

When OMMT was incorporated into PBS/PBAT, there is a reduction of the domain size of the dispersed phase (PBS) as shown by black arrows which is related to a reduction of the coalescence rate of the dispersed phase and a compatibilizing effect of the OMMT at the interface between the two phases as shown in Figure 11c and 11d. Conversely, there often appears to be an increase in the dispersed phase domain size when OMMT is located in the dispersed phase [9, 34]. So, the OMMT is located in the PBAT continuous phase in this PBS/PBAT blend system. According to Martins *et al*. [35], when the OMMT platelets are located in the continuous phase instead of the dispersed phase would lead to higher stiffness and this is in agreement with the tensile modulus results.

Some small void could be observed in PBS/PBAT/Na-MMT (Figure 11b) compared to pristine PBS/PBAT which indicates that the incompatibility of

Na-MMT with the PBS/PBAT matrix. The presence of OMMT influences the morphological structural changes of the blend. As shown in Figure 11c and 11d, the PBS/PBAT phases have affinities to make nanolevel incorporation with OMMT. It indicates a good degree of mixing between the polymer phases with addition of OMMT, since this composite totally dissolved in DMF after addition of OMMT. As a result, the nanocomposite showed more homogeneous and single phase morphology compared to unmodified clay. In other word, the OMMT induces miscibility between PBS and PBAT.

4. Conclusions

OMMTs were successfully prepared from Na-MMT via cation exchange method by using octadecylammonium and dimethyldioctadecylammonium cation as surfactant. Intercalated and exfoliated types of PBS/PBAT/OMMT nanocomposites were successfully prepared by melt blending as proven by XRD and TEM. The tensile strength of PBS/PBAT/OMMT nanocomposites was improved by reinforcing effects of OMMT and gives the maximum value at 1 wt% OMMT loading. Thermal stability was enhanced by incorporation of clay into PBS/ PBAT matrices, particularly OMMT. SEM micrographs showed that presence of OMMT in the PBS/PBAT blend improved the morphology of the compound. SEM micrographs also supported the finding of compatibility for the PBS/PBAT blend with OMMT through the homogeneous distribution which gives an improvement in mechanical properties.

References

[1] Fujimaki T.: Processability and properties of aliphatic polyesters, 'BIONOLLE', synthesized by polycondensation reaction. Polymer Degradation and Stability, **59**, 209–214 (1998).
DOI: 10.1016/S0141-3910(97)00220-6

[2] Shih Y., Wang T., Jeng R., Wu J., Teng C.: Biodegradable nanocomposites based on poly(butylene succinate)/organoclay. Journal of Polymers and the Environment, **15**, 151–158 (2007).
DOI: 10.1007/s10924-007-0055-6

[3] Chen G-X., Kim H-S., Kim E-S., Yoon J-S.: Compatibilization-like effect of reactive organoclay on the poly(l-lactide)/poly(butylene succinate) blends. Polymer, **46**, 11829–11836 (2005).
DOI: 10.1016/j.polymer.2005.10.056

[4] Okamoto K., Ray S. S., Okamoto M.: New poly(butylene succinate)/layered silicate nanocomposites. II. Effect of organically modified layered silicates on structure, properties, melt rheology, and biodegradability. Journal of Polymer Science Part B: Polymer Physics, **41**, 3160–3172 (2003).
DOI: 10.1002/polb.10708

[5] Chen G-X., Kim E-S., Yoon J-S.: Poly(butylene succinate)/twice functionalized organoclay nanocomposites: Preparation, characterization, and properties. Journal of Applied Polymer Science, **98**, 1727–1732 (2005).
DOI: 10.1002/app.22264

[6] Someya Y., Nakazato T., Teramoto N., Shibata M.: Thermal and mechanical properties of poly(butylene succinate) nanocomposites with various organo-modified montmorillonites. Journal of Applied Polymer Science, **91**, 1463–1475 (2004).
DOI: 10.1002/app.13366

[7] Yu L., Dean K., Li L.: Polymer blends and composites from renewable resources. Progress in Polymer Science, **31**, 576–602 (2006).
DOI: 10.1016/j.progpolymsci.2006.03.002

[8] Jacob J., Ramaswamy M., Mrinal B.: Evaluation of compatibility and properties of biodegradable polyester blends. Journal of Polymer Science Part A: Polymer Chemistry, **40**, 2003–2014 (2002).
DOI: 10.1002/pola.10297

[9] Khatua B. B., Lee D. J., Kim H. Y., Kim J. K.: Effect of organoclay platelets on morphology of nylon-6 and poly(ethylene-ran-propylene) rubber blends. Macromolecules, **37**, 2454–2459 (2004).
DOI: 10.1021/ma0352072

[10] Voulgaris D., Petridis D.: Emulsifying effect of dimethyldioctadecylammonium-hectorite in polystyrene/poly(ethyl methacrylate) blends. Polymer, **43**, 2213–2218 (2002).
DOI: 10.1016/S0032-3861(02)00039-3

[11] Sinha Ray S., Pouliot S., Bousmina M., Utracki L. A.: Role of organically modified layered silicate as an active interfacial modifier in immiscible polystyrene/polypropylene blends. Polymer, **45**, 8403–8413 (2004).
DOI: 10.1016/j.polymer.2004.10.009

[12] Si M., Araki T., Ade H., Kilcoyne A. L. D., Fisher R., Sokolov J. C., Rafailovich M. H.: Compatibilizing bulk polymer blends by using organoclays. Macromolecules, **39**, 4793–4801 (2006).
DOI: 10.1021/ma060125+

[13] Hong J. S., Namkung H., Ahn K. H., Lee S. J., Kim C.: The role of organically modified layered silicate in the breakup and coalescence of droplets in PBT/PE blends. Polymer, **47**, 3967–3975 (2006).
DOI: 10.1016/j.polymer.2006.03.077

[14] Su Q., Feng M., Zhang S., Jiang J., Yang M.: Melt blending of polypropylene-*blend*- polyamide 6-*blend*-organoclay systems. Polymer International, **56**, 50–56 (2007).
DOI: 10.1002/pi.2109

[15] Gelfer M. Y., Song H. H., Liu L., Hsiao B. S., Chu B., Rafailovich M., Si M., Zaitsev V.: Effects of organoclays on morphology and thermal and rheological properties of polystyrene and poly(methyl methacrylate) blends. Journal of Polymer Science Part B: Polymer Physics, **41**, 44–54 (2003).
DOI: 10.1002/polb.10360

[16] Sinha Ray S., Okamoto M.: Polymer/layered silicate nanocomposites: A review from preparation to processing. Progress in Polymer Science, **28**, 1539–1641 (2003).
DOI: 10.1016/j.progpolymsci.2003.08.002

[17] Giannelis E. P.: Polymer layered silicate nanocomposites. Advanced Materials, **8**, 29–35 (1996).
DOI: 10.1002/adma.19960080104

[18] Sharif J., Wan Yunus W. M. Z., Khairul Z. H. M. D., Mansor H. A.: Preparation and properties of radiation crosslinked natural rubber/clay nanocomposites. Polymer Testing, **24**, 211–217 (2005).
DOI: 10.1016/j.polymertesting.2004.08.008

[19] Bala P., Samantaraya B. K., Srivastava S. K.: Synthesis and characterization of Na-montmorillonite-alkylammonium intercalation compounds. Materials Research Bulletin, **35**, 1717–1724 (2000).
DOI: 10.1016/S0025-5408(00)00368-8

[20] Xue W., He H., Zhu J., Yuan P.: FTIR investigation of CTAB-Al-montmorillonite complexes. Spectrochimica Acta Part A: Molecular and Biomolecular Spectroscopy, **67**, 1030–1036 (2007).
DOI: 10.1016/j.saa.2006.09.024

[21] Xi Y., Frost R. L., He H.: Modification of the surfaces of Wyoming montmorillonite by the cationic surfactants alkyl trimethyl, dialkyl dimethyl, and trialkyl methyl ammonium bromides. Journal of Colloid and Interface Science, **305**, 150–158 (2007).
DOI: 10.1016/j.jcis.2006.09.033

[22] Agag T., Koga T., Takeichi T.: Studies on thermal and mechanical properties of polyimide-clay nanocomposites. Polymer, **42**, 3399–3408 (2001).
DOI: 10.1016/S0032-3861(00)00824-7

[23] Zhou Q., Frost R. L., He H., Xi Y., Zbik M.: TEM, XRD, and thermal stability of adsorbed paranitrophenol on DDOAB organoclay. Journal of Colloid and Interface Science, **311**, 24–37 (2007).
DOI: 10.1016/j.jcis.2007.02.039

[24] Someya Y., Sugahara Y., Shibata M.: Nanocomposites based on poly(butylene adipate-co-terephthalate) and montmorillonite. Journal of Applied Polymer Science, **95**, 386–392 (2005).
DOI: 10.1002/app.21333

[25] Wu Z., Zhou C., Qi R., Zhang H.: Synthesis and characterization of nylon 1012/clay nanocomposite. Journal of Applied Polymer Science, **83**, 2403–2410 (2002).
DOI: 10.1002/app.10198

[26] Paul D. R., Robeson L. M.: Polymer nanotechnology: Nanocomposites. Polymer, **49**, 3187–3204 (2008).
DOI: 10.1016/j.polymer.2008.04.017

[27] Sathe S. N., Devi S., Srinivasa Rao G. S., Rao K. V.: Relationship between morphology and mechanical properties of binary and compatibilized ternary blends of polypropylene and nylon 6. Journal of Applied Polymer Science, **61**, 97–107 (1996).
DOI: 10.1002/(SICI)1097-4628(19960705)61:1<97::AID-APP11>3.0.CO;2-X

[28] Sathe S. N., Srinivasa Rao G. S., Rao K. V., Devi S.: The effect of composition on morphological, thermal, and mechanical properties of polypropylene/nylon-6/polypropylene-g-butyl acrylate blends. Polymer Engineering and Science, **36**, 2443–2450 (1996).
DOI: 10.1002/pen.10642

[29] Ferrigno T. H.: Principles of filler selection and use. in 'Handbooks of fillers for plastic' (eds.: H. S. Kartz, J. V. Milewski) Van Nostrand Reinhold, New York, 6–81 (1987).

[30] Reichert P., Nitz H., Klinke S., Brandsch R., Thomann R., Mühaupt R.: Poly(propylene)/organoclay nanocomposite formation: Influence of compatibilizer functionality and organoclay modification. Macromolecular Materials and Engineering, **275**, 8–17 (2000).
DOI: 10.1002/(SICI)1439-2054(20000201)275:1<8::AID-MAME8>3.0.CO;2-6

[31] Wang J., Pyrz R.: Prediction of the overall moduli of layered silicate-reinforced nanocomposites- Part I: Basic theory and formulas. Composites Science and Technology, **64**, 925–934 (2004).
DOI: 10.1016/S0266-3538(03)00024-1

[32] Shelley J. S., Mather P. T., DeVries K. L.: Reinforcement and environmental degradation of nylon-6/clay nanocomposites. Polymer, **42**, 5849–5858 (2001).
DOI: 10.1016/S0032-3861(00)00900-9

[33] Gilman J. W., Jackson C. L., Morgan A. B., Harris R., Manias E., Giannelis E. P., Wuthenow M., Hilton D., Phillips S. H.: Flammability properties of polymer-layered-silicate nanocomposites. Polypropylene and polystyrene nanocomposites. Chemistry of Materials, **12**, 1866–1873 (2000).
DOI: 10.1021/cm0001760

[34] Kontopoulou M., Liu Y., Austin J. R., Parent J. S.: The dynamics of montmorillonite clay dispersion and morphology development in immiscible ethylene-propylene rubber/polypropylene blends. Polymer, **48**, 4520–4528 (2007).
DOI: 10.1016/j.polymer.2007.05.068

[35] Martins C. G., Larocca N. M., Paul D. R., Pessan L. A.: Nanocomposites formed from polypropylene/EVA blends. Polymer, **50**, 1743–1754 (2009).
DOI: 10.1016/j.polymer.2009.01.059

eXPRESS Polymer Letters Vol.4, No.7 (2010) 415–422
Available online at www.expresspolymlett.com
DOI: 10.3144/expresspolymlett.2010.52

Synthesis and characterizations of degradable aliphatic-aromatic copolyesters from lactic acid, dimethyl terephthalate and diol: Effects of diol type and monomer feed ratio

M. Namkajorn[1], *A. Petchsuk*[2], *M. Opaprakasit*[3], *P. Opaprakasit*[1*]

[1]School of Bio-Chemical Engineering and Technology, Sirindhorn International Institute of Technology (SIIT), Thammasat University, Pathum Thani 12121, Thailand
[2]National Metal and Materials Technology Center (MTEC), Pathum Thani 12120, Thailand
[3]Department of Materials Science, Chulalongkorn University, Bangkok 10330, Thailand

Received 17 February 2010; accepted in revised form 29 April 2010

Abstract. Lactic acid-based aliphatic/aromatic copolyesters are synthesized to incorporate the degradability of polylactic acid and good mechanical properties of aromatic species by using polycondensation of lactic acid (LA), dimethyl terephthalate (DMT), and various diols. Effects of diol lengths and comonomer feed ratios on structure and properties of the resulting copolymers are investigated. Three types of diols with different methylene lengths are employed, i.e., ethylene glycol (EG), 1,3-propanediol (PD) and 1,4-butanediol (BD). LA/DMT/diol feed ratios of 2:1:2, 1:1:2, and 1:2:4 are used in each diol system. It is found that types of the diols play an important role in the properties of the copolyester, where an increase in diol length results in an increase in the copolymers molecular weight, and a decrease in T_g, T_m and crystallinity, when a constant monomer feed ratio is employed. Monomer feed ratio also has a significant effect on properties of the copolymers, where an increase in the aromatic content leads to formation of copolymers with higher molecular weight, longer aromatic block sequence and high aromatic to aliphatic ratio in the chain structure. These, in turn, lead to an increase in T_g, T_m, crystallinity and thermal stability of the copolymer samples, and a reduction in their solubility.

Keywords: *polymer synthesis, lactic acid, aliphatic/aromatic copolyesters, degradable, diol*

1. Introduction

Degradable polymers have recently become highly attractive materials in solving the increasingly serious environmental problems due to plastic waste. Current mass-produced petroleum-based polymers are highly resistant to degradation, for example, polyethylene terephthalate (PET), a thermoplastic aromatic polyester that is widely used in the manufacturing of soft-drink bottles. Recycling has been practiced and promoted to reduce the production rate of new polymers. However, this is difficult or inexpedient due to technical and economic considerations. One of the promising solutions to this plastic waste problem is to replace conventional plastics in mass use by degradable polymers. Within the new group of degradable polymers, various types of aliphatic polyesters play a major role with respect to industrial relevance [1].

Despite their superior degradability, aliphatic polyesters have some disadvantages in weaker mechanical properties, compared to their aromatic counterparts. Physical and mechanical properties of aliphatic polyesters, however, can be slightly modified by varying their molecular weight or crys-

*Corresponding author, e-mail: pakorn@siit.tu.ac.th

tallinity. Incorporation of other groups such as aromatic esters has also proven to provide the materials with a wider range of properties. In contrast, non-degradable aromatic polyesters, such as PET exhibit much better physical and mechanical properties [2]. Recently, incorporation of aliphatic units into aromatic polyesters has been employed in improving the degradability of PET [3–8], poly (propylene terephthalate) (PPT) [3–10], poly(butylene terephthalate) (PBT) [8, 11–12], and poly(1,2-propanediyl phthalate) (PPP) [13].

Polylactic acid (PLA) is one of the widely used aliphatic polyesters, due to its environmentally-friendly properties. Its monomer, lactic acid, is derived from agricultural products, such as starch or sugar. In addition, PLA is proven as a biocompatible material with appreciable mechanical properties comparable to other commodity plastics. However, its low toughness has limited its use in certain applications. In order to improve the mechanical properties of PLA and retain its advantages of degradability, a copolymerization of lactic acid and other aromatic esters has been conducted. Olewnik *et al*. reported a synthesis and characterization of copolyester from lactic acid and bis(2-hydroxyethyl terephthalate) [14, 15]. In our previous work, lactic acid-based aliphatic/aromatic copolyester was synthesized from dimethyl terephthalate (DMT), lactic acid and ethylene glycol. The copolymer's chemical structure and properties were characterized [16].

In this study, aliphatic/aromatic copolyesters are systematically synthesized from lactic acid (LA), dimethyl terephthalate (DMT), and diols with various methylene lengths. Effects of diols and comonomer feed ratios on structure and properties of the resulting copolymers are investigated. Depending on their chain microstructure and properties, the resulting materials are suitable for a wide range of applications.

2. Experimental

2.1. Materials

Lactic acid (LA) (88 wt% aqueous solution) and 3 types of diols: ethylene glycol (EG), 1,3-propanediol (PD) and 1,4-butanediol (BD), were purchased from Carlo Erba (Rodano, Italy) and Acros Organics (Part of Thermo Fischer Scientific, Waltham, MA, USA). Dimethyl terephthalate (DMT) was supplied by Acros. Tin(II) octoate catalyst was provided by Wako Chemicals (Dalton, GA, USA). All chemicals were used without further purification.

2.2. Synthesis

The synthesis procedure of the PLA-based aliphatic/aromatic copolyesters is summarized in Figure 1. The copolymers were polymerized by a polycondensation of LA, DMT, and diols. Three types of diols with different methylene length were employed, i.e. EG, PD and BD. In each synthesis system with specific diol, LA/DMT/diol monomer feed ratios of 2:1:2, 1:1:2 and 1:2:4 were employed. The corresponding copolymers are then coded by the name of diol and the appropriated feed ratio, for example, EG212 refers to a copolymer synthesized from EG diol with a feed ratio of 2:1:2. The synthesis procedure is adopted from our previous work [16]. Essentially, the copolymers were polymerized in a 2-neck round bottom flask under N_2 atmosphere at 0.2 mbar. Appropriate amounts of DMT and LA were mixed and stirred at 150°C for 1 hour. The mixture was then heated to 200°C, followed by an addition of half of the corresponding amount of an appropriate diol using a needle injection under N_2 atmosphere. The reaction temperature was held at 200°C for 2 hours, and then raised to 220°C for 1 hour. Next, the remaining excess amount of diol was added and the reaction was further heated for 1 hour. Small-molecular byproducts were finally removed by condensation using a vacuum pump at 220°C until the total reaction time reached 7 hours. The resulting copolymers were stored in a desiccator for further characterizations.

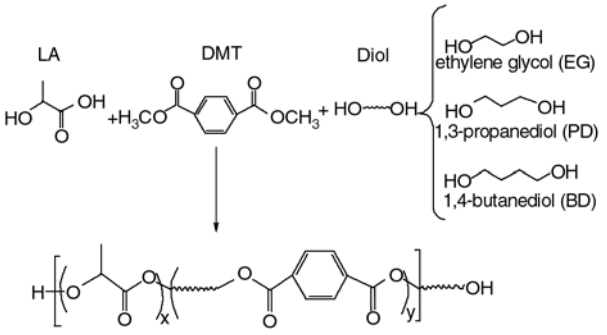

Figure 1. Summary of the synthesis reaction of aliphatic/aromatic copolyesters

2.3. Characterizations

2.3.1. ^{1}H NMR spectroscopy

^{1}H NMR spectra were recorded on a Bruker AC300 spectrometer by using 7% wt trifluoroacetic acid/$CDCl_3$ mixed solvent. The spectrum was recorded immediately in order to avoid end-group esterification by trifluoroacetic acid [17].

2.3.2. Differential Scanning Calorimetry (DSC)

DSC analyses were carried out under nitrogen on a DSC 2920 Modulated TA Instruments apparatus equipped with liquid nitrogen cooling accessory, at cooling and heating rates of 20°C/min from 0 to 240°C with a sample size of 3–5 mg. Glass transition temperatures (T_g) and melting temperatures (T_m) were measured on the second cycle heating curves.

2.3.3. Thermo Gravimetric Analysis (TGA)

TGA analyses were carried out under nitrogen on a Mettler Toledo Stare System at a heating rate of 20°C/min from 50 to 1000°C using samples of approximately 2.5 mg.

2.3.4. Fourier-Transform Infrared (FTIR) spectroscopy

FTIR spectra were recorded in transmission mode on a Thermo Nicolet 6700 model spectrometer. 16 scans were coadded, with a resolution of 2 cm^{-1}. The copolymer sample in form of KBr pellet was prepared by mixing with KBr powder.

2.3.5. Solubility test

Solubility of the copolymer samples was examined in dichloromethane (CH_2Cl_2) and tetrahydrofuran (THF) at ambient conditions. Essentially, 0.5 g of sample was dissolved in 10 ml of solvent, and vigorously stirred for 1 hour. The dissoluble portion was then separated from the solution, and its dried weight was recorded. Solubility was calculated on a weight basis.

3. Results and discussion

Chemical structure and properties of the resulting copolyesters synthesized from different diols and monomer feed ratios are characterized. Possible sequential structures of the copolymers are summarized in Figure 2. ^{1}H NMR spectra of copolymers derived from the three diol systems at a 2:1:2 monomer feed ratio, and their signal assignments are shown in Figures 3–5. Band assignments of the copolymer derived from EG are similar to those described earlier [14, 16]. ^{1}H NMR spectra of the corresponding copolymers synthesized from PD and BD show additional resonances associated with methylene units of diols. Nevertheless, other signals necessary for use in the determination of chain microstructure are similar to those of the EG derived copolyester. The actual terephthalate/lactate (T/L) molar ratios in the chain structure are calculated from the integrations of aromatic proton signals at 8.1 ppm and lactate methines (–$CH(CH_3)$–) located in the 5.2–5.5 ppm region [16]. Molecular weight (M_n), sequential length ($Y_{(L)}$, $X_{(ET)}$), and the degree of randomness of the aromatic/aliphatic

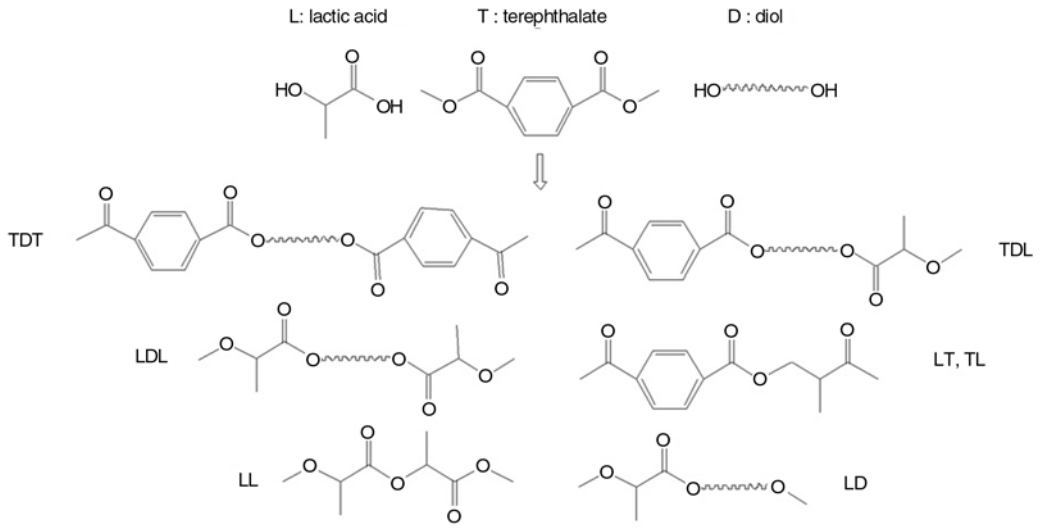

Figure 2. Possible D-centered triads and diads of the resulting copolyesters

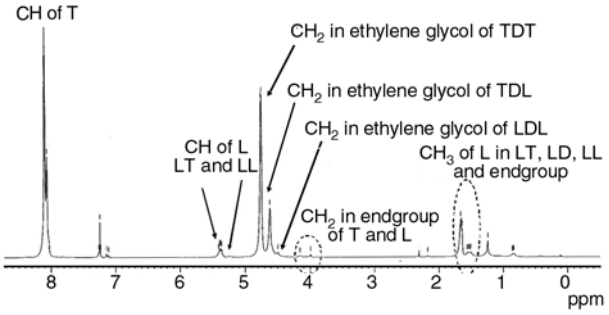

Figure 3. [1]H NMR spectrum and signal assignments of EG112

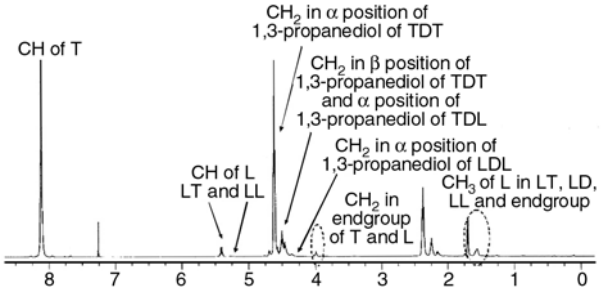

Figure 4. [1]H NMR spectrum and signal assignments of PD112

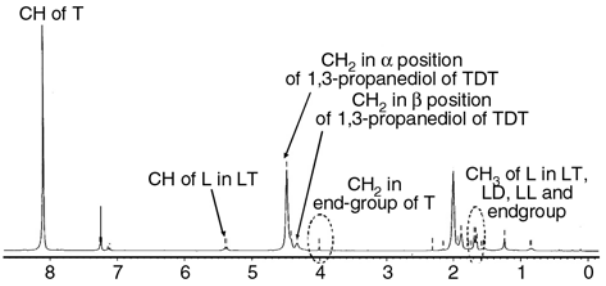

Figure 5. [1]H NMR spectrum and signal assignments of BD112

blocks (B) are also calculated from [1]H NMR spectra by employing the methodology described elsewhere [14–16,18–20]. Results on chemical structure of the as-synthesized copolyesters are summarized in Table 1, where solubility and thermal properties results are also shown.

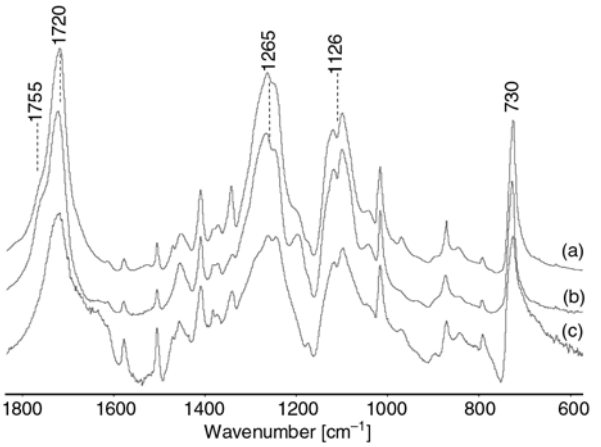

Figure 6. FTIR spectra of copolymers derived from LA/DMT/EG with various monomer feed ratios: 2:1:2 (a), 1:1:2 (b), 1:2:4 (c)

FTIR spectra of copolymers derived from EG at different monomer feed ratios are compared in Figure 6. Band characteristics of aromatic esters are observed at 1720 cm^{-1} (C=O stretching) and 730 cm^{-1} (ring C–H out of plane bending), while the unique C=O stretching band of aliphatic units is located at 1755 cm^{-1}. Strong vibrational modes observed at 1265 and 1126 cm^{-1} are associated with C–O–C asymmetric stretching modes of both aromatic and aliphatic esters. Given these band assignments, aliphatic/aromatic ratios in the copolymer chain structure can be determined from band intensity of the two corresponding C=O stretching modes. It is clearly seen that the band intensity ratio is strongly dependent on the monomer feed ratios, reflecting an incorporation of different aromatic/aliphatic ratio in the copolymer chains. This is in good agreement with those observed earlier from NMR results. Additionally, FTIR spectra of copolymers synthesized from other diols (not shown) also exhibit similar characteristics.

Table 1. Results on chain microstructure, thermal properties, and solubility of the copolyesters

Copolymers	M_n[a] [g/mol]	Sequential length[a]		T/L ratio[a]	B[a]	Transition temperatures		Solubility [%]	
		$Y_{(L)}$	$X_{(DT)}$			T_g [°C]	T_m [°C] (ΔH [J/g])	THF	CH_2Cl_2
EG212	5 200	2.43	0.47	1.7	2.75	44	–	97.6	95.6
EG112	7 200	1.21	3.49	3.3	4.39	58	199 (28)	15.3	44.1
EG124	21 000	1.03	7.98	5.6	6.74	76	218 (30)	0.4	11.2
PD212	3 000	1.72	2.86	1.4	2.34	20	136 (18)	83.7	88.7
PD112	10 200	1.18	4.24	6.1	7.26	29	198 (43)	5.6	14.2
PD124	11 700	1.05	8.96	13.2	14.41	31	214 (53)	0.2	4.3
BD212	8 100	1.63	2.74	1.6	2.59	32	134 (18)	72.8	86.3
BD112	25 200	1.25	9.08	5.2	5.87	26	191 (37)	1.4	10.0
BD124	35 000	1.11	18.08	15.6	15.80	31	210 (42)	1.0	1.3

[a] Calculated from [1]H NMR spectra

3.1. Effects of diols

Effects of diols on properties of the copolymers are examined by comparing properties of copolymers derived from the same monomer feed ratio but different diols. The characterization results, as summarized in Table 1, indicate that copolymers synthesized from all three diols show significantly similar length of lactate sequence ($Y_{(L)}$). Interestingly, the application of diols with longer methylene length in its molecule results in formation of copolymers with higher molecular weight and longer diol-terephthalate block sequence ($X_{(DT)}$). This reflects that the nature of diols does not significantly affect the formation of lactate-lactate (L-L) connections, but plays an important role in the incorporation of D and T units in the chain structure. This is probably because the longer methylene sequence in bigger size diols provides optimum flexibility and reactivity for their hydroxyl groups to react with acid functional groups of T, resulting in higher extent of polycondensation reaction and hence production of higher MW copolymers. The preference of aromatic-aromatic linkage formation through longer-length diols (T-D-T), compared to that of L-L connection, also results in the production of copolymers with higher T/L ratios and longer T block length in the chain structure, which is reflected by higher degree of deviation from unity of the degree of randomness value (B).

Effects of diols on thermal properties of the copolymers are also summarized in Table 1. Copolymers derived from different diols exhibit glass transition temperature (T_g) at temperatures ranging from 20 to 76°C. When the same monomer feed ratio is employed, a decrease in T_g values is observed in copolymers derived from EG, PD, and BD diols. This is largely due to an increase in their corresponding methylene length, which results in an increase in main chain flexibility of the copolymer structure. It should be noted that the effect of molecular weight on T_g is negligible in this comparison, as copolymers derived from the same comonomer feed ratio have comparable molecular weight. The corresponding results also indicate a decreasing trend of T_m as a function of increasing diol's length, but with lower degree of T_m reduction. This is also due to a variation of chain flexibility inherited from diol's methylene length. Surprisingly, it is observed that T/L ratio does not significantly affect T_m of the copolymer, when different diols are employed with a constant feed ratio.

Thermal stability of the copolymers is also examined. TGA thermograms and their 1st derivative traces (DTGA) of copolymers synthesized from different diols with a 1:1:2 feed ratio are shown in Figure 7. The results show that PD112 and BD112 have significantly comparable degradation temperature (T_d) at 415°C. EG112, however, shows better thermal stability with a main degradation step taking place at 450°C. The EG112 copolymer also has higher remaining mass at a temperature higher than 450°C, compared to PD112 and BD112. These are probably due to aromatic fractions containing T-D-T sequences, where T-EG-T is more stable than those of T-PD-T or T-BD-T as a result from the less flexibility of EG segments. In addition, a separate degradation step associated with aliphatic L-L sequences is clearly observed at 380°C in DTGA traces of EG112, while those of PD112 and BD112 are enveloped in the main degradation step of aromatic constituent.

Results from solubility testing indicate that all copolymers have higher solubility in CH_2Cl_2, compared to that in THF, reflecting a closer match of the solvent and copolymer solubility parameters. It is clearly observed that copolymers with lower T content in the chain structure exhibit higher solubility in both solvents, due to the hydrophobicity of TD units in the chain compared to that of the

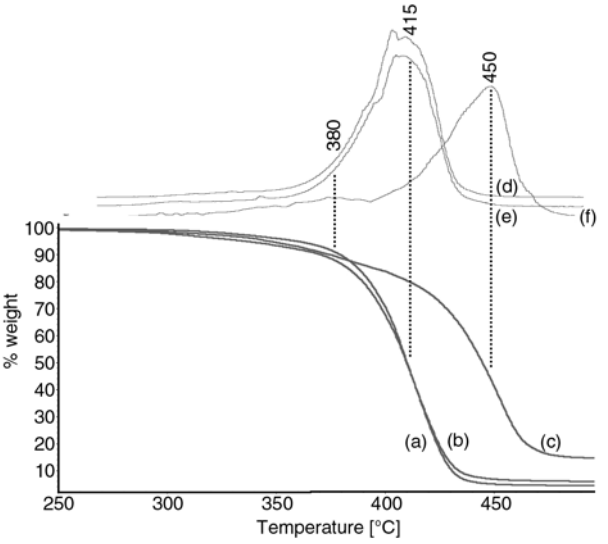

Figure 7. TGA thermograms of copolymers synthesized from different diols with a 1:1:2 feed ratio: BD (a), PD (b), EG (c), and their corresponding DTGA traces: BD (d), PD (e), EG (f)

L sequence. It should also be noted that shorter chain length may also result in the higher solubility of the samples.

3.2. Effects of monomer feed ratios

Results on properties of the copolyesters also indicate that the degree of polymerization and chain microstructure of the copolymer are strongly dependent on the monomer feed ratios, where higher molar mass polymers are produced when a feed ratio with higher aromatic content is employed. This is probably due to the relatively higher reactivity of –OH functional and carboxyl groups from diols and DMT, to undergo transesterification, compared to that of the corresponding groups present in lactic acid monomers. It is noted that the feed content of diol is kept at 2 equivalent moles with respect to that of the aromatic content, as it was observed in our early work that an excess amount of diol was required to compensate for diol loss during a vacuum condensation process [16]. The results also suggest that a decrease in sequential length of lactate, $Y_{(L)}$, and an increase in that of its aromatic sequence counterpart, $X_{(DT)}$, in the copolymer chain is observed upon increasing of aromatic content in feed. This is in concert with an increase in the degree of randomness (B), indicating higher block characteristics. The increase in aromatic block length consequently results in an increase in the T/L ratios in the copolymer chain upon increasing the aromatic content in feed.

Effect of the monomers feed ratios on thermal properties of the copolymers is also examined. It is observed that all samples exhibit melting characteristics, reflecting that these copolymers are semicrystalline in nature, except that derived from EG at a feed ratio of 2:1:2. The absence of a T_m peak in this sample is partly due to its low molecular weight and its shorter aromatic sequence than the aliphatic sequential units in the chain structure, i.e. $X_{(DT)}$ and $Y_{(L)}$ of 0.47 and 2.43 (see Table 1). The relatively longer aromatic sequence is therefore essential for the copolymers to exhibit crystalline behavior. As expected, the results indicate that copolymers synthesized from a 1:2:4 feed ratio show the highest T_m, and T_g values. In addition, an increase in T_g, T_m and crystallinity (calculated from ΔH) with an increase in aromatic content in monomer feed ratio is observed. This is partly due to the higher aromatic content in the chain and the longer aromatic block length, and the higher molecular weight of the copolymers.

TGA and DTGA traces of copolymers synthesized from PD with different feed ratios are shown in Figure 8. Thermal degradation of 'short' aliphatic L-L sequences, i.e. L-L units located next to T units, in all 3 samples is observed at 380°C. PD212, however, shows another separate degradation mechanism at 305°C with approximately 25% wt loss, which is higher than the mass loss of aliphatic domains of the other two samples. This is probably due to 'longer' L-L sequences in PD212 copolymer. The shortening of aliphatic sequences in the chain structure results in higher aliphatic-aromatic attachments, leading to higher thermal stability of the aliphatic sequences. Nevertheless, the mechanism of the degradation due to aromatic domains observed at T_d = 415°C, and the remaining weight at a temperature higher than 450°C of all samples are comparable. This indicates that thermal stability of aromatic domains is independent on the monomer feed ratio.

Solubility of the copolymers in THF and CH_2Cl_2 solvents shows a decreasing trend upon increasing of aromatic content in feed. Upon closer examination of copolymers derived from a specific diol but different feed ratios, it is observed that the reduction of solubility in the two solvents is closely correlated to an increase in molecular weight, aromatic content, aromatic block length or crystallinity of

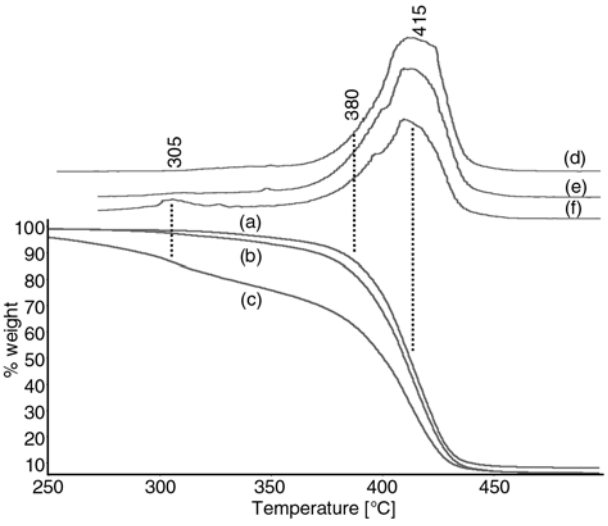

Figure 8. TGA thermograms of copolymers derived from PD at different monomer feed ratios feed ratios: 1:2:4 (a), 1:1:2 (b), 2:1:2 (c), and their corresponding DTGA traces: 1:2:4 (d), 1:1:2 (e), 2:1:2 (f)

the copolymers, which result from an increase in the aromatic content in the monomer feed ratio.

4. Conclusions

Aliphatic-aromatic copolyesters are systematically synthesized from lactic acid, dimethyl terephthalate and various diols. Results on effects of diols on properties of the copolyesters indicate that 1,4-butanediol provides copolymers with highest molecular weight, compared to that of shorter-chain diols, due to its optimum methylene flexibility and the reactivity of hydroxyl groups with acid functional groups. Types of diol and aromatic/aliphatic content in the copolymer chain play a key role in glass transition behaviors of the samples by imposing different degree of chain flexibility. In addition, molecular weight, relative length and relative content of aromatic/aliphatic sequences in the chain structure are essential parameters to govern crystalline behaviors, thermal stability, and solubility of the copolymers.

Monomer feed ratio also has a significant effect on properties of the copolymers, where an increase in the aromatic content leads to formation of copolymers with higher molecular weight, longer aromatic block sequences and high aromatic to aliphatic ratio, in the chain structure. These, in turn, lead to an increase in T_g, T_m, crystallinity and thermal stability of the copolymer samples, and a reduction in their solubility. Properties of these lactic acid/terephthalate-based copolyesters can be fine tuned by varying these two preparation conditions for use in specific applications.

Acknowledgements

Financial support of this work is provided by The Thailand Research Fund (TRF) and The Commission on Higher Education (CHE), under grant no. RSA5280029. M. Namkajorn is partially supported by The National Science and Technology Development Agency (NSTDA) and Sirindhorn International Institute of Technology (SIIT), Thammasat University.

References

[1] Awaja F., Pavel D.: Injection stretch blow moulding process of reactive extruded recycled PET and virgin PET blends. European Polymer Journal, **41**, 2614–2634 (2005).
DOI: 10.1016/j.eurpolymj.2005.05.036

[2] Ki H. C., Park O. O.: Synthesis, characterization and biodegradability of the biodegradable aliphatic-aromatic random copolyesters. Polymer, **42**, 1849–1861 (2001).
DOI: 10.1016/S0032-3861(00)00466-3

[3] Gilding D. K., Reed A. M.: Biodegradable polymers for use in surgery-poly(ethylene oxide) poly(ethylene terephthalate) (PEO/PET) copolymers: 1. Polymer, **20**, 1454–1458 (1979).
DOI: 10.1016/0032-3861(79)90008-9

[4] Reed A. M., Gilding D. K.: Biodegradable polymers for use in surgery- poly(ethylene oxide)/poly(ethylene terephthalate) (PEO/PET) copolymers: 2. *In vitro* degradation. Polymer, **22**, 499–504 (1981).
DOI: 10.1016/0032-3861(81)90169-5

[5] Kitotsukuri T., Masuda T., Tsutsumi N., Sakai W., Nagata M.: Poly(ethylene terephthalate) copolymers with a smaller amount of poly(ethylene glycol)s and poly(butylene glycol)s. Polymer, **36**, 2629–2635 (1995).
DOI: 10.1016/0032-3861(95)91211-O

[6] Heidary S., Gordon B.: Hydrolyzable poly(ethylene terephthalate). Journal of Polymers and the Environment, **2**, 19–26 (1994).
DOI: 10.1007/BF02073483

[7] Nagata M., Kitotsukuri T., Minami S., Tsutsumi N., Sakai W.: Enzymatic degradation of poly(ethylene terephthalate) copolymers with aliphatic dicarboxylic acids and/or poly(ethylene glycol). European Polymer Journal, **33**, 1701–1705 (1997).
DOI: 10.1016/S0014-3057(97)00063-3

[8] Witt U., Müller R-J., Deckwer W-D.: Biodegradation behavior and material properties of aliphatic/aromatic polyesters of commercial importance. Journal of Polymers and the Environment, **5**, 81–89 (1997).
DOI: 10.1007/BF02763591

[9] Witt U., Müller R-J., Augusta J., Widdecke H., Deckwer W-D.: Synthesis, properties and biodegradability of polyesters based on 1,3-propanediol. Macromolecular Chemistry and Physics, **195**, 793–802 (1994).
DOI: 10.1002/macp.1994.021950235

[10] Witt U., Müller R-J., Deckwer W-D.: Biodegradation of polyester copolymers containing aromatic compounds. Journal of Macromolecular Science Part A: Pure and Applied Chemistry, **32**, 851–856 (1995).
DOI: 10.1080/10601329508010296

[11] Witt U., Müller R-J., Deckwer W-D.: New biodegradable polyester-copolymers from commodity chemicals with favorable use properties. Journal of Environmental Polymer Degradation, **3**, 215–223 (1995).
DOI: 10.1007/BF02068676

[12] Marten E., Müller R-J., Deckwer W-D.: Studies on the enzymatic hydrolysis of polyesters. II. Aliphatic-aromatic copolyesters. Polymer Degradation and Stability, **88**, 371–381 (2005).
DOI: 10.1016/j.polymdegradstab.2004.12.001

[13] Valiente N., Lalot T., Brigodiot M., Maréchal E.: Enzymic hydrolysis of phthalic unit containing copolyesters as a potential tool for block length determination. Polymer Degradation and Stability, **61**, 409–415 (1998).
DOI: 10.1016/S0141-3910(97)00226-7

[14] Olewnik E., Czerwinski W., Nowaczyk J., Sepulchre M. O., Tessier M., Salhi S., Fradet A.: Synthesis and structural study of copolymers of L-lactic acid and bis(2-hydroxyethyl terephthalate). European Polymer Journal, **43**, 1009–1019 (2007).
DOI: 10.1016/j.eurpolymj.2006.11.025

[15] Olewnik E., Czerwinski W., Nowaczyk J.: Hydrolytic degradation of copolymers based on L-lactic acid and bis-2-hydroxyethyl terephthalate. Polymer Degradation and Stability, **92**, 24–31 (2007).
DOI: 10.1016/j.polymdegradstab.2006.10.003

[16] Opaprakasit M., Petchsuk A., Opaprakasit P., Chongprakobkit S.: Effects of synthesis conditions on chemical structures and physical properties of copolyesters from lactic acid, ethylene glycol and dimethyl terephthalate. Express Polymer Letters, **3**, 458–468 (2009).
DOI: 10.3144/expresspolymlett.2009.56

[17] Kenwright A. M., Peace S. K., Richards R. W., Bunn A., MacDonald W. A: End group modification in poly(ethylene terephthalate). Polymer, **40**, 2035–2040 (1999).
DOI: 10.1016/S0032-3861(98)00433-9

[18] Tessier M., Fradet A.: Determination of the degree of randomness in condensation copolymers containing both symmetrical and unsymmetrical monomer units: A theoretical study. e-Polymers, no.30 (2003).

[19] Grzebieniak K.: Copolyesters of ethylene terephthalate and lactic acid susceptible to hydrolytic degradation. Fibres and Textiles in Eastern Europe, **4**, 34–37 (1996).

[20] Grzebieniak K., Ratajska M., Strobin G.: Estimation of hydrolysis and biodegradation processes in ethylene terephthalate and lactic acid copolymers. Fibres and Textiles in Eastern Europe, **9**, 61–65 (2001).

eXPRESS Polymer Letters Vol.4, No.7 (2010) 423–430
Available online at www.expresspolymlett.com
DOI: 10.3144/expresspolymlett.2010.53

Biodegradation of flax fiber reinforced poly lactic acid

R. Kumar[1*], *M. K. Yakubu*[2], *R. D. Anandjiwala*[1,3]

[1]CSIR Materials Science and Manufacturing, Port Elizabeth, South Africa
[2]Department of Textile Science and Technology, Ahmadu Bello University, Zaria, Nigeria
[3]Department of Textile Science, Faculty of Sciences, Nelson Mandela Metropolitan University, Port Elizabeth, South Africa

Received 24 February 2010; accepted in revised form 30 April 2010

Abstract. Woven and nonwoven flax fiber reinforced poly lactic acid (PLA) biocomposites were prepared with amphiphilic additives as accelerator for biodegradation. The prepared composites were buried in farmland soil for biodegradability studies. Loss in weight of the biodegraded composite samples was determined at different time intervals. The surface morphology of the biodegraded composites was studied with scanning electron microscope (SEM). Results indicated that in presence of mandelic acid, the composites showed accelerated biodegradation with 20–25% loss in weight after 50–60 days. On the other hand, in presence of dicumyl peroxide (as additive), biodegradation of the composites was relatively slow as confirmed by only 5–10% loss in weight even after 80–90 days. This was further confirmed by surface morphology of the biodegraded composites. We have attempted to show that depending on the end uses, we can add different amphiphilic additives for delayed or accelerated biodegradability. This work gives us the idea of biodegradation of materials from natural fiber reinforced PLA composites when discarded carelessly in the environment instead of proper waste disposal site.

Keywords: *biodegradable polymers, amphiphilic additives, scanning electron microscope*

1. Introduction

Biocomposites are usually fabricated with biodegradable/nonbiodegradable polymers as matrix and natural fibres as reinforcement. A number of lignocellulosic fibres, such as jute, hemp, sisal, abaca etc. are used as reinforcement for biodegradable biocomposites because of their good mechanical properties and low specific mass [1–4]. Extensive research is carried out on plastics and composites from poly(lactic acid) (PLA), a synthetic aliphatic polyester which is biodegradable and synthesized from renewable agriculture products, with properties comparable to some fossil-oil-based polymers [2]. Generally, biodegradation studies are carried out in soil and/or compost, in particular, enhanced biodegradation of these materials may occur in the presence of compost, a complex biological environment, in which microbial diversity is relatively high and therefore an increased degradation potential for polymeric compounds may result [5–7]. The improper disposal and treatment of solid waste is one of the gravest environmental problems faced by most of the countries. With the increasing globalization and modernization, generation of waste for disposal is likely to increase still further. In near future, biocomposite products that will be discarded by the consumer after use will become biocomposite wastes and these products do break down naturally by the air, moisture, climate, or soil and disintegrate in the surrounding land. But as more and more biodegradable materials pile up, there is increased threat to the environment so dur-

*Corresponding author, e-mail: krrakesh72@gmail.com

ing processing of the materials, additives can be included for enhancing the rate of biodegradability of the biocomposites depending upon the end-uses of the products. Importantly, in many parts of the world proper waste disposal facilities do not exist and the wastes are simply discarded in the surrounding areas. Ultimately, we have to depend on the nature for biodegradation of the materials. In view of this thought it is of interest to conduct the biodegradation studies of the biocomposites for natural fiber reinforced PLA in farmland soil in presence of amphiphilic additives and thereby assess the effectiveness of the various additives on the biodegradability of the material.

In this short communication we report the biodegradation studies conducted in the farmland soil for woven and nonwoven flax fibres reinforced PLA composites using amphiphilic additives. The physico-mechanical properties of these composites are discussed in detail in two of our recent papers under publication [8, 9]. PLA used in this study contains cereal starch (wheat, potato and tapioca) for improved biodegradability. Biodegradation studies were based on the estimation of the loss in weight of the composites with time. Fourier transform infrared spectra (FTIR) and scanning electron microscopy (SEM) were used to assess the degradation of the material. The application areas of the biocomposites from PLA will expand further if the materials degrade faster after their end-uses. The objective of this work is to investigate the rate of biodegradation of flax/PLA biocomposites in the presence of different additives. An attempt is made to ascertain the extent of acceleration that can be achieved.

2. Experimental

2.1. Materials

PLA resin (CP-INJ-1001EZC) was obtained from Cereplast, Inc, Hawthorne, USA (MFI@190° as determined by D1238 method is 10–12 g/min, HDT is 44.4°C at 4.6 MPa (66 psi)). To improve the biodegradability of the PLA resin, supplier has incorporated cereal starch (wheat, potato and tapioca) in this grade of resin. Flax nonwoven web of 110±20 g/m^2 was prepared by needle punching technique on a pilot plant at CSIR, Port Elizabeth, South Africa. Flax woven fabric of 180±10 g/m^2 was purchased from Libeco, Belgium with 19 warp/cm and 21 weft/cm. Benzilic acid, mandelic acid and dicumyl peroxide (DCP) were procured from Sigma-Aldrich, Germany. Zein protein was obtained from Scientific Polymer Products, New York, USA and chloroform was purchased from Minema Chemicals, South Africa. All laboratory grade chemicals were used without further purification.

2.2. Preparation of the composites

In a typical process, a square nonwoven or woven web of 15 cm×15 cm in dimensions with an average mass of 2.5 g (for nonwoven) or 4 g (for woven) was cut and dried in an oven at 60°C for 24 h to remove moisture. PLA pellets equivalent to 0.8 and 0.7 weight fractions of the nonwoven web and woven fabric, respectively were dissolved in chloroform. It is to be noted that nonwoven flax fiber requires higher amount of PLA than woven ones. The dried nonwoven web/woven fabric was then placed inside a square metal frame mold of 15 cm×15 cm in dimensions and the PLA solution was poured over the nonwoven web or woven fabric. It was observed that 5 to 6 g of PLA in 100 ml chloroform gave homogeneous solution for wetting the fibres in the nonwoven web or woven fabric. We are using chloroform to dissolve PLA in the initial stage of our research although we are aware of the fact that chloroform is not suitable for the environment. Once we get the idea of suitable additives for accelerated degradation we will prepare the samples by injection molding without using the solvent. The assembly was kept at a room temperature for 24 h to evaporate the solvent. The solution-cast samples with one layer of nonwoven web/woven fabric were subsequently hot pressed at 190°C under 50 bar pressure for 15 min to get the composite samples. The solution-cast composites followed by compression molding with different additives (1% w/w w.r.t PLA) were prepared at 0.2 and 0.3 weight fraction of the fibers (W_f) of the nonwoven web and woven fabric, respectively by following the procedure described above. The composites, thus prepared from nonwoven web, were designated as PFB-NW, PFM-NW, PFD-NW, PFZ-NW where B, M, Z, and D represent benzilic acid, mandelic acid, zein, and DCP, respectively. PF-NW represents the composites prepared without additives. Similarly, the composites prepared from

woven web were designated as PFB-W, PFM-W, PFD-W, PFZ-W. PLA-fibre composite prepared without additive is designated as PF-W. PF represents flax fiber reinforced PLA composites while NW and W represent nonwoven and woven flax fabric, respectively. The thickness of the composites with one layer of nonwoven or woven fabric, prepared by compression molding at 50 bar pressure, was found to be 0.65±0.05 mm. The composites thus prepared were free from voids and solvent as the samples obtained after solution casting were pressed (50 bar pressure) in compression molding machine at 190°C for 15 min.

2.3. Characterizations

For biodegradability test, the composite sheets were cut into 40×20 mm rectangular specimens. Biodegradability test was carried out in a flower pot containing farmland soil having pH 7.5–7.7 by maintaining high relative humidity (~98%) by daily sprinkling water. Each specimen was buried in the soil kept in a flower pot (30 cm diameter) at room temperature (25±5°C). Each specimen was dug out of the farmland soil after buried for 20, 30, 40, 50, 60, 70, 80 and 90 days, respectively, and then washed with water and dried at 60°C in an air oven for 48 h. Biodegradability was determined by measuring loss in weight of the specimens. To maintain uniformity in the results only one sample was tested at each condition.

Scanning electron microscopy (SEM) images of the surface of the biodegraded composites were taken on FEI Quanta 200 (Eindhoven, The Netherlands) electron microscope at an accelerating voltage of 10 kV in low vacuum. Differential scanning calorimetry (DSC) of the composites was carried out on a Diamond DSC (Perkin Elmer) in the temperature range of 25 to 220°C. Fourier transform infrared spectra (FTIR) of the composites before and after degradation were carried out on a Spectrum 100 FT-IR (Perkin Elmer USA) in the range from 4000 to 600 cm^{-1} using composite powders.

3. Results and discussion

Films prepared from neat PLA degraded rapidly compared to natural fiber reinforced composites. About 4.2% weight loss was observed in neat PLA after 20 days of burial in soil degradation test. After

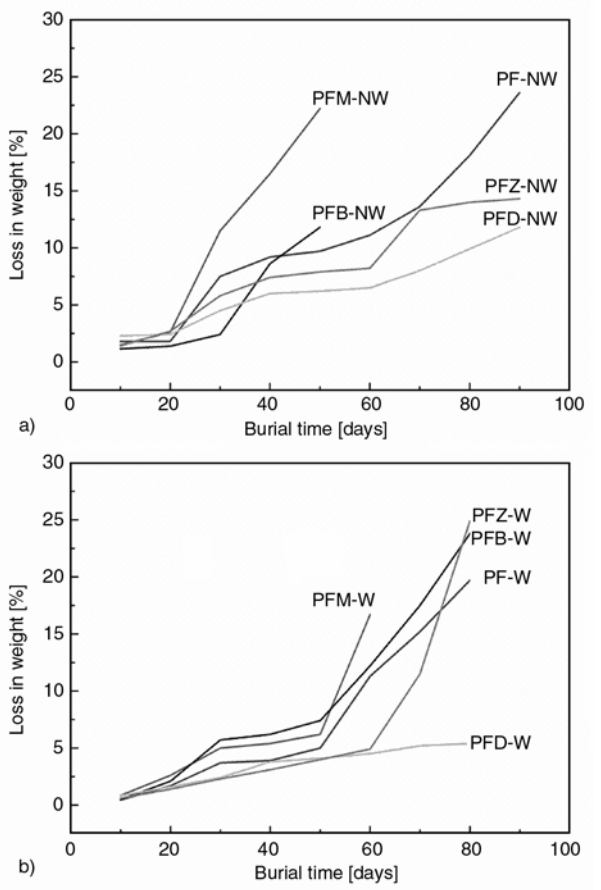

Figure 1. Loss in weight of the buried composite samples in farmland soil with different additives. In the above figures, PF represents flax fiber reinforced PLA composites while NW and W represent nonwoven and woven flax fabric, respectively. M, B, Z and D represent mandelic acic, benzilic acid, zein protein and dicumyl peroxide, respectively that has been added to the composites during preparation.

20 days, neat PLA samples were brittle so further study on PLA film was discontinued. Figure 1 shows the loss in weight of the biodegraded flax fiber reinforced composites over the soil burial degradation period of 90 days. After 90 days, composite samples partially disintegrated so further studies on the biodegradation of the composites in soil was discontinued. Lag phase/time of about 20 days was observed in the biodegradation curves. Woven and nonwoven reinforced composites showed 5–25% of weight loss after the designated lag time. The loss in weight increased with the increase in burial time for all the specimens. The presence of DCP delayed the rate of biodegradation of the composites in soil with resultant loss in weight of 11.4% (after 90 days) and 5.5% (after 80 days) for PFD-NW and PFD-W, respectively.

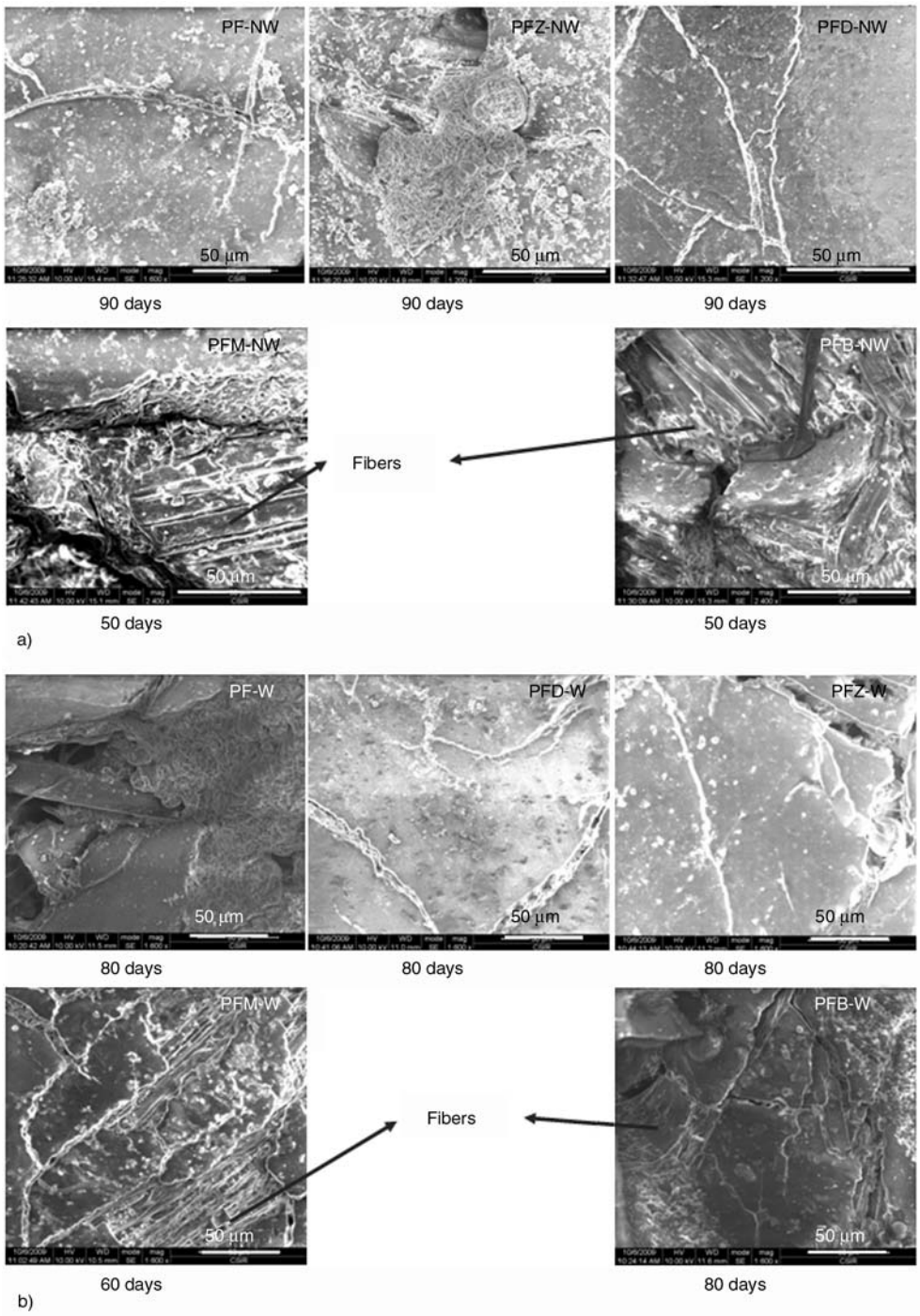

Figure 2. Surface morphology of nowoven reinforced PLA composites in presence of different additives. Cracks in the PFD-NW are observed indicating stability of composites. Fibers are observed on the surface of the PFM-NW, PFB-NW (a) and PFM-W, PFB-W (b) composites after biodegradation indicating accelerated degradation in presence of that particular additive.

On the other hand, the presence of mandelic acid accelerated the rate of degradation of the composites in the soil with resultant loss in weight of 22% (after 50 days) and 16.7% (after 60 days) for PFM-NW and PFM-W, respectively. Higher rate of degradation of the composites in presence of mandelic acid may be due to the removal of PLA from the surface upon biodegradation as confirmed by Figure 2 [10]. Additionally, in presence of benzilic acid composites also showed accelerated biodegradation in soil. The percentage loss in weight after biodegradation in nonwoven composites is higher than woven ones. This is due to the fact that in case of nonwoven reinforced composites, due to higher

amount of PLA, the microorganisms in soil can degrade the composites more effectively. Thus in addition to hydrolysis in PLA biological degradation has also taken place in the composites.

Figures 2a and 2b show the surface morphology of the composites degraded in the soil. After 80 and 90 days, the cracks on the surface of the PF-NW, PF-W, PFD-NW, PFD-W, PFZ-NW and PFZ-W composites are apparent. Additionally, one or two fibers are also seen in PF-W and PFZ-W. The pres-

Table 1. Percentage crystallinity ($\%\chi_c$) of woven and nonwoven fiber reinforced PLA composites determined by DSC thermal scans

Nonwoven fiber reinforced PLA composites		Woven fiber reinforced PLA composites	
Sample	**$\%\chi_c$**	**Sample**	**$\%\chi_c$**
PLA	11.0	PLA	11.0
PF-NW	8.0	PF-W	5.8
PFB-NW	9.4	PFB-W	6.8
PFD-NW	5.4	PFD-W	7.0
PFM-NW	10.3	PFM-W	7.1
PFZ-NW	9.3	PFZ-W	6.6

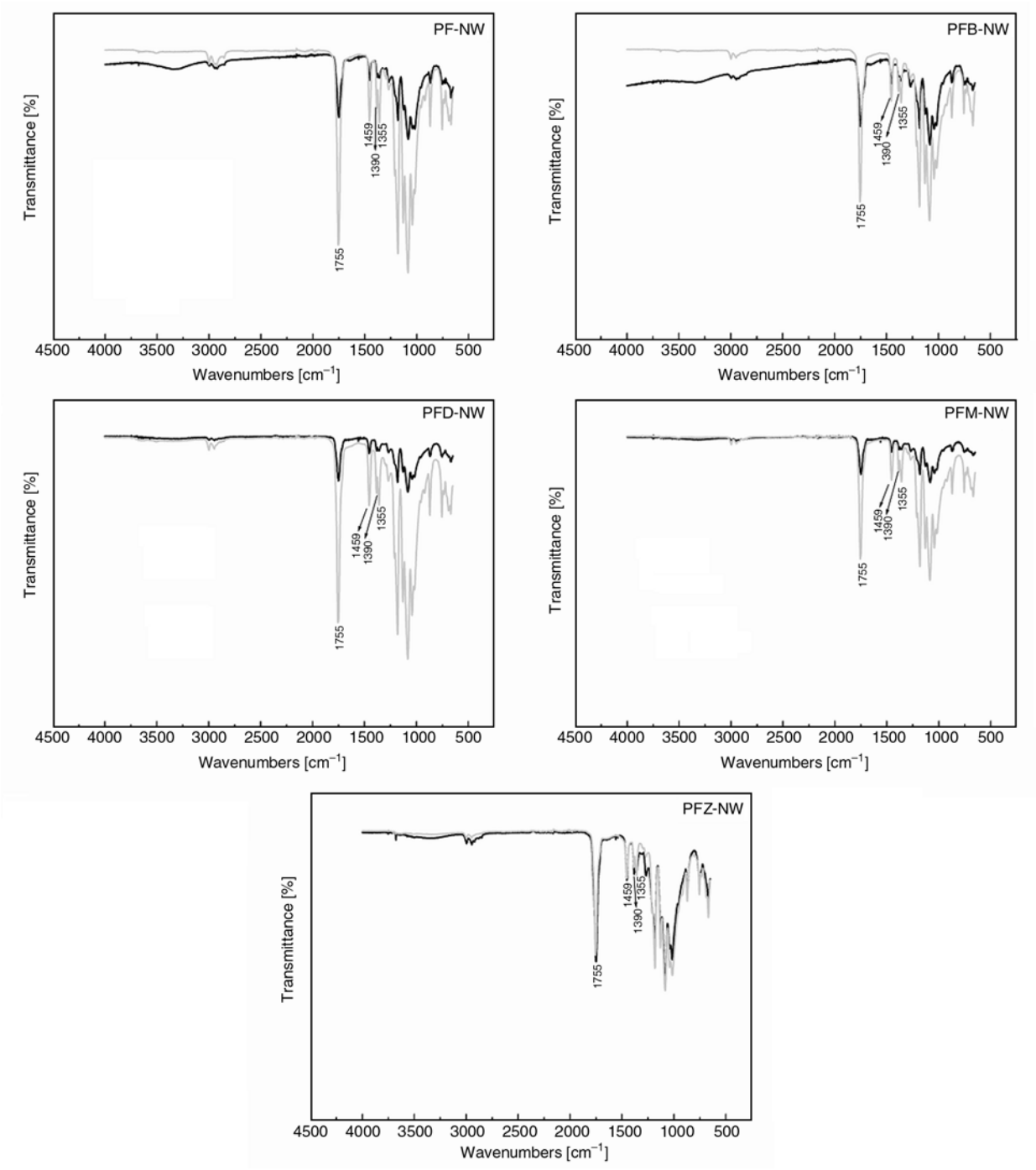

Figure 3. FTIR spectra of nonwoven fiber reinforced PLA composites in presence of different additives. In the FTIR spectra black line represents composite samples before degradation and grey line represents after degradation.

ence of cracks in PFD-NW and PFD-W samples showed the stability of the composites towards degradation in soil and is well confirmed from the low percentage loss in weight even after 90 days. In the case of biodegraded PFM-NW, PFB-NW, PFM-W and PFB-W composites, the fibers are being observed on surface as evidenced from SEM study indicating removal of PLA from the surface of the composites in presence of mandelic acid. This directly refers to the accelerated degradation of the composites in the presence of mandelic and benzilic acids and is well confirmed by the high percentage loss in weight for PFM-NW/PFM-W or PFB-NW/PFB-W after degradation (Figure 1). To ascertain the reason for high or low stability of composites towards degradation we have estimated gel content of the composites before degradation. The gel content of the composites was determined according to ASTM D 2765. Each sample of about 0.2 g was oven dried at 70°C for 24 h and then

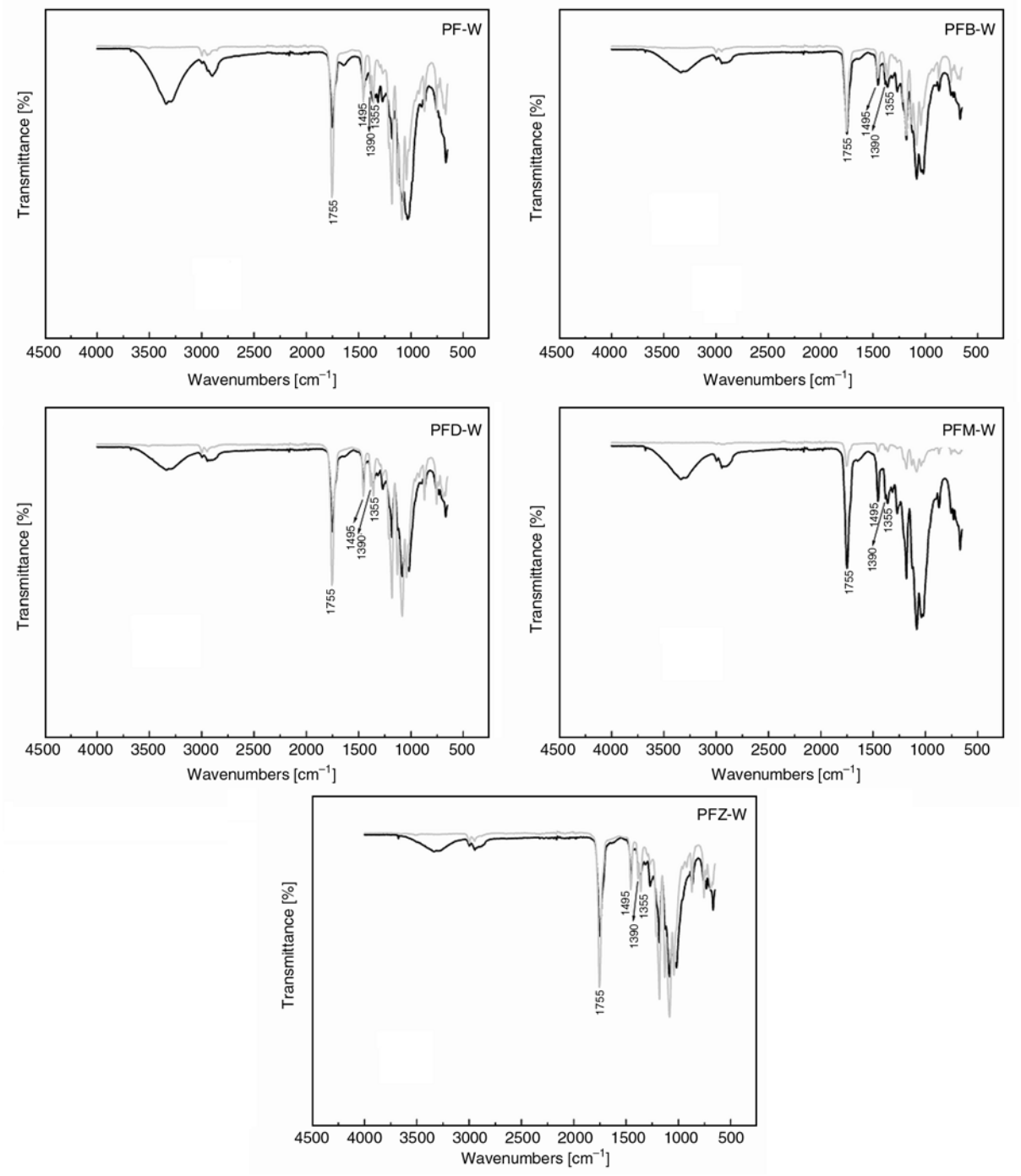

Figure 4. FTIR spectra of woven fiber reinforced PLA composites in presence of different additives. In the FTIR spectra black line represents composite samples before degradation and grey line represents after degradation.

immersed in 20 ml of chloroform for 24 h at a room temperature. The gel content was calculated as a fraction of residual PLA in the composite after subtracting the weight of the fibre. PFD-NW and PFD-W showed highest gel content (~12.3%) among all the composites, which indicates possible crosslinking in the presence of DCP attributable to free radical initiator nature of DCP.

The DSC results on percentage crystallinity ($\%\chi_c$) of PLA based composites are shown in Table 1. The melting enthalpy of 100% crystalline PLA was taken as 135 J/g [11]. There is an increase in $\%\chi_c$ for PFM-NW, which may have resulted from the presence of nucleating site from the amphiphilic additives. Both mandelic acid and benzilic acids are highly crystalline in nature. Presence of only one aromatic ring in mandelic acid provided more crystallising tendency in PLA in comparison to benzilic acid with two aromatic rings. The crystallization of PLA based composites tends to shift to higher temperature than PLA alone (not shown). Overall, the $\%\chi_c$ of the PLA decreased with the introduction of additives. $\%\chi_c$ of the PLA used in this study is much lower than that reported in the literature [12], and this is attributed to the fact that to improve the biodegradability of the PLA resin, supplier has incorporated cereal starch (wheat, potato and tapioca) in this grade of resin.

The influence of biological environment on the changes in chemical structure of the native and biodegraded composites can be investigated by the analysis of the infrared spectra. The FTIR spectra for woven and nonwoven reinforced composites were measured for samples before and after burial in soil and are presented in Figures 3 and 4. Degradation of composites is indicated mostly by increase of the band intensity corresponding to the C–H deformational vibrations of CH_3 groups present in polylactide segments (1355, 1390 cm^{-1}). The intensities of the –C=O bands of PLA show sharpening and increase after biodegradation. The changes of –C=O band are associated with the increase in the number of carboxylic end groups in the polymer chain during the hydrolytic degradation as well as in the cycle of microbial attack [13]. In the case of PFM-W (Figure 4) there is decrease in all the band intensities after biodegradation. FTIR spectra of PFM-W support the fact that there is removal of PLA from the surface upon biodegradation. In the case of PFM-NW (Figure 3) the PLA content is more and the fibers are well dispersed and that is the reason why the FTIR spectra of PFM-NW and PFM-W are not the same. However, surface morphology of both the degraded composites appears almost similar. The presence of degraded fibers with less PLA adhered in PFM-W and PFM-NW composites are also confirmed by the SEM micrographs (Figures 2a, 2b).

4. Conclusions

Biodegradability of flax fiber reinforced PLA based composites in presence of amphiphilic additives was investigated by soil burial test. Regarding the effect of amphiphilic additives on the biodegradability of composites, the higher loss in weight is obtained in the presence of mandelic acid. This is confirmed by the removal of PLA from the surface of the composites upon biodegradation as evidenced from the SEM study. In the presence of DCP, the biodegradability of the composites was comparatively delayed. Depending on the end-uses of the biocomposites, we can add suitable amphiphilic additives as triggers for inducing controlled biodegradation.

Acknowledgements

One of the authors, M. K. Yakubu is grateful to the Macarthur Foundation for providing the Post Doctoral Research Fellowship to work at CSIR MSM, Port Elizabeth, South Africa.

References

[1] Lee S-H., Wang S.: Biodegradable polymers/bamboo fiber biocomposite with bio-based coupling agent. Composites Part A: Applied Science and Manufacturing, **37**, 80–91 (2006).
DOI: 10.1016/j.compositesa.2005.04.015

[2] Oksman K., Skrifvars M., Selin J-F.: Natural fibres as reinforcement in polylactic acid (PLA) composites. Composites Science and Technology, **63**, 1317–1324 (2003).
DOI: 10.1016/S0266-3538(03)00103-9

[3] Mohanty A. K., Mubarak A. K., Hinrichsen G.: Surface modification of jute and its influence on performance of biodegradable jute-fabric/Biopol composites. Composites Science and Technology, **60**, 1115–1124 (2000).
DOI: 10.1016/S0266-3538(00)00012-9

[4] Sinha Ray S., Yamada K., Okamoto M., Ueda K.: Control of biodegradability of polylactide via nanocomposite technology. Macromolecular Materials and Engineering, **288**, 203–208 (2003).
DOI: 10.1002/mame.200390013

[5] Itävaara M., Karjomaa S., Selin J-F.: Biodegradation of polylactide in aerobic and anaerobic thermophilic conditions. Chemosphere, **46**, 879–885 (2002).
DOI: 10.1016/S0045-6535(01)00163-1

[6] Shogren R. L., Doane W. M., Garlotta D., Lawton J. W., Willett J. L.: Biodegradation of starch/polylactic acid/poly(hydroxyester-ether) composite bars in soil. Polymer Degradation and Stability, **79**, 405–411 (2003).
DOI: 10.1016/S0141-3910(02)00356-7

[7] Martucci J. F., Ruseckaite R. A.: Biodegradation of three-layer laminate films based on gelatin under indoor soil conditions. Polymer Degradation and Stability, **94**, 1307–1313 (2009).
DOI: 10.1016/j.polymdegradstab.2009.03.018

[8] Kumar R., Yakubu M. K., Anandjiwala R. D.: Flax fibre reinforced poly lactic acid composites with amphiphilic additives. Plastic Rubber and Composites: Macromolecular Engineering, in press (2010).

[9] Kumar R., Yakubu M. K., Anandjiwala R. D.: Effect of montmorillonite clay on flax fabric reinforced poly lactic acid composites with amphiphilic additives. Composites Part A: Applied Science and Manufacturing, in press (2010)

[10] Fukuzaki H., Aiba Y., Yoshida M., Asano M., Kumakura M.: Synthesis of biodegradable poly(L-lactic acid-co-D,L-mandelic acid) with relatively low molecular weight. Die Makromolekulare Chemie, **190**, 2407–2415 (1989).
DOI: 10.1002/macp.1989.021901007

[11] Miyata T., Masuko T.: Crystallization behaviour of poly(L-lactide). Polymer, **39**, 5515–5521 (1998).
DOI: 10.1016/S0032-3861(97)10203-8

[12] Yang S-L., Wu Z-H., Yang W., Yang M-B.: Thermal and mechanical properties of chemical crosslinked polylactide (PLA). Polymer Testing, **27**, 957–963 (2008).
DOI: 10.1016/j.polymertesting.2008.08.009

[13] Chlopek J., Morawska-Chochol A., Paluszkiewicz C., Jaworska J., Kasperczyk J., Dobrzyński P.: FTIR and NMR study of poly(lactide-co-glycolide) and hydroxyapatite implant degradation under *in vivo* conditions. Polymer Degradation and Stability, **94**, 1479–1485 (2009).
DOI: 10.1016/j.polymdegradstab.2009.05.010

eXPRESS Polymer Letters Vol.4, No.7 (2010) 431–441
Available online at www.expresspolymlett.com
DOI: 10.3144/expresspolymlett.2010.54

Ring-opening copolymerization of (*R,S*)-β-butyrolactone and ε-caprolactone using sodium hydride as initiator

M. Monsalve[1], *J. M. Contreras*[1*], *E. Laredo*[2], *F. López-Carrasquero*[1]

[1]Grupo de Polímeros, Departamento de Química, Facultad de Ciencias, Universidad de Los Andes, Mérida, 5101-A, Venezuela
[2]Grupo FIMAC, Departamento de Física, Universidad Simón Bolívar, Caracas 1080A, Venezuela

Received 3 March 2010; accepted in revised form 7 May 2010

Abstract. Copolymers of racemic β-butyrolactone ((*R,S*)-BL) and ε-caprolactone (CL), were synthesized by ring-opening polymerization initiated by sodium hydride (NaH). The initiator exhibited a satisfactory catalytic activity, producing copolymers whose yields are greatly influenced by the feed monomer ratio, CL/BL. All polymers obtained were characterized by nuclear magnetic resonance (NMR), gel permeation chromatography (GPC), thermogravimetric analysis (TGA), differential scanning calorimetry (DSC) and wide angle X-rays scattering, WAXS. The molar composition of copolyesters determined by ^{1}H-NMR spectra, showed that the incorporation of CL is favoured over the incorporation of (*R,S*)-BL. Gel permeation chromatography and ^{13}C-NMR spectra indicated that CL/BL copolymers had block sequence distribution.
The TGA analysis of copolymers showed that these copolymers are stable up to temperatures near 200°C, followed by a decomposition process in two steps; the first one is attributed to the (*R,S*)-BL block degradation and the second to the remaining PCL block. The crystallization process of these copolymers was studied by DSC and WAXS showing that the amorphous (*R,S*)-BL segments chains did not affect the crystallinity of the PCL blocks.

Keywords: *biodegradable polymers, sodium hydride, ε-caprolactone, β-butyrolactone, block copolymers*

1. Introduction

Biodegradable polymers have received much attention as materials for medical applications [1–3]. Linear aliphatic polyesters such as poly(glycolide) (PGL), poly(lactide) (PLA), poly(β-butyrolactone) (PBL) and poly(ε-caprolactone) (PCL) and their co- and terpolymers are the most popular bioabsorbable polymers. Because of the wide range of applications in biomedicine, it is necessary for the polyesters to present different mechanical and physical properties to adjust the adequate time of their degradation; in this sense copolymerization constitutes an attractive mean for modulating the basic properties of each homopolymer [4–6]. In particular, block copolymerization may offer a broader spectrum of mechanical and degradation properties in order to meet the demands of a larger number of applications. Blocks with different physical properties, for example, a soft, amorphous segment together with a hard semicrystalline one, can be used to modulate the thermal and mechanical material behaviour [4, 7–9]. The mechanical properties can be controlled by the hard/soft segment ratio [7] and copolymers with various morphologies such as solid, pasty and waxy states, can be obtained according to the monomer composition [6, 10]. The soft phase provides elasticity and the degradation behaviour, whereas the rigid phase gives mechanical strength and also acts as a physical crosslinker [6].
Polymerization of racemic monomer (*R,S*)-β-butyrolactone ((*R,S*)-BL) has given an atactic poly

*Corresponding author, e-mail: jeco@ula.ve

(*R,S*)-(β-butyrolactone) ((*R,S*)-PBL) with elastomeric properties because of its low crystallinity [7, 11, 12]. However, for its applications as biodegradable elastomer, it is necessary to decrease their creep behaviour. This has been done by the introduction of a biodegradable hard segment, by means of the successive ring-opening polymerization of (*R,S*)-BL and *L*-lactide [7] or ε-caprolactone [8, 13]. The resultant block copolymers, consisting of (*R,S*)-PBL as the soft segment and PLLA or PCL as the hard segment, could be the biodegradable thermoplastic elastomer.

On the other hand, the choice of a proper initiator is another important parameter in the synthesis of polyesters. Many effective catalysts based on tin-compounds, have been employed for this purpose [4, 7, 8, 13–21]. However, many are relatively toxic and impossible to remove completely from the synthesized material, this being undesirable for pharmaceutical or biomedical applications [2, 6].

Therefore, several attempts to use a catalyst based on much less toxic metal compounds are being undertaken [2, 6, 11, 22–27]. The anionic polymerization of β-butyrolactone had been widely studied [27–40], and in general polymers with low molecular weight were obtained. Relatively low toxic alkali metal hydrides are among the initiators used for this purpose [27], nevertheless, they have not been used so far for the synthesis of copolymers of (*R,S*)-BL and CL. It is for this reason that the possibility of utilizing sodium hydride as the initiator of the copolymerization of (*R,S*)-BL and CL is undertaken in this work.

2. Experimental

2.1. Materials

ε-caprolactone (CL) and racemic β-butyrolactone ((*R,S*)-BL) (from Aldrich) were dried over calcium hydride for 24 h at room temperature an then distilled under reduced pressure in a nitrogen atmosphere prior use. Sodium hydride (from Aldrich) was used as received.

2.2. Polymerization procedure

CL and (*R,S*)-BL were polymerized in bulk using sodium hydride (NaH) as initiator, in a glass reactor equipped with magnetic stirring bar. The reactors were charged with the previously established amounts of initiator, CL and (*R,S*)-BL under nitrogen atmosphere, in a dry-box. The sealed reaction vessels were placed into an oil bath preheated at 70°C, for the duration requested. The resultant polymeric products were washed by ethylic ether several times in order to separate (*R,S*)-(butirolactone) oligomers from the copolymer. Finally, the copolymers obtained were dissolved in chloroform, filtered in order to eliminate the traces of remaining initiator and precipitated into an excess amount of methanol. The precipitated products were then separated by filtration and thoroughly dried at 50°C in vacuum.

2.3. Characterization

^{1}H-NMR and ^{13}C-NMR spectroscopy was carried out with a Bruker AVANCE DRX 400 Spectrometer. $CDCl_3$ was used as solvent for the NMR measurements. The GPC measurements were carried out with THF as the eluent using a Waters chromatograph, model 150CV, operated at 40°C and equipped with three columns connected in series and packed with Ultrastyragel 10^3, 10^4 and 10^5. Calibration was performed with polystyrene standards with a narrow molecular weight distribution.

Thermogravimetric curves were obtained in a Perkin-Elmer TGA 7, from a heating scan of a sample of about 10 mg from 25 to 500°C, at 10°C/min under a nitrogen atmosphere.

Thermal volatilization analysis (TVA) was carried out in a vacuum line heating the samples of about 100 mg from room temperature to 270°C during 30 minutes under a moderate primary vacuum. Volatile fractions were condensed at room temperature and analyzed by IR and ^{1}H-NMR.

DSC measurements were carried out with a Perkin-Elmer DSC-7, the sample mass was 10–15 mg and the heating rate was 10°C/min.

Wide angle X-ray scattering (WAXS) experiments were performed in an Analytical X'Pert Pro automatic horizontal θ-θ axis diffractometer with an X'celerator detector, using CuK_α-Ni filtered radiation. The excitation voltage was 45 kV and the tube current 40 mA. Spectra were taken at temperatures ranging from 25 to 70°C in an Anton PAAR Variable Temperature Attachment with the scattering angle 2θ varying from 3 to 50°.

3. Results and discussion

3.1. Synthesis of the copolymers

Among the initiators used in anionic polymerization of BL are the alkali metal hydrides, which give rise to polymers with low yield and low molecular weight [27]. However, to the best of our knowledge, there are no literature reports in which these have been used to start the copolymerization of BL and CL. Results of the copolymerization of a mixture of BL and CL using NaH as the initiator are presented here.

All copolymerizations of CL and (*R,S*)-BL were conducted in bulk with sodium hydride (NaH) as initiator. The effect of monomer to initiator (M/I) molar ratio of on the copolymerization was first examined. As may be seen in Table 1, above M/I = 20 (exp. 3 and exp. 4), no polymer formation was observed even after 72 hours. This fact can be attributed to the copolymerization rate which is suppressed due to a small amount of initiator [24, 25]. Also, the results reported in Table 1 show that for M/I = 4 and 20 the conversion of monomers to copolymer decreases with the increase of M/I; CL content in copolyesters is higher than in (*R,S*)-BL.

Taking into account that for M/I = 20 (exp. 2) the product was a stiff white solid, while for M/I = 4 (exp. 1) it was a softer solid, it may be suggested that the molecular weight increases with the content of CL in the copolymers, which increases with molar ratio M/I. On the basis of these results, subsequent polymerizations were carried out at M/I = 20.

The effects of feed ratio on the copolymerization is shown in Table 2 using a constant relation M/I = 20, at 70°C, for 96 h. There it can be seen that the proportion of butyroyl units in the copolymers is quite constant regardless the feed ratio; in addition, its content is lower than expected from the feed ratio for (*R,S*)-BL feed content up to 40 mol% (exp. 6 to exp. 8), while for contents lower that 40 mol% (exp. 9 and exp. 10) the instantaneous composition of the copolymers (F_{CL}/F_{BL}) is nearly equal to the monomer feed composition. On the other hand, the increase of CL in the feed mixture raises the copolymers yields. This is consistent with the results of homopolymerization of CL and (*R,S*)-BL (exp. 11 and exp. 5, respectively), in which CL polymerization is much faster than that of (*R,S*)-BL. In general, the molecular weight of the copolymers obtained tends to increase with F_{CL}, and this could be due to the fact that the molecular weight of the PCL homopolymer is higher than that of the

Table 1. Effect of molar ratio of comonomers (M) to initiator (I) on the copolymerization of CL and (*R,S*)-BL[a]

Exp. No.	NaH [mmol]	M/I [mol/mol]	F_{CL}[b] [%]	$F_{(R,S)\text{-}BL}$[b] [%]	Yield[c] [%]	Physical appearance
1	5.20	4	55.00	45.00	87.72	white soft solid
2	1.06	20	66.30	33.70	17.33	white rigid solid
3	0.35	60	–	–	–	–
4	0.21	100	–	–	–	–

[a] at 70°C for 72 h, n_{CL} = 9.02 mmol (f_{CL} = 0.42, 1 mmol = 0.086 g); $n_{(R,S)\text{-BL}}$ = 12.3 mmol ($f_{(R,S)\text{-BL}}$ = 0.58, 1 mmol = 0.114 g), 1 mmol NaH = 0,024 g

[b] Content of CL and (*R,S*)-BL in copolymer [mol%]

[c] Based on initial comonomers

Table 2. Results of the copolymerization of CL and BL at various feed monomer ratios using sodium hydride (NaH) as initiator

Exp. No.	NaH [mmol]	CL/BL [mmol/mmol]	Feed monomer ratio CL/BL [mol%]	FCL/FBL[a] [%]	Yield[b] [%]	GPC[c]		
						$\overline{M}_n \cdot 10^{-3}$	$\overline{M}_w \cdot 10^{-3}$	D
5	0.61	12.30	0/100	0/100	19.08	1.94	2.51	1.29
6	2.71	16.24/37.88	30/70	88/12	7.35	18.63	26,26	1.41
7	1.23	12.30/12.30	50/50	75/25	14.96	8.96	13.91	1.55
8	1.50	18.04/12.02	60/40	75/25	37.17	8.67	12.84	1.48
9	1.29	18.04/7.73	70/30	80/20	63.25	11.23	16.46	1.47
10	1.13	18.04/4.51	80/20	83/17	74.17	12.05	16.28	1.35
11	0.45	9.02	100/0	100/0	87.37	32.21	44.21	1.37

M/I = 20, in bulk at 70°C for 96 h

[a] Content of CL and BL in copolymer [mol%], obtained by means ^{1}H-NMR

[b] Based on initial comonomers

[c] From GPC, measured in THF at 40°C

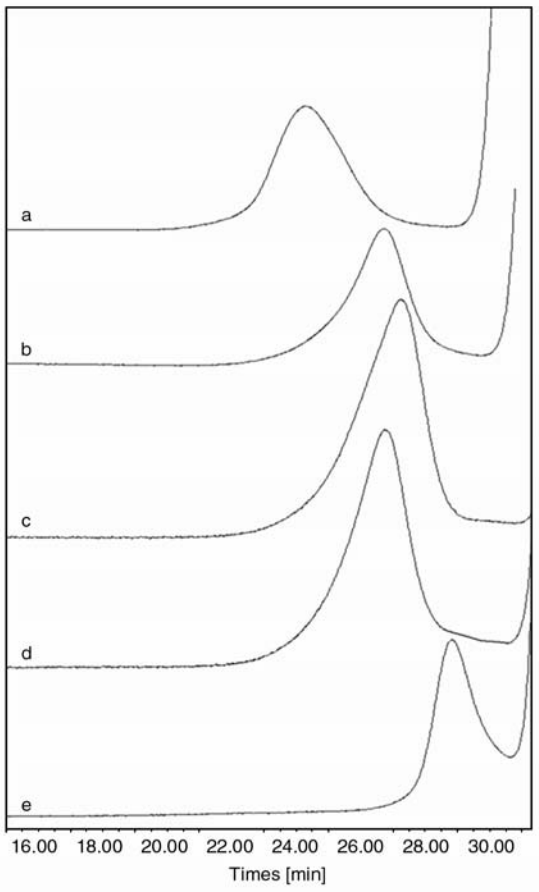

Figure 1. Gel permeation chromatograms of copolymers obtained using NaH at various molar ratios CL/(*R,S*)-BL: a) PCL, b) block PCL/(*R,S*)-PBL 75/25, c) block PCL/(*R,S*)-PBL 80/20, d) block PCL/(*R,S*)-PBL 83/17, e) (*R,S*)-PBL

(*R,S*)-PBL homopolymer (exp. 11 and exp. 5, respectively). These results are in agreement with the fact the anionic polymerization of (*R,S*)-BL leads to low yield and chains of a relatively low molecular weight [27–33].

Figure 1 displays the GPC chromatograms of the obtained polymers. There it can be noted that the curves show a monomodal pattern which indicates that the polymerization product is a true copolymer not contaminated by PCL and (*R,S*)-PBL.

3.2. Structural analysis of copolymers:

Analysis of copolymer microstructure was performed by means of NMR spectroscopy. The typical ^{1}H-NMR and ^{13}C-NMR spectra copolymer of CL with BL are shown in Figure 2. The assignments of the peaks were made according to previous results [24, 25, 32]. It can be noted that the copolymers spectra show signals of both homopolymers. The resonances at $\delta = 1.8$ ppm, $\delta = 5.8$ ppm and $\delta = 6.8$ ppm observed in the ^{1}H-NMR spectrum, can be attributed to the presence of a crotonyl end-group [32]; this group is formed at the initiation step of the polymerization where the α-proton abstraction of the (*R,S*)-BL could occur resulting in the salt of the unsaturated carboxylic acid as propagating species of reaction, as shown in Figure 3 [27, 33].

To determine the comonomer sequencing (random or in block), the most convenient spectrum range is the corresponding to carbonyl carbon [10, 13, 41]. The expanded ^{13}C-NMR spectrum of the carbonyl (CO) region of the copolymer shown in Figure 2 indicates the formation of a diblock, because the two CO signals of the blocks BL-BL and CL-CL are strong, whereas the signals of the BL-CL and CL-BL sequences are absent [6]. The CO signal of BL-BL sequences exhibits a splitting resulting from isotactic and syndiotactic dyads [13, 41]. This result may be explained, taking into account the higher strain in bond angle in the (*R,S*)-BL with respect to CL; this could facilitate in the medium of reaction the occurrence as first step the anionic polymerization of (*R,S*)-BL via carboxylate anions as propagating species, leading to blocks of PBL of a relatively low molecular weight [27–33]. The latter could then initiate the polymerization of CL trough alkoxide anions as propagating species leading to blocks of PCL of a relatively higher molecular weight [5, 23].

3.3. Thermal properties of the obtained copolymers

3.3.1. Thermogravimetric analysis (TGA)

Thermal stability was evaluated by TGA and traces of most of the polymers are shown in Figure 4 where it may be observed that the PCL is significantly more stable than the PBL and the degradation of both polymers occurs in a single stage. On the other hand, the PCL-*block*-(*R,S*)-PBL copolymers exhibit an intermediate stability between both homopolymers and their stability increases with the content of CL. In addition, these copolymers show two stages of degradation where the first one corresponds to a weight-loss comparable to the fraction in weight of the PBL in the copolymer as may be observed in Table 3.

The temperature values and mainly the comparison between the percentage of volatilized material after

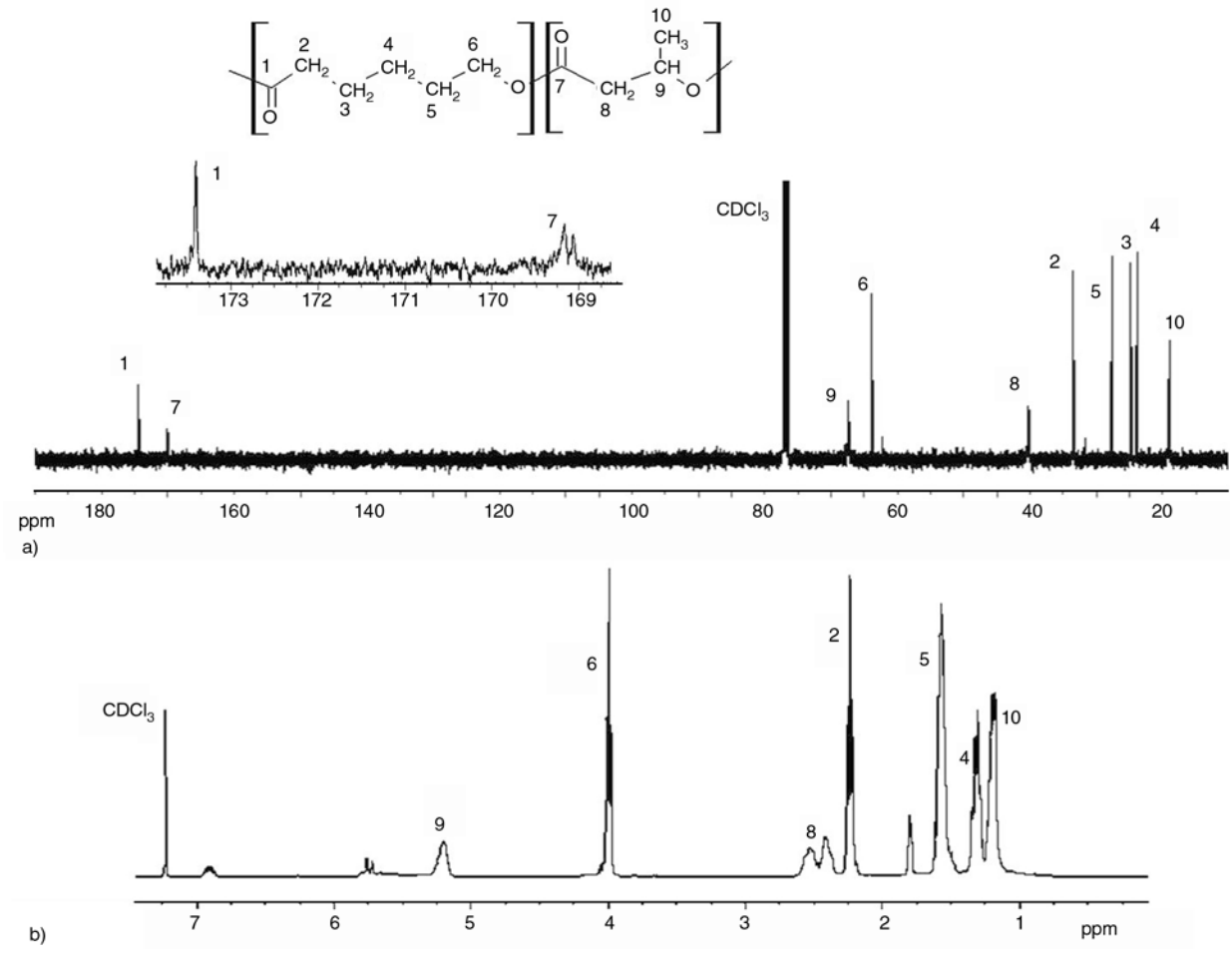

Figure 2. NMR spectra of the PCL-*block*-(*R,S*)-PBL 55/45 copolymer. a) ^{13}C-NMR, b) ^{1}H-NMR

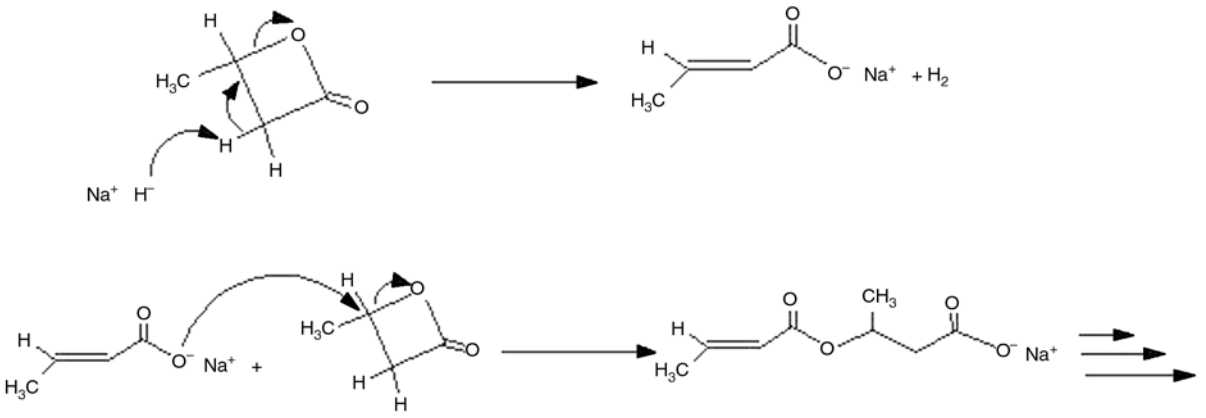

Figure 3. Initiating step in ring-opening copolymerization of (*R,S*)-PBL with CL [27, 33]

each step, and the composition of the copolymers suggest that the first step can be essentially attributed to the degradation of (*R,S*)-PBL moiety and the second one to the remaining PCL fraction.

On the other hand, the analysis by TVA was carried out to examine the volatiles produced during the degradation process. The degradation products were analyzed by ^{1}H-NMR. Figure 5 depicts the spectra of volatile fraction produced during the first degradation stage, in the range of 120 to 270°C, and it shows appreciable quantities of crotonic acid, which is well known to be one of the main degradation products of PBL, together with low molecular weight fractions of the (*R,S*)-PBL having crotonyl end groups [28, 42–45]. Additionally, the NMR spectra of the solid residue were identical to the

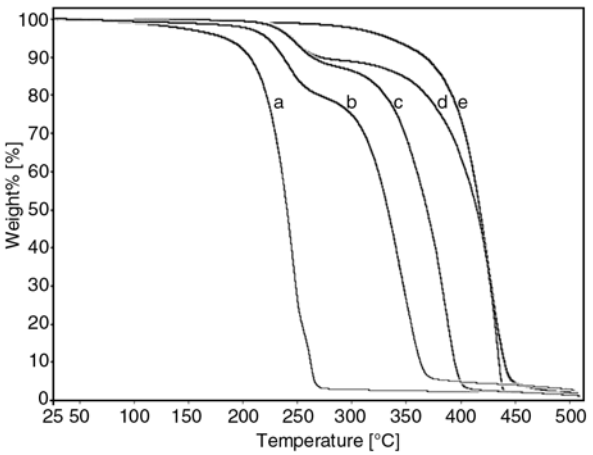

Figure 4. TGA curves under nitrogen atmosphere (10°C/min) of: a) (*R,S*)-PBL, b) block PCL/(*R,S*)-PBL 75/25, c) block PCL/(*R,S*)-PBL 83/17, d) block PCL/(*R,S*)-PBL 88/12, e) PCL

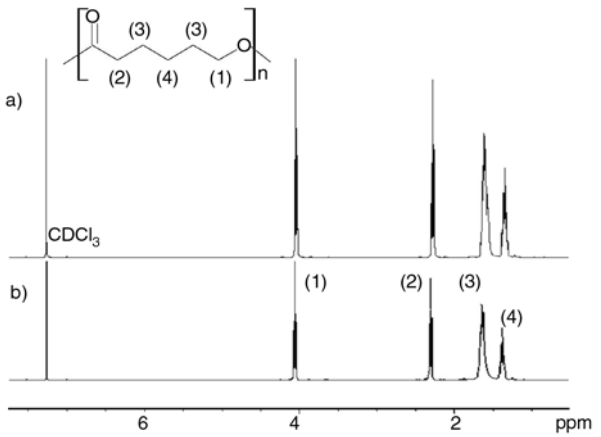

Figure 6. [1]H-NMR spectrum: a) PCL homopolymer (exp. 5, Table 2), b) solid residue obtained in the analysis by TVA

PCL homopolymer (Figure 6). These results confirm those obtained by TGA, which indicated that thermal degradation involves the occurrence of two distinct processes. The first one mainly involves the degradation of (*R,S*)-PBL block for which it has been proposed a random chain scission by β-elimination [43, 44] or an E1cB mechanism proceeding via α-deprotonation by carboxilate anion [45], both alternatives lead the same products: crotonic acid and oligomers with a crotonate end group [28, 42–45]. The second process is due to the degradation of the remaining PCL block.

3.3.2. Differential scanning calorimetry (DSC) and Wide angle X-ray scattering WAXS

In order to study the effect of the (*R,S*)-PBL blocks in the crystallization of PCL on the copolymer a combined study of DSC and WAXS was carried out.

In the DSC study all copolymers were first heated from –40 to 120°C to erase thermal history and

Table 3. TGA data of PCL, PBL and copolymers

Sample	Composition CL/(R,S)-BL [%p/p]		First step		Second step	
			Ti[a] [°C]	ΔW[b] [%]	Ti[a] [°C]*	ΔW[b] [%]
PCL	100	–	389.70	97.86	–	–
PCL-*block*-(*R,S*)-PBL (88/12)	90.67	9.33	229.35	11.07	411.31	88.85
PCL-*block*-(*R,S*)-PBL (83/17)	86.62	13.38	221.53	13.43	340.92	85.46
PCL-*block*-(*R,S*)-PBL (80/20)	84.13	15.87	219.65	18.08	327.24	77.85
PCL-*block*-(*R,S*)-PBL (75/25)	79.91	20.09	214.40	20.27	309.79	75.75
PBL	–	100	191.18	94.80	–	–

[a] Temperature at the inflection point

[b] Total weight loss percentage at the end of the step

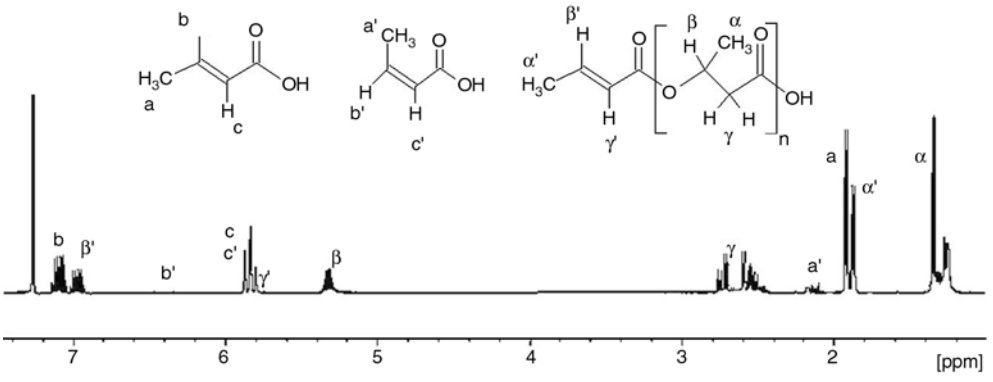

Figure 5. [1]H-NMR spectrum of volatile fraction obtained in the analysis by TVA

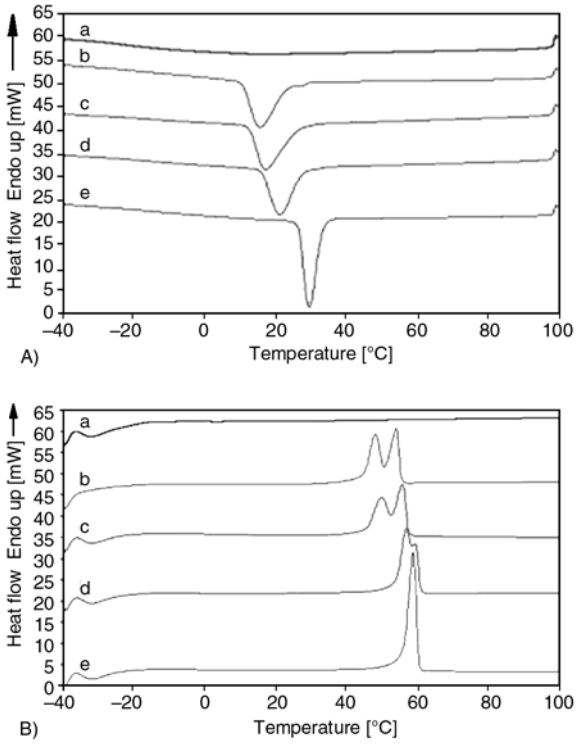

Figure 7. DSC (7-A) cooling and (7-B) second heating curves (10°C/min) of the (*R,S*)-PBL, PCL and the copolyesters obtained: a) (*R,S*)-PBL, b) block PCL/(*R,S*)-PBL 75/25, c) block PCL/(*R,S*)-PBL 80/20, d) block PCL/(*R,S*)-PBL 88/12, e) PCL

subsequently cooled to –40°C and heated back to 120°C. Analyses are based on first cooling and second heating and the resulting thermograms are plotted in Figure 7. The transition temperatures values are listed in Table 4. It can be observed in Figure 7A, that, as expected, the (*R,S*)-PBL do not show any exothermal peak, whereas the PCL shows one at about 33°C; for the copolyesters the peak moves towards lower temperatures when the butyroyl units content increases. This could be indicating that the (*R,S*)-PBL segment in the copolyesters may hinder crystallization of the PCL segment as their crystallization needs greater undercooling during the crystallization process. On the other hand, the DSC heating curves (Figure 7B), for (*R,S*)-PBL homopolymer doesn't show any melting endotherms, whereas the PCL exhibit a melting endotherm at about 55°C. The copolyesters display endotherms very close to the melting temperature of PCL homopolymer and the melting enthalpies of these are not influenced by the (*R,S*)-PBL content; they remain about 63 $J \cdot g^{-1}$.

Additionally, the most striking feature in Figure 7B is that all the DSC melting traces of the copolyesters show bimodal melting peaks, whereas the DSC melting curve of PCL only reveals a single peak in the absence of (*R,S*)-BL. In general, these peaks are attributed to a crystalline reorganization via melting, re-crystallization and re-melting at higher temperature [8, 46–48].

The lower temperature peak in DSC curves corresponds to the melting of unstable crystals formed during the cooling process due a (*R,S*)-PBL block in the copolymer. The slight shift of the melting peak to lower temperatures with increased (*R,S*)- BL content, suggests that crystals with lower thermal stability had been formed [46]. The higher temperature peak should be attributed to crystals recrystallized during the DSC heating process [8, 48].

The DSC results were confirmed by WAXS experiments carried out for some PCL-*block*-(*R,S*)-PBL copolymers at different temperatures. In Figure 8 the X-ray diffraction patterns of PCL-*block*-(*R,S*)-PBL, 80/20, recorded at different temperatures are shown. At 45°C the diffractograms are identical to those obtained at room temperature. In Figure 8a, the Bragg peaks characteristic of the orthorhombic PCL crystals [49] (Space group $P2_12_12_1$, a = 7.496 Å, b = 4.974 Å, c = 17.297 Å) are observed together with broad bands which correspond to the scattering by disordered regions. At 60°C (Figure 8b) the amount of crystalline regions has decreased significantly and the spectrum recorded at 70°C show a total absence of crystalline order,

Table 4. DSC results of PCL and copolymers in the cooling and second heating scans

Sample	ΔH_{total} [$J \cdot g^{-1}$]	T_{m1} [°C]	T_{m2} [°C]	ΔH_c [$J \cdot g^{-1}$]	T_c [°C]
PCL	75.04	55.45	–	–72.09	33.13
PCL-*block*-(*R,S*)-PBL (88/12)	63.26	54.20	57.03	–63.98	21.47
PCL-*block*-(*R,S*)-PBL (80/20)	63.62	47.37	53.20	–61.93	17.47
PCL-*block*-(*R,S*)-PBL (75/25)	63.50	46.87	53.03	–60.76	17.47

T_{m2} denotes the melting point of the second peak in the bimodal endotherm
ΔH_{total} denote total heat of melting
ΔH_c denotes heat of crystallization
T_c denotes temperature of crystallization

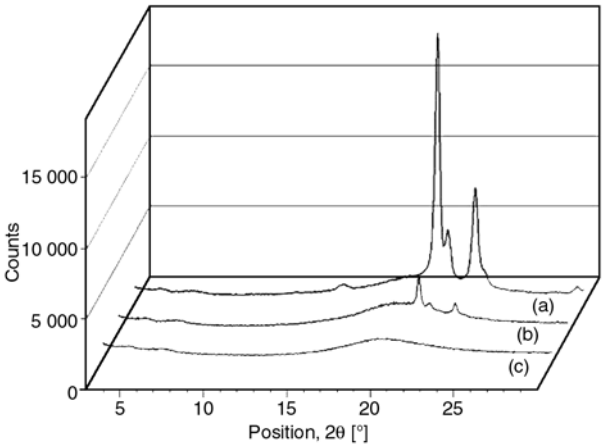

Figure 8. Diffractograms of copolymer 80/20 at different temperatures: (a) 45°C, (b) 60°C, (c) 70°C

the sample is 100% amorphous as revealed by the sole presence of broad amorphous halos. These results confirm the DSC determinations and show that the melting peaks are due to the PCL blocks whose behaviour is not affected by the presence of PBL blocks. This behaviour is to be expected as the blending [50, 51] or copolynerization of PCL [52] with a broad variety of homopolymers have always preserved the crystralline strcture of PCL.

4. Conclusions

Copolymers of CL/(*R,S*)-BL could be synthesized by ring-opening copolymerization using NaH as initiator. NMR spectroscopic analysis show block sequences in these copolyesters, in which the content of (*R,S*)-BL units was in all cases lower than expected from the feed ratio; its proportion in the copolymers is almost constant regardless of the feed ratio. This indicates that in the reaction mixture, the first stage polymerization could consist of BL, thus obtaining relatively short chain segment of PBL with active carboxylate ions which subsequently induce the polymerization of CL via alkoxide ion producing chain segment PCL relatively longer. The catalyst concentration and the monomer feed ratios had strong effects on yield, while the molecular weights do not depend significantly on the feed ratio.

The thermal stability of the prepared copolymers studied by TGA and TVA showed that they are stable up to temperatures near 200°C, when the decomposition process begins in two steps, the first one due to the (*R,S*)-BL block degradation and the second to the remaining PCL block. The DSC and WAXS results indicate that the copolymers contain one cristallizable block of PCL, which crystallization and melting behaviors are slightly affected by composition.

Acknowledgements

This work has been supported by CDCHT-ULA (grants C-1517-07-08-A and C1522-07-08-F) and by DID-USB (DID-G15) and FONACIT (F2005-000284). The authors also thank the Laboratorio Nacional de RMN Nodo ULA (Mérida Venezuela) for NMR facilities.

References

[1] Vert M.: Bioresorbable polymers for temporary therapeutic applications. Die Angewandte Makromolekulare Chemie, **166**, 155–168 (1989).
DOI: 10.1002/apmc.1989.051660111

[2] Dobrzynski P.: Synthesis of biodegradable copolymers with low-toxicity zirconium compounds. III. Synthesis and chain-microstructure analysis of terpolymer obtained from L-lactide, glycolide, and ε-caprolactone initiated by zirconium(IV) acetylacetonate. Journal of Polymer Science Part A: Polymer Chemistry, **40**, 3129–3143 (2002).
DOI: 10.1002/pola.10401

[3] Ashammakhi N., Mäkelä E. A., Vihtonen K., Rokkanen P., Törmälä P.: Effect of self-reinforced polyglycolide membranes on cortical bone: An experimental study on rats. Journal of Biomedical Materials Research, **29**, 687–694 (1995).
DOI: 10.1002/jbm.820290603

[4] Stridsberg K., Albertsson A-C.: Controlled ring-opening polymerization of L-lactide and 1,5-dioxepan-2-one forming a triblock copolymer. Journal of Polymer Science Part A: Polymer Chemistry, **38**, 1774–1784 (2000).
DOI: 10.1002/(SICI)1099-0518(20000515)38:10<1774::AID-POLA620>3.0.CO;2-F

[5] Vanhoorne P., Dubois P., Jerome R., Teyssie P.: Macromolecular engineering of polylactones and polylactides. 7. Structural analysis of copolyesters of ε-caprolactone and L- or D,L-lactide initiated by triisopropoxyaluminum. Macromolecules, **25**, 37–44 (1992).
DOI: 10.1021/ma00027a008

[6] Kricheldorf H. R., Rost S.: A-B-A-triblock and multiblock copolyesters prepared from ε-caprolactone, glycolide and L-lactide by means of bismuth subsalicylate. Polymer, **46**, 3248–3256 (2005).
DOI: 10.1016/j.polymer.2005.02.004

[7] Hiki S., Miyamoto M., Kimura Y.: Synthesis and characterization of hydroxy-terminated [RS]-poly(3-hydroxybutyrate) and its utilization to block copolymerization with L-lactide to obtain a biodegradable thermoplastic elastomer. Polymer, **41**, 7369–7379 (2000).
DOI: 10.1016/S0032-3861(00)00086-0

[8] Chen C., Peng S., Wu H., Zhuang Y., Chen X., Dong L., Feng Z.: Synthesis and characterizacion of poly(β-hydroxibutyrate) and poly(ε-caprolactone) copolyesters by transesterification. Journal of Polymer Science Part B: Polymer Physics, **40**, 1893–1903 (2002).
DOI: 10.1002/polb.10242

[9] Zhong Z., Yu D., Meng F., Gan Z., Ping X.: Controlled synthesis of L-lactide-*b*-ε-caprolactone block copolymers using a rare earth complex as catalyst. Polymer Journal, **31**, 633–636 (1999).
DOI: 10.1295/polymj.31.633

[10] Fukuzaki H., Yoshida M., Asano M., Kumakura M., Mashimo T., Yuasa H., Imai K., Yamanaka H.: Synthesis of low-molecular-weight copoly(L-lactic acid/ε-caprolactone) by direct copolycondensation in the absence of catalysts, and enzymatic degradation of the polymers. Polymer, **31**, 2006–2014 (1990).
DOI: 10.1016/0032-3861(90)90031-S

[11] Vivas M., Mejías N., Contreras J.: Ring-opening polymerization of lactones initiated by diphenylzinc-coinitiator systems. Polymer International, **52**, 1005–1009 (2003).
DOI: 10.1002/pi.1183

[12] Abe H., Matsubara I., Doi Y., Hori Y., Yamaguchi A.: Physical properties and enzymic degradability of poly(3-hydroxybutyrate) stereoisomers with different stereoregularities. Macromolecules, **27**, 6018–6025 (1994).
DOI: 10.1021/ma00099a013

[13] Kricheldorf H. R., Lee S-R.: Polylactones. 35. Macrocyclic and stereoselective polymerization of β-D,L-butyrolactone with cyclic dibutyltin initiators. Macromolecules, 28, 6718–6725 (1995).
DOI: 10.1021/ma00124a004

[14] Kohn F. E., Van Den Berg J., Van De Ridder G.: The ring-opening polymerization of D,L-lactide in the melt initiated with tetraphenyltin. Journal of Applied Polymer Science, **29**, 4265–4277 (1984).
DOI: 10.1002/app.1984.070291255

[15] Grijpma D. W., Pennings A. J.: Polymerization temperature effects on the properties of L-lactide and ε-caprolactone copolymers. Polymer Bulletin, **25**, 335–341 (1991).
DOI: 10.1007/BF00316903

[16] Storey R. F., Herring K. R., Hoffman D. C.: Hydroxy-terminated poly(ε-caprolactone-co-δ-valerolactone) oligomers: Synthesis, characterization, and polyurethane network formation. Journal of Polymer Science Part A: Polymer Chemistry, **29**, 1759–1777 (1991).
DOI: 10.1002/pola.1991.080291209

[17] Kricheldorf H. R., Lee S., Scharnagl N.: Polylactones. 28. Syndiotactic poly(β-D,L-hydroxybutyrate) by ring-opening polymerization of β-D,L-butyrolactone with butyltin methoxides. Macromolecules, **27**, 3139–3146 (1994).
DOI: 10.1021/ma00090a005

[18] Kricheldorf H.R., Eggerstedt S.: Polylactones: 41. Polymerization of β-D,L-butyrolactone with dialkyltinoxides as initiators. Macromolecules, **30**, 5693–5697 (1997).
DOI: 10.1021/ma970244c

[19] Nakayama A., Kawasaki N., Maeda Y., Arvanitoyannis I., Aiba S., Yamamoto N.: Study of biodegradability of poly(δ-valerolactone-*co*-L-lactide)s. Journal of Applied Polymer Science, **66**, 741–748 (1997).
DOI: 10.1002/(SICI)1097-4628(19971024)66:4<741::AID-APP14>3.0.CO;2-U

[20] Nakayama A., Kawasaki N., Aiba S., Maeda Y., Arvanitoyannis I., Yamamoto N.: Synthesis and biodegradability of novel copolyesters containg γ-butyrolactone units. Polymer, **39**, 1213–1222 (1998).
DOI: 10.1016/S0032-3861(97)00401-1

[21] Kricheldorf H. R., Bornhorst K., Hachmann-Thiessen H.: Bismuth(III) n-hexanoate and Tin (II) 2-ethylhexanoate initiated copolymerizations of ε-caprolactone and L-lactide. Macromolecules, **38**, 5017–5024 (2005).
DOI: 10.1021/ma047873o

[22] Piao L., Deng M., Chen X., Jiang L., Jing X.: Ring-opening of ε-caprolactone and L-lactide using organic aminocalcium catalyst. Polymer, **44**, 2331–2336 (2003).
DOI: 10.1016/s0032-3861(03)00118-6

[23] Zhong Z., Ankoné M., Dijkstra P. J., Birg C., Westerhausen M., Feijen J.: Calcium methoxide initiated ring-opening polymerization of ε-caprolactone and L-lactide. Polymer Bulletin, **46**, 51–57 (2001).
DOI: 10.1007/s002890170088

[24] Vivas M., Contreras J.: Ring-opening polymerization of ε-caprolactone initiated by diphenylzinc. European Polymer Journal, **39**, 43–47 (2003).
DOI: 10.1016/S0014-3057(02)00190-8

[25] Contreras J., Dávila D.: Ring-opening copolymerization of L-lactide with ε-caprolactone initiated by diphenylzinc. Polymer International, **55**, 1049–1056 (2006).
DOI: 10.1002/pi.2050

[26] Dobrzynski P.: Synthesis of biodegradable copolymers with low-toxicity zirconium compounds. II. Copolymerization of glycolide with ε-caprolactone initiated by zirconium(IV) acetylacetonate and zirconium(IV) chloride. Journal of Polymer Science Part A: Polymer Chemistry, **40**, 1379–1394 (2002).
DOI: 10.1002/pola.10222

[27] Kurcok P., Matuszowics A., Jedliński Z.: Anionic polymerization of β-lactones initiated with potassium hydride. A convenient route to polyester macromonomers. Macromolecular Rapid Communication, **16**, 201–206 (1995).
DOI: 10.1002/marc.1995.030160308

[28] Kurcok P., Kowalczuk M., Hennek K., Jedlinsky Z.: Anionic polymerization of β-lactones initiated with alkali-metal alkoxides: Reinvestigation of the polymerization mechanism. Macromolecules, **25**, 2017–2020 (1992).
DOI: 10.1021/ma00033a027

[29] Kurcok P., Dubois P., Sikorska W., Jedlinsky Z., Jèrôme R.: Macromolecular engineering of lactones and lactides. 24. Controlled synthesis of (R,S)-β-butyrolactone-*b*-ε-caprolactone block copolymers by anionic and coordination polymerization. Macromolecules, **30**, 5591–5595 (1997).
DOI: 10.1021/ma970212p

[30] Liu K., Goh S., Li J.: Controlled synthesis and characterizations of amphiphilic poly[(R,S)-3-hydroxybutyrate]-poly(ethylene glycol)-poly[(R,S)-3-hydroxybutyrate] triblock copolymers. Polymer, **49**, 732–741 (2008).
DOI: 10.1016/j.polymer.2007.12.017

[31] Adamus G., Kowalczuk M.: Anionic ring-opening polymerization of β-alkoxymethyl-substituted β-lactones. Biomacromolecules, **9**, 696–703 (2008).
DOI: 10.1021/bm701077v

[32] Yu G., Marchessault R. H.: Characterization of low molecular weight poly(β-hydroxybutyrate)s from alkaline and acid hydrolysis. Polymer, **41**, 1087–1098 (2000).
DOI: 10.1016/S0032-3861(99)00230-X

[33] Jedliński Z., Kowalczuk M., Kurcok P.: Polymerization of β-lactones initiated by alkali metal naphthalenides. A convenient route to telechelic polymers. Journal of Macromolecular Science Part A, **29**, 1223–1230 (1992).
DOI: 10.1080/10601329208054152

[34] Duda A.: Anionic polymerization of 4-methyl-2-oxetanone (β-butyrolactone). Journal of Polymer Science Part A: Polymer Chemistry, **30**, 21–29 (1992).
DOI: 10.1002/pola.1992.080300103

[35] Kurcok P., Matuszowicz A., Jedliński Z., Kricheldorf H. R., Dubois P., Jèrôme R.: Substituent effect in anionic polymerization of β-lactones initiated by alkali metal alkoxides. Macromolecular Rapid Communication, **16**, 513–519 (1995).
DOI: 10.1002/marc.1995.030160709

[36] Jedlińsky Z., Kowalczuk M., Kurcok P., Adamus G., Matuszuwicz A., Sikorska W., Gross R. A., Xu J., Lenz R. W.: Stereochemical control in the anionic polymerization of β-butyrolactone initiated with alkali-metal alkoxides. Macromolecules, **29**, 3773–3777 (1996).
DOI: 10.1021/ma951888s

[37] Kurcok P., Dubois P., Jèrôme R.: Polymerization of β-butyrolactone initiated with $Al(O^iPr)_3$. Polymer International, **41**, 479–485 (1999).
DOI: 10.1002/(SICI)1097-0126(199612)41:4<479::AID-PI652>3.0.CO;2-w

[38] Kurcok P., Śmiga M., Jedlińsky Z.: β-butyrolactone polymerization initiated with tetrabutylammonium carboxylates: A novel approach to biomimetic polyester synthesis. Journal of polymer Science Part A: Polymer Chemistry, **40**, 2184–2189 (2002).
DOI: 10.1002/pola.10285

[39] Arkin A. H., Hazet B., Adamus G., Kuwalczuk M., Jedlińsky Z., Lenz R. W.: Synthesis of poly(2-methyl-3-hydroxyoctanoate) via anionic polymerization of α-methyl-β-pentyl-β-propiolactone. Biomacromolecules, **2**, 623–627 (2001).
DOI: 10.1021/bm015528q

[40] Kawalec M., Śmiga-Matuszowicz M., Kurcok P.: Counterion and solvent effects on the anionic polymerization of β-butyrolactone initiated with acetic acid salts. European Polymer Journal, **44**, 3556–3563 (2008).
DOI: 10.1016/j.eurpolymj.2008.09.008

[41] Kricheldorf H. R., Mang T., Jonté J. M.: Polylactones. 1. Copolymerizations of glycolide and ε-caprolactone. Macromolecules, **17**, 2173–2181 (1984).
DOI: 10.1021/ma00140a051

[42] Aoyagi Y., Yamashita K., Doi Y.: Thermal degradation of poly[(R)-3-hydroxybutyrate], poly[ε-caprolactone], and poly[(S)-lactide]. Polymer Degradation and Stability, **76**, 53–59 (2002).
DOI: 10.1016/S0141-3910(01)00265-8

[43] Gonzalez A., Irusta L., Fernández-Berridi M. J., Iriarte M., Iruin J. J.: Application of pyrolysis/gas chromatography/Fourier transform infrared spectroscopy and TGA techniques in the study of thermal degradation of poly (3-hydroxybutyrate). Polymer Degradation and Stability, **87**, 347–354 (2005).
DOI: 10.1016/j.polymdegradstab.2004.09.005

[44] Ariffin H., Nishida H., Shirai Y., Hassan M. A.: Determination of multiple thermal degradation mechanisms of poly(3-hydroxybutyrate). Polymer Degradation and Stability, **93**, 1433–1439 (2008).
DOI: 10.1016/j.polymdegradstab.2008.05.020

[45] Kawalec M., Adamus G., Kurcok P., Kowalczuk M., Foltran I., Focarete M. L., Scandola M.: Carboxylate-induced degradation of poly(3-hydroxybutyrate)s. Biomacromolecules, **8**, 1053–1058 (2007).
DOI: 10.1021/bm061155n

[46] Pearce R., Marchessault R. H.: Multiple melting in blends of isotactic and atactic poly(β-hydroxybutyrate). Polymer, **35**, 3990–3997 (1994).
DOI: 10.1016/0032-3861(94)90285-2

[47] Gunaratne L. M., Shanks R. A.: Multiple melting behaviour of poly(3-hydroxybutyrate-co-hydroxyvalerate) using step-scan DSC. European Polymer Journal, **41**, 2980–2988 (2005).
DOI: 10.1016/j.eurpolymj.2005.06.015

[48] Yoo E. S., Im S. S.: Melting behavior of poly(butylene succinate) during heating scan by DSC. Journal of Polymer Science Part B: Polymer Physics, **37**, 1357–1366 (1999).
DOI: 10.1002/(SICI)1099-0488(19990701)37:13<1357::AID-POLB2>3.0.CO;2-Q

[49] Bittiger H., Marchessault R. H., Niegisch W.D.: Crystal structure of poly-ε-caprolactone. Acta Crystallographica, **B26**, 1923–1927 (1970).
DOI: 10.1107/S0567740870005198

[50] Herrera D., Zamora J-C., Bello A., Grimau M., Laredo E., Müller A. J., Lodge T.: Miscibility and crystallization in polycarbonate/poly(ε-caprolactone) blends: Application of the self-concentration model. Macromolecules, **38**, 5109–5120 (2005).
DOI: 10.1021/ma050481c

[51] Balsamo V., Newman D., Gouveia L., Herrera L., Grimau M., Laredo E.: Molecular dynamics and crystallization kinetics in PSMA14/PCL blends. Polymer, **47**, 5810–5820 (2006).
DOI: 10.1016/j.polymer.2006.06.019

[52] Laredo E., Hernández M. C., Bello A., Grimau M., Müller A., Balsamo V.: Local and segmental dynamics in homopolymer and triblock copolymers with one semicrystalline block. Physical Review E, **65**, 021807/1–021807/13 (2002).
DOI: 10.1103/PhysRevE.65.021807

eXPRESS Polymer Letters Vol.4, No.7 (2010) 442–449
Available online at www.expresspolymlett.com
DOI: 10.3144/expresspolymlett.2010.55

Synthesis, characterization of polytridecamethylene 2,6-naphthalamide as semiaromatic polyamide containing naphthalene-ring

S. H. Yang[1], P. Fu[1], M. Y. Liu[1], Y. D. Wang[1], Y. C. Zhang[2], Q. X. Zhao[1]*

[1]School of Materials Science and Engineering, Zhengzhou University, 75 Daxue Road, Zhengzhou 450052, China
[2]High and New Technology Research Center of Henan Academay of Sciences, 56 Hongzhuan Road, Zhengzhou 450002, China

Received 17 March 2010; accepted in revised form 7 May 2010

Abstract. A novel engineering plastic polytridecamethylene 2,6-naphthalamide (PA13N) was prepared via a reaction of 2,6-naphthalene dicarboxylic acid and 1,13-tridecanediamine through a three-step procedure. The structure of synthesized PA13N was characterized by elemental analysis, Fourier transform infrared (FT-IR) spectroscopy and proton nuclear magnetic resonance (^{1}H-NMR). The thermal behaviors were determined by differential scanning calorimetry (DSC), thermogravimetric analysis (TGA) and dynamic mechanical analysis (DMA). The solubility, water-absorbing capacity, and mechanical properties of PA13N have also been investigated. Melting temperature (T_m), glass transition temperature (T_g) and decomposition temperature (T_d) of PA13N are 288, 129 and 492°C, respectively. The results show that the heat resistance and mechanical properties of PA13N are near to those of polynonamethylene terephthalamide (PA9T), and PA13N is a promising heat-resistant and processable engineering plastic.

Keywords: *mechanical properties, thermal properties, polyamides, synthesis, polycondensation*

1. Introduction

Aromatic polyamides and semiaromatic polyamides have been widely used in many industrial and commercial applications, especially in surface-mount technology and automobile industries, by virtue of their excellent characteristics such as good thermal stability, chemical resistance, low creep and high modulus [1–3]. The commonly mentioned aromatic and semiaromatic polyamides [4–15] cannot be processed by melt methods due to their high melting temperature and relatively lower decomposition temperatures [16–18]. Therefore, several approaches have been made through synthetic modification by the incorporation of flexible linkages [19, 20], bulky pendant groups [21] and non-coplanar biphenylene moieties [22] into the polymer backbones. Polynonamethylene terephthalamide (PA9T) inherits the merits of the heat resistance of aromatic polyamides and the processability of aliphatic polyamides [23]. However, the high cost of PA9T limited its applications.

In order to increase the processability and decrease the cost of semiaromatic polyamides, long flexible aliphatic chains are usually introduced into their backbones [24–26]. It has been reported that diacids with long molecular chains can be prepared from petroleum fermentation process using light wax as raw material [27], and the long chain diamines can be prepared from the corresponding long chain diacids by cyanation and amination process [28]. The cost of obtained long chain diacids and diamines was reduced accordingly.

*Corresponding author, e-mail: zhaoqingxiang1@126.com

It was noticeable that naphthalene-ring can be also introduced into the molecular chain of polyamides and high thermal stability was retained, as expected. However, the semiaromatic polyamides containing naphthalene-ring presented relatively low molecular weight and unsatisfactory performance which would not meet the requirements for commercialization [29–33]. Therefore, it is of great significance to synthesize novel, low-cost, high-performance and processable semiaromatic polyamides containing naphthalene-ring.

In this work, the polytridecamethylene 2,6-naphthalamide (PA13N) was successfully synthesized by the polycondensation reaction of 2,6-naphthalenedicarboxylic acid and 1,13-tridecanediamine in water. PA13N was investigated by Fourier transform infrared (FT-IR) spectroscopy, proton nuclear magnetic resonance (^{1}H-NMR), differential scanning calorimetry (DSC), thermo-gravimetric analysis (TGA) and dynamic mechanical analysis (DMA). Intrinsic viscosity, water-absorbing capacity and mechanical properties of PA13N were also studied.

2. Experimental

2.1. Materials

2,6-naphthalenediacrboxylic acid was purchased from Mitsubishi Gas Chemical Company, Inc (MGC, Japan). 1,13-tridecanediamine was provided commercially by Zibo Guangtong Chemical Limited Company (China), and purified by vacuum distillation prior to use.

2.2. Synthesis

PA13N was synthesized through a three-step procedure (Figure 1). 1,13-tridecanediamine (321 g, 1.5 mol) was dissolved in distilled water (1000 ml) at 90°C. Then the solution was added slowly into 500 ml of distilled water mixture of 2,6-naphthalene diacrboxylic acid (324 g, 1.5 mol) with vigorous stirring and then stirred for 2 h at 90°C. Finally a slight excess of 1,13-tridecanediamine (2 g, 0.01 mol) was added into the solution with continuous stirring for 1 h at 90°C. The pH value of the solution was adjusted to 7.2. The white 1,13-tridecanediamine-2,6-naphthalene diacrboxylic acid salt (PA13N salt) precipitated from the solution.

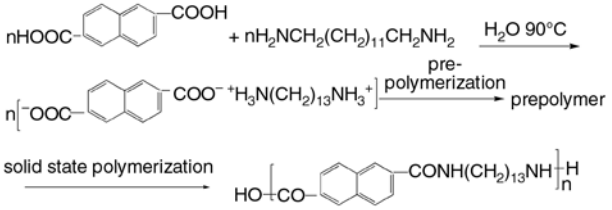

Figure 1. The synthetic route of PA13N

After filtering over a Buchner funnel and drying in a vacuum desiccator for 12 h, the white salt of PA13N (608.2 g) and distilled water (500 ml) were added into an autoclave. The autoclave was filled with carbon dioxide and then heated to 210°C while increasing the pressure to 2.1 MPa. After 2 h, the pressure of the autoclave was gradually decreased to normal pressure in 2 h by deflating and the reaction temperature of the autoclave was increased to 230°C. After reaction for another 1.5 h, the ivory-white prepolymer of PA13N was obtained (559.5 g).

The prepolymer of PA13N was ground into particles with diameter of 0.1~2 mm and dried at 90°C in a vacuum oven for 4 h. Then the prepolymer of PA13N was added into a solid-state polymerization kettle, the reaction was carried out at 230°C for 15 h with a vacuum of 10 Pa. Finally, the kettle was cooled to room temperature and straw yellow polymer of PA13N was obtained (539.9 g).

2.3. Characterizations

FT-IR, ^{1}H-NMR and elemental analysis were used to confirm the structure of PA13N. The thermal behaviors were determined by DSC, TGA and DMA. The solubility, intrinsic viscosity, water-absorbing capacity and mechanical properties of PA13N were also studied.

The intrinsic viscosity of PA13N dissolved in concentrated sulfuric acid was determined in an Ubbelohde viscometer at 25±0.1°C. The water-absorbing capacity of PA13N was measured according to GB/T1034 (Chinese standard).

The FT-IR measurement was carried out on a NICOLET 460 spectrometer (KBr pellet) in the range of 4000–400 cm^{-1} with the resolution of 4 cm^{-1}. The concentration of PA13N in KBr pellet (200 mg) was 1%. ^{1}H-NMR spectra was recorded with a Bruker DPX-400 (400 MHz), using deuterated trifluoroacetic acid as solvent and tetramethylsilane (TMS) as an internal reference. Elemental analysis was performed on a Perkin-Elmer 2400

CHNS/O elemental analyzer at 975°C under nitrogen.

Thermal analysis (DSC and TGA) was recorded on a NETSCH 204 calorimeter, using dry nitrogen flow as atmosphere with a flowing rate of 70 ml·min^{-1}. The conditions for the thermal analysis were summarized as follows: for DSC, the sample of PA13N (about 2 mg) was sealed in aluminum pan, then heated from 50 to 350°C at a heating rate of 10°C·min^{-1}; for TGA, the sample of PA13N (about 2 mg) was put in platinum open pan with a heating rate of 10°C·min^{-1} from 50 to 550°C. DMA was carried out on a NETZSCH DMA-242 apparatus with a heating rate of 3°C·min^{-1} from –170 to 170°C at 1 Hz. The sample geometry was 60 mm×12 mm×3.0 mm. The clamp configuration was 3-point bending, and the stress on the sample was 2 N. The static atmosphere was used in the DMA test.

All samples for mechanical tests were prepared by injection molding. The Izod impact strength was measured according to GB/T 1843 (Chinese standard). Tensile strength and elongation at break were measured according to GB/T 1040 (Chinese standard). Bending strength was measured according to GB/T 9341 (Chinese standard). All tests were carried out at room temperature (23°C). The resulting value of each sample was the average of five specimens.

3. Results and discussion

3.1. Synthesis of PA13N

PA13N was prepared from the reaction of 2,6-naphthalene dicarboxylic acid and 1,13-tridecanediamine through a three-step procedure: salt formation, prepolymerization and solid-state polymerization. In order to assure an accurate equivalent ratio of 1,13-tridecanediamine to 2,6-naphthalene dicarboxylic acid, PA13N salt was prepared firstly. Then a slight excess of 1,13-tridecanediamine was added into the salt solution to compensate reaction system for the loss during the prepolymerization reaction. It is noticeable that the solvent for the salt formation reaction is water, which is cheaper and environmental friendly compared with ethanol, usually used in preparing other common polyamides [34]. In order to obtain high vapor pressure, the distilled water was added to reduce volatilization of diamine during the prepolymerization. The prepolymer was ground into small particles, which are convenient for removing water. In order to avoid side reaction and to improve the molecular weight of the polyamide, the high vacuum was maintained during the solid-state polymerization reaction. The molecular weight of the PA13N was characterized by intrinsic viscosity. The intrinsic viscosity of PA13N is 1.91 dl·g^{-1}.

3.2. Fourier transform infrared spectra

FT-IR spectrum of the PA13N is shown in Figure 2. All the characteristic peaks of amide groups and methylene segments of polyamide are listed as follows: 1630 cm^{-1} (amide I, C=O stretching vibration), 1535 cm^{-1} (amide II, C–N stretching and CO–N–H bending vibration), 2921 cm^{-1} (N–H in-plane bending vibration and CH_2 vibration), 3291 cm^{-1} (hydrogen-bonded and N–H stretching vibration), 3074 cm^{-1} (N–H in-plane bending), 910 cm^{-1} (amide IV, C–CO stretching vibration), 820 cm^{-1} (CH_2 wagging), 766 cm^{-1} (C–H of naphthalene ring vibration).

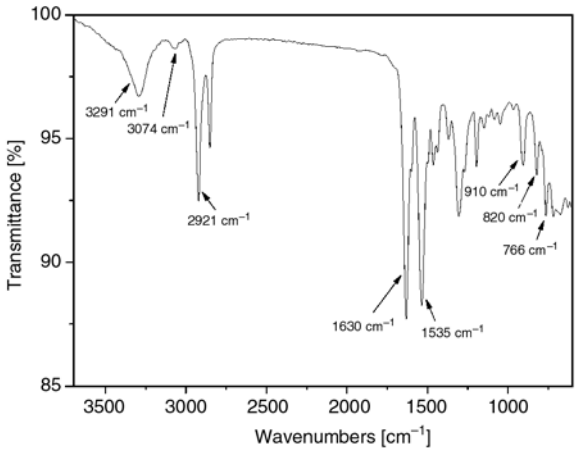

Figure 2. FT-IR spectra of PA13N

3.3. Proton nuclear magnetic resonance

Figure 3 presents the ^{1}H-NMR spectrum of PA13N in deuterated trifluoroacetic acid. The chemical shifts at 8.46 ppm (2H), 7.95 ppm (2H) and 8.16 ppm (2H) are attributed to the naphthalene ring protons (*a*, *b* and *c*). The chemical shift at 3.83 ppm (4H) originates from the protons at the position *d* while that at 1.88 ppm (4H) comes from the protons at the position *e*. The peak at 1.42 ppm

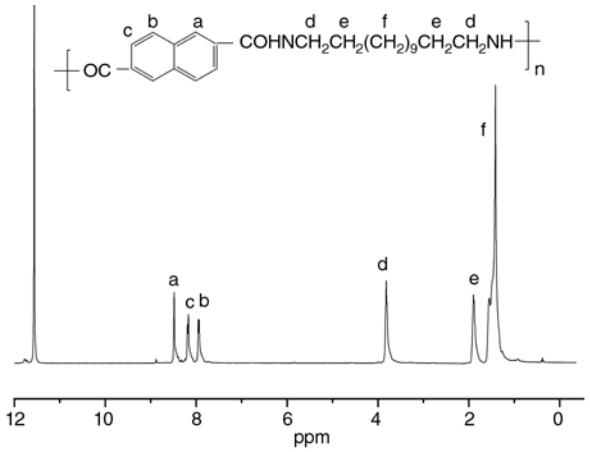

Figure 3. [1]H-NMR spectra of PA13N

(18H) belongs to the other protons of the aliphatic chains (*f*). The peak at 11.6 ppm was assigned to trifluoroacetic acid.

3.4. Elemental analysis

The elemental analysis data of PA13N are listed in Table 1. The calculated components are presented for comparison. The hydrogen content of PA13N is higher than the theoretical value owing to the absorption of water. The other measurement results are in agreement with the theoretical values.

3.5. Water absorption

The water-absorbing capacity of PA13N was measured according to GB/T1034 (Chinese standard), and the result is 0.07. The water-absorbing capacity of polydodecamethylene 2,6-naphthalamide (PA12N) was measured according to the same standard, and the result is 0.10. The low water absorption, close to PA9T (0.17), polydecamethylene 2,6-naphthalamide (PA10N) (0.14), polyundecamethylene 2,6-naphthalamide (PA11N) (0.12) and PA12N [35–37], is conducive to maintain dimensional and mechanical stability of products.

3.6. Solubility

The solubilities (sample 100 mg, solvent 10 ml) of PA13N were tested in different organic solvents. PA13N can easily dissolve in acidic solvents such as concentrated sulfuric acid and trifluoroacetic acid (TFA) at room temperature, while it is insoluble in dimethylsulphoxide (DMSO), N,N-dimethylformamide (DMF), 1-methyl-2-pyrrolidinone (NMP), dimethylacetamide (DMAc), m-cresol, tetrahydrofuran (THF), tetrachloroethane, chlorobenzene, pyridine, methanol, toluene, chloroform, phenol and formic acid.

3.7. Thermal behaviors

Figure 4 depicts the DSC curves of PA13N. Curve A is the second heating DSC curve with a heating rate of 10°C·min^{-1} from 50 to 320°C, while B is the cooling curve with a cooling rate of 10°C·min^{-1} from 320 to 50°C. The melting temperature (T_m) of PA13N is 288°C based on curve A, and the crystallization temperature (T_c) of PA13N is 251°C based on curve B. PA13N exhibits double-melting endotherms, which is a common phenomenon observed in semicrystalline polymers [38–40].

TGA curves of PA13N are shown in Figure 5. The curve A of PA13N shows a one-stage weight loss process in nitrogen. The decomposition temperature (T_d) is approximately 492°C, and the termination temperature of thermal degradation is about 500°C. The maximum degradation temperature (T_{max}) of PA13N is 474°C.

The T_m of PA13N is far below T_d of PA13N. Therefore, the melt processability of PA13N is excellent. In addition, the T_d of PA13N is higher than that of

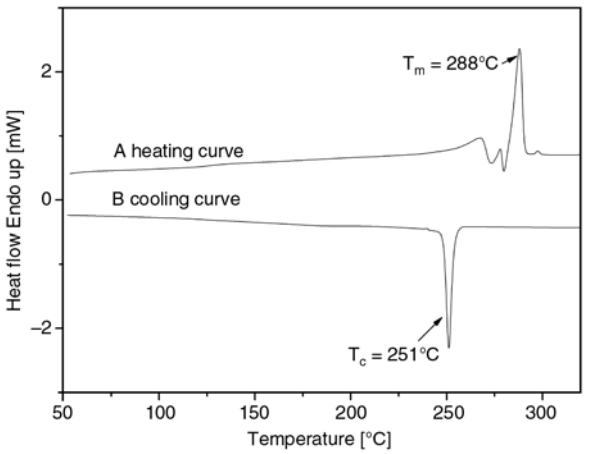

Figure 4. DSC curves of PA13N

Table 1. Elemental analysis data of PA13N

Sample	Carbon [%]		Hydrogen [%]		Nitrogen [%]		Oxygen [%]	
	Calculated	Measured	Calculated	Measured	Calculated	Measured	Calculated	Measured
PA11N	76.1	76.0	8.62	8.69	7.10	7.04	8.18	8.27

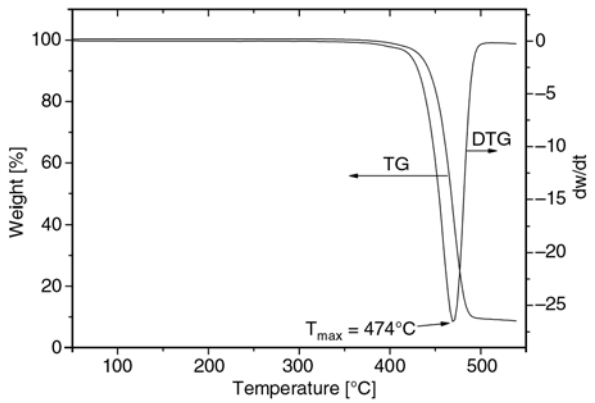

Figure 5. TGA curves of PA13N

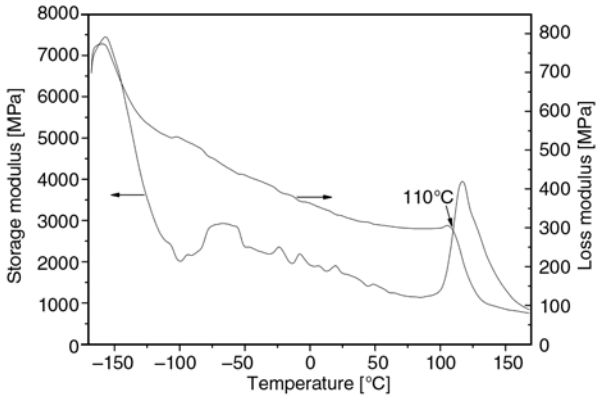

Figure 7. The storage modulus and loss modulus curves of PA13N (1 Hz)

aliphatic polyamides [41, 42]. The results show that the thermal stability of PA13N has been improved by inserting naphthalene linkage into the polymeric backbone.

DMA was also used to characterize the thermal property of PA13N (Figure 6 and Figure 7). As shown in Figure 6, three obvious transition behaviors can be observed, and are defined as α, β and γ relaxation, respectively. The glass transition temperature (T_g) of the PA13N is 129°C according to α relaxation. T_g of aliphatic polyamides such as poly(ε-caprolactam) (nylon6) (T_g = 60°C) and poly(hexamethylene adipamide) (nylon66) (T_g = 50°C) are all below 90°C. The results show that T_g of PA13N is higher than aliphatic polyamides. As expected, the heat-resistance of PA13N was improved by the introduction of naphthalene-ring. The β relaxation reflects the mobility of carbonyl group of amorphous region, and the γ relaxation reflects the simultaneous movement of amido and methane groups. Figure 7 displays the storage modulus and loss modulus curves of PA13N and illustrate the viscoelastic behavior of the PA13N. As shown in Figure 7, the PA13N has high storage moduli beyond $2 \cdot 10^3$ MPa below 110°C. When the temperature increased above 110°C, the storage modulus begins to decrease precipitously. The thermal data of PA13N in this work are listed in Table 2.

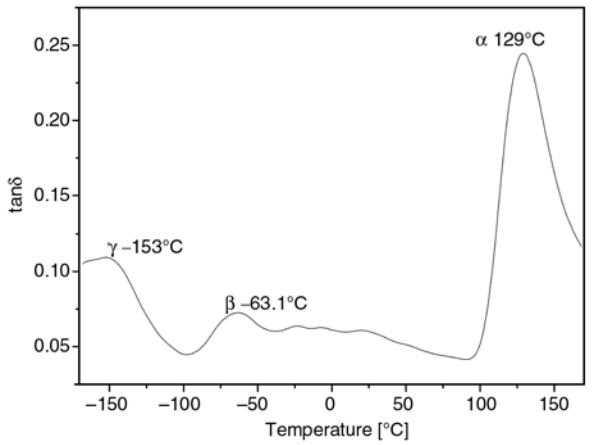

Figure 6. The tan delta curve of PA13N (1 Hz)

Table 2. The Intrinsic viscosity, thermal data and water-absorbing capacity of of PA10N, PA11N, PA12N and PA13N

Sample	[η] [dl·g^{-1}]	Tm [°C]	Tc [°C]	Td [°C]	Tg [°C]	Water-absorbing capacity [%]
PA13N	1.91	288	251	492	129	0.07
PA12N	1.84	299	273	498	120	0.10
PA11N	1.81	294	255	455	139	0.12
PA10N	1.85	320	297	495	144	0.14

Table 3. The mechanical properties of PA13N compared with PA10N, PA11N, PA12N and PA9T

Samples	Tensile strength [MPa]	Tensile modulus [GPa]	Breaking elongation [%]	Bending strength [MPa]	Bending modulus [GPa]	Izod impact strength [kJ·m^{-2}]
PA13N	90	1.7	56	80	1.9	5.1
PA12N	88	1.7	29	53	1.5	5.3
PA11N	89	1.8	54	76	1.8	5.3
PA10N	94	1.7	40	92	1.9	5.2
PA9T	92	–	20	120	2.6	4.9

3.8. Mechanical properties

All dry and standard samples of PA13N for mechanical tests were prepared by injection molding in an injection-molding machine. Based on Table 3, it can be observed that the tensile strength of PA13N is almost as same as that of PA9T [43], PA10N [36], PA11N [37] and PA12N [44] at room temperature.

4. Conclusions

PA13N with high molecular weight was prepared from the reaction of 2,6-naphthalene dicarboxylic acid and 1,13-tridecanediamine. The characterization of FT-IR, ^{1}H-NMR spectroscopy and elemental analysis confirmed that the obtained product has the expected chemical structure and composition. T_m, T_g and T_d of PA13N are 288, 129 and 492°C, respectively. The intrinsic viscosity of PA13N is 1.91 dl·g^{-1}. The results show that PA13N has better thermal stability than aliphatic polyamides. The low water absorption, close to PA9T, is conducive to maintain dimensional and mechanical stability of products for surface-mount technology. Compared with PA9T, the low cost and good performance of PA13N demonstrate it could be a promising, heat-resisting and well processable engineering plastic, and it can be a candidate nylon for the industrial production.

References

[1] Cassidy P. E.: Thermally stable polymers. Marcel Dekker, New York (1980).

[2] Persyn O., Miri V., Lefebvre J-M., Ferreiro V., Brink T., Stroeks A.: Mechanical behavior of films of miscible polyamide 6/polyamide 6I-6T blends. Journal of Polymer Science Part B: Polymer Physics, **44**, 1690–1701 (2006).
DOI: 10.1002/polb.20825

[3] Endo M., Morishima Y., Yano S., Tadano K., Murata Y., Tsunashima K.: Miscibility in binary blends of aromatic and alicyclic polyamides. Journal of Applied Polymer Science, **101**, 3971–3978 (2006).
DOI: 10.1002/app.22912

[4] Kwolek S. L.: Reflections on 'Interfacial polycondensation. II. Fundamentals of polymer formation at liquid interfaces'. Journal of Polymer Science Part A: Polymer Chemistry, **34**, 517–518 (1996).
DOI: 10.1002/pola.1996.813

[5] Liu X., Li T., Tian N., Liu W.: Study on tribological properties of frictional material based aromatic polyamide. Journal of Applied Polymer Science, **80**, 2790–2794 (2001).
DOI: 10.1002/app.1395

[6] Kudo K., Suguie T., Hirami M.: Melt-polymerized aliphatic-aromatic copolyamides. I. Melting points of nylon 66 copolymerized with aromatic diamines and terephthalic acid. Journal of Applied Polymer Science, **44**, 1625–1629 (1992).
DOI: 10.1002/app.1992.070440916

[7] Koichi U., Hirofumi K., Takashi Y., Hiroki Y.: Semi-aromatic polyamide resin. EP Patent: 1860134A1, Europe (2007).

[8] Ihara H., Kawahara N.: Injection molding nozzle for resin of highly temperature-dependent viscosity. U.S. Patent: 20020102323A1, USA (2002).

[9] Eersels K. L., Groeninckx G.: Influence of interchange reactions on the crystallization and melting behaviour of polyamide blends as affected by the processing conditions. Polymer, **37**, 983–984 (1996).
DOI: 10.1016/0032-3861(96)87281-8

[10] Ballistreri A., Garozzo D., Giuffrida M., Maravigna P.: Thermal decomposition processes in aliphatic-aromatic polyamides investigated by mass spectrometry. Macromolecules, **19**, 2693–2699 (1986).
DOI: 10.1021/ma00165a005

[11] Siciliano A., Severgnini D., Seves A., Pedrelli T., Vicini L.: Thermal and mechanical behavior of polyamide 6/polyamide 6I/6T blends. Journal of Applied Polymer Science, **60**, 1757–1764 (1996).
DOI: 10.1002/(SICI)1097-4628(19960606)60:10<1757::AID-APP29>3.0.CO;2-#

[12] Hu Y. S., Prattipati V., Mehta S., Schiraldi D. A., Hiltner A., Baer E.: Improving gas barrier of PET by blending with aromatic polyamides. Polymer, **46**, 2685–2698 (2005).
DOI: 10.1016/j.polymer.2005.01.056

[13] Uddin A. J., Ohkoshi Y., Gotoh Y., Nagura M., Hara T.: Influence of moisture on the viscoelastic relaxations in long aliphatic chain contained semiaromatic polyamide, (PA9-T) fiber. Journal of Polymer Science Part B: Polymer Physics, **41**, 2878–2891(2003).
DOI: 10.1002/polb.10602

[14] Uddin A. J., Ohkoshi Y., Gotoh Y., Nagura M., Endo R., Hara T.: Melt spinning and laser-heated drawing of a new semiaromatic polyamide, PA9-T fiber. Journal of Polymer Science Part B: Polymer Physics, **42**, 433–444 (2004).
DOI: 10.1002/polb.10710

[15] Uddin A. J., Gotoh Y., Ohkoshi Y., Nagura M., Endo R., Hara T.: Hydration in a new semiaromatic polyamide observed by humidity-controlled dynamic viscoelastometry and X-ray diffraction. Journal of Polymer Science Part B: Polymer Physics, **43**, 1640–1648 (2005).
DOI: 10.1002/polb.20446

[16] Ferreiro J. J., de la Campa J. G., Lozano A. E., de Abajo J.: Polyisophthalamides with heteroaromatic pendent rings: Synthesis, physical properties, and water uptake. Journal of Polymer Science Part A: Polymer Chemistry, **43**, 5300–5311 (2005). DOI: 10.1002/pola.21000

[17] Yang H. H.: Aromatic high-strength fibers. Wiley, New York (1989).

[18] Rao Y., Waddon A. J., Farris R. J.: Structure-property relation in poly(p-phenylene terephthalamide) (PPTA) fibers. Polymer, **42**, 5937–5946 (2001). DOI: 10.1016/S0032-3861(00)00905-8

[19] Spiliopoulos I. K., Mikroyannidis J. A., Tsivgoulis G. M.: Rigid-rod polyamides and polyimides derived from 4,3″-diamino-2′,6′-diphenyl- or di(4-biphenylyl)-p-terphenyl and 4-amino-4″-carboxy-2′,6′-diphenyl-p-terphenyl. Macromolecules, **31**, 522–529 (1998). DOI: 10.1021/ma9709664

[20] Liaw D-J., Liaw B-Y., Tseng J-M.: Synthesis and characterization of novel poly(amide-imide)s containing hexafluoroisopropylidene linkage. Journal of Polymer Science Part A: Polymer Chemistry, **37**, 2629–2635 (1999). DOI: 10.1002/(SICI)1099-0518(19990715)37:14<2629::AID-POLA37>3.0.CO;2-3

[21] Liaw D. J., Hsu P. N., Chen W. H., Lin S. L.: High glass transitions of new polyamides, polyimides, and poly(amide-imide)s containing a triphenylamine group: Synthesis and characterization. Macromolecules, **35**, 4669–4676 (2002). DOI: 10.1021/ma001523u

[22] Liaw D-J., Chang F-C., Leung M-K., Chou M-Y., Muellen K.: High thermal stability and rigid rod of novel organosoluble polyimides and polyamides based on bulky and noncoplanar naphthalene-biphenyl-diamine. Macromolecules, **38**, 4024–4029 (2005). DOI: 10.1021/ma048559x

[23] Ahmed J. U., Ohkoshi Y., Gotoh Y.: Melt spinning and laser-heated drawing of a new semiaromatic polyamide, PA9-T fiber. Journal of Polymer Science Part B: Polymer Physics, **42**, 433–444 (2004). DOI: 10.1002/polb.10710

[24] Wang W., Wang X., Li R., Liu B., Wang E., Zhang Y.: Environment-friendly synthesis of long chain semiaromatic polyamides with high heat resistance. Journal of Applied Polymer Science, **114**, 2036–2042 (2009). DOI: 10.1002/app.30774

[25] Wang W-Z., Zhang Y-H.: Environment-friendly synthesis of long chain semiaromatic polyamides. Express Polymer Letters, **3**, 470–476 (2009). DOI: 10.3144/expresspolymlett.2009.58

[26] Pei X., Zhao Q., Liu M., Wang Y., Wang W., Cao S.: Synthesis and characterization of two new semiaromatic polyamides (in Chinese). China Plastics Industrial, **33**, 7–9 (2005).

[27] Liu M., Zhao Q., Wang Y., Zhang C., Li X.: Synthesis, property and application of petroleum fermentation nylon 1212 (in Chinese). Engineering Plastics Application, **30**, 37–39 (2002).

[28] Jiang T., Liu M., Fu P., Wang Y., Fang Y., Zhao Q.: Melting behavior, isothermal and nonisothermal crystallization kinetics of nylon 1111. Polymer Engineering and Science, **49**, 1366–1374 (2009). DOI: 10.1002/pen.21269

[29] Wang C-H., Chen L-W.: Preparation and properties of aramids based on naphthalenedicarboxylic acid and their molecular composites with amorphous nylon. Angewandte Makromolekulare Chemie, **237**, 173–189 (1996). DOI: 10.1002/apmc.1996.052370110

[30] Caldwell J. R.: Verwendung von hochschmelzenden linearen Polyamiden zur Herstellung von Folien, Faeden oder Formteilen. German Patent DE1254347, Germany (1967).

[31] Yang C-P., Hsiao S-H., Lin Y-S.: Synthesis and properties of polyamides and copolyamides based on 2,6-naphthalene dicarboxylic acid. Journal of Applied Polymer Science, **51**, 2063–2072 (1994). DOI: 10.1002/app.1994.070511212

[32] Yang C-P., Hsiao S-H., Yang C-C.: Synthesis and properties of aromatic polyamides derived from 2,6-bis(4-aminophenoxy)naphthalene and various aromatic dicarboxylic acids. Journal of Polymer Science Part A: Polymer Chemistry, **35**, 2147–2156 (1997). DOI: 10.1002/(SICI)1099-0518(199708)35:11<2147::AID-POLA5>3.0.CO;2-V

[33] Hsiao S-H., Liou G-S.: Preparation and characterization of aromatic polyamides from 4,4′-(2,6-naphthylenedioxy)dibenzoic acid and aromatic diamines. Macromolecular Chemistry and Physics, **199**, 2321–2328 (1998). DOI: 10.1002/(SICI)1521-3935(19981001)199:10<2321::AID-MACP2321>3.3.CO;2-I

[34] Cui X. W., Li W. H., Yan D. Y.: Investigation on odd-odd nylons based on undecanedioic acid: 1. Synthesis and characterization. Polymer International, **53**, 1729–1734 (2004). DOI: 10.1002/pi.1546

[35] Zou S.: Heat resistant polyamide PA9T (in Chinese). Modern Plastics, **12**, 62–64 (2000).

[36] Yang S. H., Fu P., Liu M. Y., Wang Y. D., Li Z. P., Zhao Q. X.: Synthesis, characterization and thermal decomposition of poly(decamethylene 2,6-naphthalamide). Express Polymer Letters, **4**, 346–354 (2010). DOI: 10.3144/expresspolymlett.2010.44

[37] Yang S., Fu P., Liu M., Wang Y., Zhao Q.: Synthesis of polyundecamethylene 2,6-naphthalamide as semiaromatic polyamide containing naphthalene-ring. Journal of Applied Polymer Science. in press (2010). DOI: 10.1002/app.32471

[38] Li Y. J., Zhu X. Y., Tian G. H., Yan D. Y., Zhou E.: Multiple melting endotherms in melt-crystallized nylon 10,12. Polymer International, **50**, 677–678 (2001).
DOI: 10.1002/pi.682

[39] Ramesh C., Keller A., Eltink S. J.: Studies on the crystallization and melting of nylon 66: 3. Melting behaviour of negative spherulites by calorimetry. Polymer, **35**, 5300–5302 (1994).
DOI: 10.1016/0032-3861(94)90483-9

[40] Hybart F. J., Platt J. D.: The melting of 66 nylon: Observations by differential thermal analysis. Journal of Applied Polymer Science, **11**, 1449–1453 (1967).
DOI: 10.1002/app.1967.070110808

[41] Wang Y., Liu M., Zhao Q.: Studies on the process and kinetics of thermal degradation in nylon 109 (in Chinese). Polymeric Materials Science and Engineering, **15**, 78–80 (1999).

[42] Zhao Q., Wang Y., Liu M., Du B., Li H., Li X.: Study on process and kinetics of thermal degradation in nylon 69 (in Chinese). Polymeric Materials Science and Engineering, **11**, 52–56 (1995).

[43] Ma J. M., Song S. W., Guo J.: New heat resistance polyamide (in Chinese). Modern Plastics, **15**, 41–44 (2003).

[44] Yang S., Liu M., Wang Y., Fu P., Chen Z., Zhang Y., Zhao Q.: Synthesis and characterization of PA12N (in Chinese). Material Science and Technology, **16**, 117–119 (2008).

eXPRESS Polymer Letters Vol.4, No.7 (2010) 450–454
Available online at www.expresspolymlett.com
DOI: 10.3144/expresspolymlett.2010.56

A novel reversible thermo-swelling hydrogel

J. Q. Wang[1,2*], *M. Satoh*[2]

[1]School of Materials Science and Engineering, Beijing Institute of Technology, Beijing, 100081, P. R. China
[2]Department of Chemistry and Materials Science, Tokyo Institute of Technology, Tokyo, 152-8550, Japan

Received 23 March 2010; accepted in revised form 7 May 2010

Abstract. A novel reversible thermo-swelling gel was prepared from poly(vinyl alcohol)-trimellitate (PVA-T) by crosslinking with ethylene glycol diglycidyl ether (EGDGE). Only in the presence of sulfate anion, this polymer gel showed a significant and reversible swelling behavior with increasing the temperature from 5 to 40°C, and vice versa, probably due to the scission and formation of the inter- and/or intramolecular hydrogen-bondings (HBs) between the carboxyls on the side groups. The involvement of inter- and/or intramolecular HBs for the thermo-swelling behavior was also suggested by a significant dependence on HCl concentration of the swelling degree. In addition, the swelling reversibility and reproducibility were confirmed via the temperature jump between 5 and 40°C, well satisfying for a candidate as a thermo-sensitive material.

Keywords: *polymer gels, reversible thermo-swelling, Hofmeister Series*

1. Introduction

In a hydrogel, a few interactions, such as van der Waals, ionic, hydrophobic and hydrogen-bonding, are exerted among macromolecules, water and other substances to determine the swelling degree. Any change in the interactions will cause a variation in the gel size, sometimes dramatically as the volume phase transition [1]. Thus, an external stimulus such as temperature, pH, ionic strength, solvent, and so on may change the gel size via alteration in the interactions.

Among the external stimuli, the temperature effect has been most extensively studied and hydrogels prepared from poly(N-isopropylacrylamide) (PNIPAAm) must be the most typical as a thermo-responsive polymer gel. This polymer has a lower critical solution temperature (LCST) in water, and the LCST could be changed to different extents by various modifications [2]. In addition, it has also been found that poly(N,N-diethylacrylamide), poly(N-vinylcaprolactam), poly(2-isopropyl-2-oxazoline) and poly(vinyl methyl ether) have LCST in water [3–6]. For these thermo-responsive polymers, one common feature is that the hydrophobic interaction drives the aggregation of macromolecules to induce the collapse above the LCST, and another is that the swollen (or hydrated) state can be recovered by decreasing the temperature, namely, the swelling-collapse cycle can be reversibly repeated. The hydrogen bond is also sensitive to temperature and may be utilized as a main interaction causing a thermo-swelling of relevant hydrogels. In fact, Tanaka *et al.* [1] firstly found that poly(acrylamide)/ poly(acrylic acid) interpenetrating network (PAAm/ PAA IPN) gel revealed a reversible discontinuous transition with temperature. Further they also proved that hydrogen-bonding (HB) is the driving force for the transition on the basis of the urea effect because HB is the only attractive force in PAAm/PAA IPN to induce the collapse at low temperature. To our best knowledge, this somewhat sophisticatedly prepared hydrogel is the only one

*Corresponding author, e-mail: jqwang@bit.edu.cn

example that shows a reversible gel swelling and deswelling with temperature increasing and decreasing, respectively, on the basis of HB interaction.

Recently, Suzuki and coworkers reported that poly(sodium acrylate) (PSA) and poly(N-isopropylacrylamide-co-sodium acrylate) (NIPA-SA) gels deswelled under repeated exchange of external water, which was attributed to protonation of the carboxyl groups and the resultant formation of inter- and/or intramolecular HBs between –COOHs. Further interestingly, the gels showed a discontinuous reswelling at a certain elevated temperature because of the destruction of HBs [7, 8]. However, the thermo-swelling was not reversible; namely, with decreasing the temperature the gel kept the swollen state.

In the present letter, we report a novel reversible thermo-swelling gel prepared from poly(vinyl alcohol)-trimellitate (PVA-T) by a chemical crosslinking. This polymer gel is collapsed in water due to intermolecular HBs among –COOHs at the side groups [9, 10], and shows no appreciable thermo-swelling. In the presence of sulfate anion, however, a significant and reversible swelling occurs with increasing the temperature, and vice versa. Although this swelling behavior is not a volume phase transition, the PVA-T gel is a first example showing a reversible thermo-swelling as a hydrogel that was prepared with a simple chemical crosslinking.

2. Experimentals

2.1. Preparation of PVA-T hydrogel samples

According to a procedure that was reported previously [10], PVA-T polymer was prepared by the esterification of PVA (degree of hydrolysis: 99–100 mol%, M_w: 86000, Acros) and trimellitic anhydride (Tokyo Chemical Industry) in dimethyl sulfoxide (Kanto Chemical), under the catalysis of 4-(N,N-dimethylamino)pyridine (Kanto Chemical) and triethylamine (Kanto Chemical). In this work, we used a PVA-T polymer with a rather high esterification degree (ED), i.e. 82 mol%, to get hydrogels crosslinked with ethylene glycol diglycidyl ether (Aldrich). The detailed procedure is given elsewhere [10], with the exception that the crosslinker was used as 10 mol% with respect to the amount of PVA-T side groups in this work. The rod-type gel samples were prepared in glass capillaries (φ = 0.69 mm) at 30°C for 24 h. After taken out, they were equilibrated to pure water and then to 1 mM HCl solution for several days with daily exchanging of the external solution. With this pretreatment, the carboxyl groups introduced to PVA at the side group (ca. 1.6 mol per vinyl alcohol residue) were protonized and kept in the undissociated state.

2.2. Temperature dependence of hydrogel swelling

The equilibrium gel diameter in 1 mM aqueous HCl was first determined as d_0 with an optical microscope (DIAPHOT 200, NIKON) at room temperature (ca. 25°C). Then the samples were immersed in different salt solutions (0.1–1 M Li_2SO_4, 1 M LiCl or LiSCN) containing 1 mM HCl or in pure water. In those experiments, the gel samples were small enough compared to the immersing solution (gel diameter: ca. 0.4 mm, length: ca. 3 mm, solution volume: 4 ml), and held in screw cap vials with 10 ml capacity. The swelling degree, defined as d/d_0 (d: gel diameter in the acidic salt solutions or in pure water), was measured as a function of temperature; the respective gel samples were first equilibrated in a water bath at 40±0.5°C for 48 h, and then the temperature was decreased by 5°C down to 5±0.5°C, by changing the bath temperature. It is worth noting that the gels were kept at a certain temperature for 24 h and the swelling was equilibrated. As for the sulfate system, the temperature dependence of the swelling degree was measured as a function of the Li_2SO_4 concentration (0.1–1 M with 1 mM HCl) and HCl concentration (0.1–5 mM with 0.5 M Li_2SO_4). Aside from the swelling measurement with the gradual temperature change, response and reversibility of the swelling degree to a temperature jump were measured by setting a gel sample, which had been measured in 0.5 M Li_2SO_4/1 mM HCl at 5±0.5°C, in a water bath of 40±0.5°C. After 24 h, the gel sample was set in another water bath of 5±0.5°C. This temperature jump was repeated twice as (5°C) – 40°C – 5°C – 40°C – 5°C.

3. Results and discussion

Hydrogel swelling properties reflect the nature of crosslinkages including chemical and physical ones within gels. In the present study, the latter involves

HBs between –COOH groups, –OH groups, –COOH/–OH, –COOH(–OH)/π electrons and π–π stacking of the benzene rings. All of them, especially the first one between –COOH groups, seemed to be responsible for the collapse of PVA-T gels in pure water [10] and such a low water content as 25 wt%. Further, the observed marked swelling in sulfate solutions was ascribed to the breakage of the inter- and/or intramolecular HB between the carboxyl groups [10]. On the other hand, the chemical crosslinkage with 10 mol% EGDGE may only restrict the swelling degree of the PVA-T gel in a non-specific way. Therefore we focus on the discussion of HBs relevant to –COOHs instead of the chemical crosslinkage in the present study.

As reported in our previous papers [9, 10], the PVA-T gels swelled significantly only in sulfate solutions and we called this unique behavior anti-Hofmeister Series property. In addition to the anion-specificity, an appreciable cation-specificity was also observed. Thus, Li_2SO_4 revealed more significant salting-in effect than Na_2SO_4, because of the much stronger interaction of Li^+ with the substituted trimellitic acid groups than that of Na^+ [10]. Therefore lithium salts/PVA-T gel systems were chosen as the most typical one to examine the thermo-sensitivity of the relevant gel. Swelling degrees of PVA-T hydrogels in various lithium salt solutions containing 1 mM HCl and in pure water were investigated as a function of temperature, as shown in Figure 1. The hydrogels significantly swelled with temperature only in the presence of Li_2SO_4, while in pure water and 1 M LiCl or LiSCN solution, no appreciable changes were observed with temperature changes.

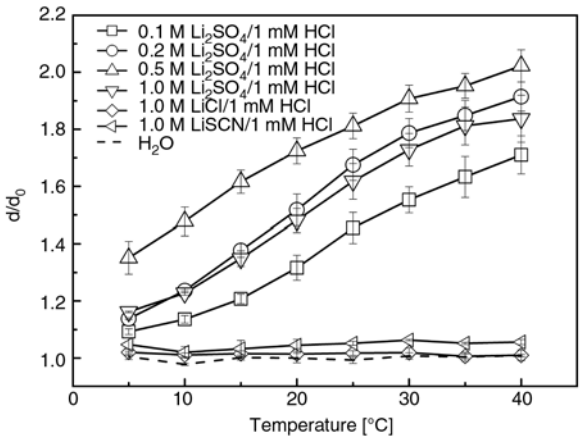

Figure 1. The swelling degree of PVA-T hydrogels in different aqueous solutions as a function of temperature

The significant swelling of PVA-T gels only in sulfate systems might be ascribed to the specific stabilization of hydrogen-bonding hydration (HBH) to the acidic protons of the carboxyl groups by the sulfate anion, as shown in Figure 2 as a schematic for the salt- and thermo-swelling mechanism [9, 10]. The stabilization of the HBH to the –COOH protons should be favorable for breaking those HBs involving carboxyls to cause the salt-induced gel swelling. Thus, the present 'thermo-swelling' that was observed only in the presence of sulfate anion may be safely ascribed to the scission of the intra- and/or intermolecular HBs. In fact, no other reasonable explanation seems to be given for the sulfate anion effect to induce the thermo-swelling. The insensitivity to temperature change in the absence of the sulfate anion, in turn, strongly suggests that the inter- and/or intramolecular HBs are too strong to be broken without the help of SO_4^{2-}. Namely, for the HBs to be effectively broken by heating, the presence of sulfate anion seems to be prerequisite.

It is known that the parent polymer PVA is largely subject to salting-out effect induced by SO_4^{2-} [11]. Thus, the great salting-in effect of this anion

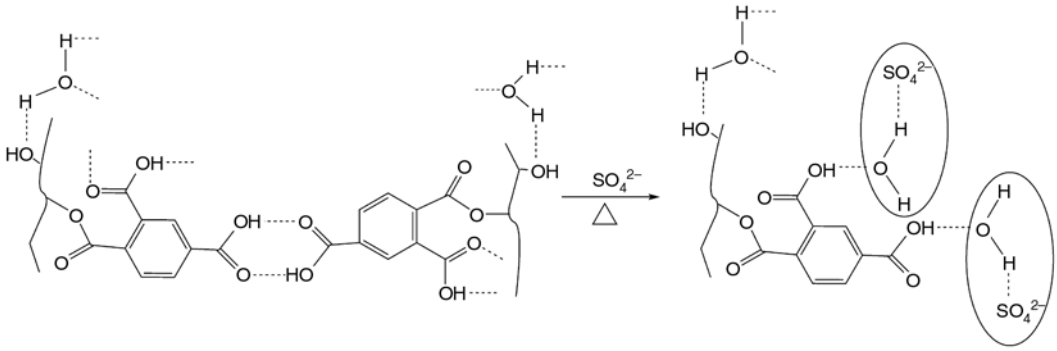

Figure 2. The scission of HBs involving –COOH groups in the presence of SO_4^{2-} during heating. Here the HBHs to the acidic protons are significantly stabilized by SO_4^{2-} because the partial negative charges on the water oxygen is enhanced [12].

observed for the PVA-T hydrogel must be ascribed to the trimellitic residue introduced to PVA. The salting-in effect may be attributed to the stabilization of HBH to carboxylic acid proton by SO_4^{2-} via enhancement of electron pair donicity (EPD) of the hydration water, because the partial negative charge on the water oxygen is enhanced via ionic hydration to small anions [12]. As a matter of fact, the improvement of PVA-T hydration in sulfate systems and the temperature effect are also proved by FTIR and NMR, which will be published in our forthcoming paper.

As for the effect of SO_4^{2-} concentration, the maximum swelling emerged at 0.5 M at any temperature. The deswelling at 1.0 M relative to 0.5 M results from the salting-out effect to the unesterified PVA OH group and the vinyl main chain [10]. Of course, the deswelling may be considered as a result of enhanced osmotic pressure from inside out because the salting-out of the sulfate means that the salt ions are rejected from around the polymer to reduce the concentration in gel phase compared with that in the external solution. Comparing the swelling degrees variation of PVA-T hydrogels with temperature, the ratio at 40 to 5°C are 2.8, 2.5, 3.0 and 2.7 for samples swollen in 0.1, 0.2, 0.5 and 1.0 M Li_2SO_4 solution, respectively. Thus, the thermo-swelling profiles are nearly parallel and slightly sigmoidal irrespective of the sulfate concentrations studied.

In order to examine whether the breakage/formation of HBs between –COOH groups is the driving force for the thermo-responsibility of PVA-T gel in Li_2SO_4 solutions, dissociation of the –COOH groups was changed by altering HCl concentration in 0.5 M Li_2SO_4 solution. As shown in Figure 3, the thermo-swelling behavior was only observed in the presence of moderate concentrations of HCl. It is noteworthy that the swelling degrees of samples in 0.1 and 0.5 mM HCl systems become saturated at higher temperatures (nearly equal values are observed at over 30°C). This may be ascribed to almost a complete breakage of inter- and intramolecular HBs in the hydrogels due to the stabilization of the HBH by sulfate anion as well as to inherent partial dissociation of the carboxyl groups. (At pH = 4–3.3, the dissociation degree of –COOH would be less than 50%.) On the other hand, at 5 mM HCl, no appreciable swelling was observed. Under such a rather acidic condition (pH ~ 2.3), the dissociation may be almost suppressed to stabilize the intermolecular HBs. Thus, these behaviors suggest that the thermo-swelling found for the PVA-T hydrogels occurs with a subtle balance of two counteracting factors: concentrations of HCl (H_3O^+) and Li_2SO_4 (SO_4^{2-}). An increment of the former would suppress the dissociation of –COOH groups and favor the inter- and/or intramolecular HBs, while the latter may cause the scission of the HBs via stabilization of the HBH to the acidic proton. As a result of the subtle balance between the two factors, the present gel may also be taken as a pH-sensitive material; in fact, e.g. at 30°C, the water content increases from ca. 25% in 5 mM HCl to ca. 90% in 0.5 mM HCl.

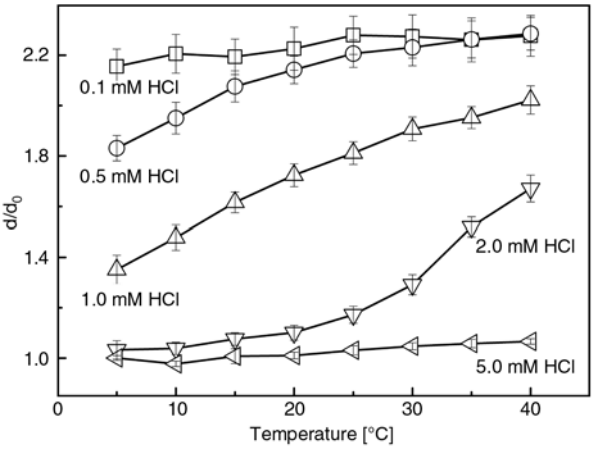

Figure 3. The influence of HCl concentration on the temperature-dependence of PVA-T hydrogels swollen in 0.5 M Li_2SO_4 system

Finally, taken the hydrogel swollen in 0.5 M Li_2SO_4/1 mM HCl system as an example, the reversibility of the thermo-swelling was tested by repeating a temperature jump between 5 and 40°C (Figure 4). When the equilibrated gel samples at 5°C were placed into the bath of 40°C, they swelled quickly to the value of $d/d_0 = 2.10$ after 3.5 h, approaching to the equilibrium value of 2.14 after 24 h. Then the highly swollen sample at 40°C was put into the environment of 5°C, the significant deswelling was observed within 6 h. The first and the second swelling degrees obtained after 24 h kept nearly constant at 40 and 5°C, respectively. Although the kinetics of the swelling-deswelling processes is rather slow, the reversibility and the reproducibility are well satisfying for a thermo-sensitive gel material that significantly swells upon heating.

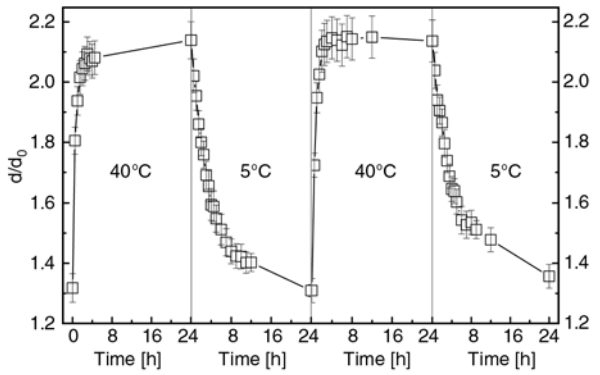

Figure 4. The swelling sensitivity to temperature jump between 5 and 40°C for PVA-T hydrogel swollen in 0.5 M Li_2SO_4/1 mM HCl solution

4. Conclusions

In the temperature range from 5 to 40°C, PVA-T hydrogels showed reversible and continuous thermo-swelling behavior only in the presence of SO_4^{2-}. This rather specific behavior was ascribed to scission and formation of the inter- and/or intramolecular HBs in the course of the heating and the cooling, respectively. Although the PVA-T hydrogel only continuously responded to temperature under the Li_2SO_4/HCl conditions tested in the present study, it may be expected that a reversible volume-phase transition driven by HB may be realized through optimizing the composition of swelling medium such as sulfate salt and HCl. To delve into the mechanism of salt- and thermo-swelling of PVA-T gels in sulfate solutions, a spectroscopic study with NMR and FTIR are now being undertaken, which will be published in our coming paper.

Acknowledgements

This study was supported by Grant-in-Aid for foreign post-doctoral fellows (19.07798) from Japan Society for the Promotion of Science (JSPS).

References

[1] Ilmain F., Tanaka T., Kokufuta E.: Volume transition in a gel driven by hydrogen bonding. Nature, **349**, 400–401 (1991).
DOI: 10.1038/349400a0

[2] Dimitrov I., Trzebicka B., Müller A. H. E., Dworak A., Tsvetanov C. B.: Thermosensitive water-soluble copolymers with doubly responsive reversibly interacting entities. Progress in Polymer Science, **32**, 1275–1343 (2007).
DOI: 10.1016/j.progpolymsci.2007.07.001

[3] Idziak I., Avoce D., Lessard D., Gravel D., Zhu X. X.: Thermosensitivity of aqueous solutions of poly(*N,N*-diethylacrylamide). Macromolecules, **32**, 1260–1263 (1999).
DOI: 10.1021/ma981171f

[4] Laukkanen A., Valtola L., Winnik F. M., Tenhu H.: Formation of colloidally stable phase separated poly(N-vinylcaprolactam) in water: A study by dynamic light scattering, microcalorimetry, and pressure perturbation calorimetry. Macromolecules, **37**, 2268–2274 (2004).
DOI: 10.1021/ma035124l

[5] Diab C., Akiyama Y., Kataoka K., Winnik F. M.: Microcalorimetric study of the temperature-induced phase separation in aqueous solutions of poly(2-isopropyl-2-oxazolines). Macromolecules, **37**, 2556–2562 (2004).
DOI: 10.1021/ma0358733

[6] Meeussen F., Bauwens Y., Moerkerke R., Nies E., Berghmans H.: Molecular complex formation in the system poly(vinyl methyl ether)/water. Polymer, **41**, 3737–3743 (2000).
DOI: 10.1016/S0032-3861(99)00513-3

[7] Hirashima Y., Sato H., Suzuki A.: ATR-FTIR spectroscopic study on hydrogen bonding of poly(*N*-isopropylacrylamide-*co*-sodium acrylate) gel. Macromolecules, **38**, 9280–9286 (2005).
DOI: 10.1021/ma051081s

[8] Sato H., Hirashima Y., Suzuki A.: Reswelling transition of poly(sodium acrylate) gels due to destruction of hydrogen bonds observed by ATR FTIR spectroscopy. Journal of Applied Polymer Science, **105**, 3811–3816 (2007).
DOI: 10.1002/app.26626

[9] Mori M., Wang J., Satoh M.: Anti-Hofmeister series properties found for a polymer having a π electron system and acidic protons. Colloid and Polymer Science, **287**, 123–127 (2009).
DOI: 10.1007/s00396-008-1965-0

[10] Wang J., Satoh M.: Novel PVA-based polymers showing an anti-Hofmeister series property. Polymer, **50**, 3680–3685 (2009).
DOI: 10.1016/j.polymer.2009.05.050

[11] Muta H., Miwa M., Satoh M.: Ion-specific swelling of hydrophilic polymer gels. Polymer, **42**, 6313–6316 (2001).
DOI: 10.1016/S0032-3861(01)00098-2

[12] Muta H., Kawauchi S., Satoh M.: Ion effects on hydrogen-bonding hydration of polymer an approach by 'induced force model'. Journal of Molecular Structure: THEOCHEM, **620**, 65–76 (2003).
DOI: 10.1016/S0166-1280(02)00585-7